**Università degli Studi di Salerno**

Dipartimento di Informatica

Dottorato di Ricerca in Informatica
Curriculum «IoT and Smart Technologies»
XXXVIII Ciclo

Tesi di Dottorato / Ph.D. Thesis

# Analysis and Optimization of Next-Generation SWIPT-Enabled Heterogeneous IoT Networks

**Biagio BOI**

Supervisor: **Prof. Christian ESPOSITO**

PhD Program Director: **Prof. Andrea DE LUCIA**

A.A 2024/2025

# ABSTRACT

Internet of Things (IoT) devices face significant challenges in maintaining continuous operation due to the limited capacity of their batteries. Despite the adoption of low-power communication protocols, many devices are unable to meet their energy demand, leading to frequent battery replacements in scenarios where electric power is unavailable. This affects data reliability and causes service interruptions, with repercussions across the entire data-driven IoT infrastructure.

Energy accumulation mechanisms based on environmental sources offer a promising way to extend the operational lifetime of such devices. However, sources such as sunlight and wind are highly variable and unreliable for systems that require continuous operation, and they are difficult to implement in small-scale devices. A more promising approach is to exploit the electromagnetic energy available within the network itself: the Simultaneous Wireless Information and Power Transfer (SWIPT) technique enables energy harvesting from wireless signals, allowing devices to recharge their batteries while receiving data.

Although extensively studied in the literature, SWIPT protocols have limitations related to the poor modeling of network parameters in heterogeneous context, where cellular and energy harvesting devices co-exist. It is therefore essential to develop network models and protocols capable of maximizing the collected energy by intelligently exploiting the properties of the channel, the environment, and the device density.

This thesis proposes a modeling and analysis framework for SWIPT-enabled networks in heterogeneous scenarios characterized by multiple devices and interference conditions. The analysis, initially focused on random spatial patterns, is then extended to vehicular and future smart city contexts, where node density and mobility play a critical role in the network's energy and communication performance.

Considering the growing relevance of 5G and future 6G networks, the thesis introduces a more realistic implementation that

defines adaptive patterns and optimization strategies accounting for network-specific characteristics. The achieved energy gains and optimization policies are examined as functions of the network configuration and operational conditions.

Taking into account the progressive decentralization of network policies, two device-side optimization policies are proposed for device-side energy harvesting, designed according to the criticality of the operating context, aiming to balance energy efficiency and quality of service.

The results of this work, beyond their methodological contribution, establish a solid knowledge foundation for the study and enhancement of SWIPT-based networks. The findings provide practical and non-trivial guidelines on how to model networks according to spatial geometries and environmental factors. Overall, the outcomes confirm the potential of SWIPT and self-sustainable network paradigms in enabling the transition toward autonomous, batteryless IoT infrastructures.

## ABSTRACT

I dispositivi dell'Internet of Things (IoT) incontrano notevoli difficoltà nel mantenere un funzionamento continuo a causa delle limitate capacità delle loro batterie. Nonostante l'adozione di protocolli a basso consumo energetico, molti dispositivi non riescono a soddisfare la richiesta energetica, con conseguenti frequenti sostituzioni delle batterie in scenari dove non è possibile l'alimentazione elettrica. Ciò compromette l'affidabilità dei dati raccolti e causa interruzioni nei servizi offerti, con impatti sull'intera infrastruttura basata su dati provenienti dai dispositivi IoT.

Meccanismi per l'accumulo di energia tramite fonti ambientali presentano una buona possibilità per estendere la vita di questi dispositivi. Tuttavia, fonti come sole e vento risultano altamente variabili e poco affidabili per sistemi che richiedono continuità operativa, nonchè difficili da implementare in dispositivi di piccole diminensioni. Una strategia più promettente consiste nello sfruttare l'energia elettromagnetica della rete stessa: la tecnica Simultaneous Wireless Information and Power Transfer (SWIPT)

permette di ricavare energia dal segnale wireless, ricaricando le batterie dei dispositivi durante la ricezione del segnale.

Nonostante i numerosi studi presenti in letteratura, SWIPT presenta ancora limitazioni legate alla modellazione dei parametri delle reti in contesti eterogenei al fine di sfruttarli al meglio. È quindi necessario sviluppare protocolli e modelli di rete in grado di massimizzare l'energia raccolta, sfruttando in modo intelligente le caratteristiche del canale, dell'ambiente e la densità dei dispositivi.

Questa tesi propone un modello di rete SWIPT e la relativa analisi in scenari eterogenei caratterizzati dalla presenza di molteplici dispositivi e da condizioni di interferenza. L'analisi, inizialmente condotta su pattern randomici, viene successivamente estesa a contesti veicolari e smart city di futura generazione, dove la densità e la mobilità dei dispositivi influenzano in modo significativo le prestazioni energetiche e di comunicazione.

Considerando la crescente rilevanza delle reti 5G e delle future 6G, la tesi introduce nella seconda parte una modellazione più realistica, che integra strategie di ottimizzazione e definisce pattern adattivi basati sulle caratteristiche del canale e della rete. In questo contesto vengono esaminati i guadagni energetici ottenibili e le strategie di configurazione più efficaci per massimizzare l'energia raccolta dai dispositivi.

Infine, tenendo conto della progressiva decentralizzazione delle scelte a opera dei dispositivi, vengono proposte due politiche di ottimizzazione del processo di energy harvesting lato dispositivo, definite in funzione del livello di criticità del contesto operativo, con l'obiettivo di bilanciare l'efficienza energetica e la qualità del servizio.

I risultati della tesi, oltre al contributo metodologico, costituiscono una base di conoscenza solida per lo studio e il miglioramento delle reti SWIPT, offrendo linee guida pratiche e non banali su come modellare la rete in relazione alle geometrie e alle condizioni ambientali. Tali risultati confermano il potenziale delle tecniche SWIPT e delle reti auto-sostenibili nel favorire la transizione verso infrastrutture IoT autonome, alimentate senza batterie.

# PUBLICATIONS

The research outcomes presented in this thesis have been partially published in international journals and conference proceedings, while additional manuscripts are currently under review or in preparation. The complete list is provided below.

## PUBLISHED

1. Rizzo, G., Marsan, M. A., Esposito, C., & Boi, B. (2025). Green operations of SWIPT networks: The role of end-user devices. *IEEE Transactions on Green Communications and Networking*.

2. Rizzo, G., Boi, B., Esposito, C., & Marsan, M. A. (2024, October). A stochastic geometry approach to performance modeling of SWIPT vehicular networks. In *Proc. 22nd International Symposium on Modeling and Optimization in Mobile, Ad Hoc, and Wireless Networks* (*WiOpt*) (pp. 76–83). IEEE.

3. Boi, B., Finarelli, L., Dressler, F., Esposito, C., & Rizzo, G. (2025). Energy-aware load shifting in SWIPT-enabled IoT networks. In *Proc. 9th IEEE International Conference on Smart Internet of Things* (*SmartIoT 2025*). IEEE.

## UNDER REVIEW / IN PREPARATION

1. Boi, B., Zhao, F., Esposito, C., & Yang, H. (2025). Age of information optimization in heterogeneous energy-harvesting networks. *Submitted to IEEE INFOCOM 2026*.

2. Boi, B., de Veciana, G., Rizzo, G., & Esposito, C. (2025). Design and analysis of energy-efficient beamforming for SWIPT networks. *In preparation*.

# CONTENTS

Publications vii
1 Introduction 1
1.1 Challenges 3
1.2 Research Questions 5
1.3 Document outline 8

I Context and State of The Art
2 Theoretical Background 13
2.1 Energy Harvesting and SWIPT 13
2.1.1 Receiver Architectures and Splitting Strategies 14
2.1.2 Practical Non-Linear Energy Harvesting 17
2.1.3 Interference 21
2.1.4 Safety 22
2.2 Analytical Models of Wireless Networks 22
2.2.1 Random Variables and Random Processes 23
2.2.2 Poisson Point Process (PPP) 24
2.2.3 Poisson Line Cox Process (PLCP) 26
2.3 Performance Modeling Tools 28
2.3.1 Queue Theory 29
2.3.2 Markov Chains 32
3 State of The Art 35
3.1 System-Level Trade-offs in SWIPT Networks 35
3.1.1 Deployment Strategies and Configurations 36
3.1.2 Stochastic Geometry Approaches 37
3.1.3 Research Gaps 38
3.2 Next-Generation Communication Enablers for SWIPT Networks 39
3.2.1 Antenna Directivity and Array-Based Energy Focusing 40
3.2.2 Spatial Scheduling 41
3.2.3 Research Gaps 42
3.3 Device-Side Optimization Policies 43
3.3.1 Information Freshness Strategies 43
3.3.2 Energy Efficient Strategies 45

3.3.3 Research Gaps 47

II Approaches for Design and Optimization of SWIPT-Enabled Heterogeneous Networks

4 System-Level Design of SWIPT HetNets 51
4.1 Planar Deployment Model 51
4.1.1 Problem Statement and Motivation 51
4.1.2 Methodological Approach 53
4.1.3 Optimization Problem 69
4.1.4 Limitations 71
4.2 Vehicular Deployment Model 71
4.2.1 Problem Statement and Motivation 71
4.2.2 Methodological Approach 72
4.2.3 Optimization Problem 79
4.3 Conclusion 81
5 Next-Gen Enablers for SWIPT 83
5.1 Analysis and Optimization of Energy-Efficient Beamforming for SWIPT Networks 83
5.1.1 Problem Statement and Motivation 83
5.1.2 Methodological Approach 85
5.1.3 Dynamic Optimization Framework 91
5.1.4 Analytical Modeling 93
5.2 Conclusion 97
6 Optimizing User Transmission Policies in SWIPT Networks 99
6.1 The Optimal Age of Information Policy 99
6.1.1 Problem Statement and Motivation 99
6.1.2 Methodological Approach 101
6.1.3 Optimization Problem 113
6.2 The Optimal Load Shifting Policy 119
6.2.1 Problem Statement and Motivation 120
6.2.2 Methodological Approach 121
6.2.3 Analytical Model 124
6.2.4 Optimization Problem 129
6.3 Conclusion 130

III Results and Discussion

7 Performance Outcomes for System Parameter Optimization 135

7.1 Planar Deployment Analysis 135
7.1.1 Parameter Setup 135
7.1.2 Receiver Architectures and Splitting Strategies 137
7.1.3 Traffic Patterns and Base Station Density 140
7.1.4 Impact of Splitting Factor 144
7.1.5 Nonlinear Energy Harvesting Effects 145
7.2 Vehicular Deployment Analysis 147
7.2.1 Network Power Consumption and Deployment Strategies 147
7.2.2 Transmit Power and Splitting Optimization 150
7.2.3 Harvested Energy Performance 151
7.3 Summary of Findings 152
8 NextGen Enablers Results 155
8.1 Beamforming Design and Optimization 155
8.1.1 Parameter Setup 155
8.1.2 Optimal antenna design 156
8.1.3 Optimal non-overlapping beam scheduling 159
8.1.4 Heuristic for beam overlapping 160
8.2 Summary of Findings 161
9 Device-Side Policy Results 165
9.1 Analysis of Time-Sensitive Policy 165
9.1.1 Parameter Setup 165
9.1.2 Effect of Energy Availability and Thresholds 166
9.1.3 Effect of Interference on Freshness 168
9.2 Load-Shifting Policy 171
9.2.1 Parameter Setup 171
9.2.2 Delay Constraints and BS Utilization 174
9.2.3 IoT Duty Cycling Impact 176
9.3 Summary of Findings 177

IV Conclusions and Future Work
10 Conclusion 183
10.1 Practical Implications 184
10.2 Limitations 185
11 Future Work 187
11.1 Relying Architectures 187
11.2 Opportunistic Energy Scheduling 188

Bibliography 189

# LIST OF FIGURES


Figure 2.1 Typical PS based Architecture [139] 16
Figure 2.2 Comparison of analytical model for linear vs. nonlinear harvesting in [5] 19
Figure 2.3 Manhattan PLP vs. Classical PLP [29] 28
Figure 2.4 Battery Markov chain with non-adjacent transitions. Rates $\lambda$ (harvest jumps) and $\mu$ (consumption jumps) illustrate generalized dynamics. 34
Figure 4.1 Outline of the system model for the SWIPT wireless network considered in this work. 53
Figure 4.2 Difference in the harvesting process between SPS and DPS receiver operating modes. 55
Figure 4.3 Downlink time scheduling scheme for a SWIPT BS, for a network with time switching EH receiver architecture, with GPS weights. 55
Figure 4.4 Two tiers proposed architecture composed by UE (green), vehicular BS (blue) placed on roads (yellow), and planar BS (red). 74
Figure 6.1 System model characterized by a grid-powered device $S_1$ with a data queue $Q(t)$, and an energy-harvesting device $S_2$ equipped with an energy buffer $B(t)$. Interference arises when both nodes transmit simultaneously to the destination $D$. 101
Figure 6.2 Illustration of a SWIPT network where the base station provides connectivity for both BB and IoT UEs while actively charging IoT UEs. 121
Figure 7.1 Power per $km^2$ consumed by the network at the optimum vs user density, for different target minimum harvested power and IoT UE receiver configurations. Markers denote values from simulations, derived with a 95% confidence interval of at most 8%. 138

Figure 7.2 Power consumed by the network for each user (broadband or IoT) vs. user density, for different target minimum harvested power and IoT UE receiver configurations. 140
Figure 7.3 Increase in the power per $km^2$ consumed by the network with respect to linear EH, as a function of user density, for HLP 1 mW target minimum harvested power, and for different IoT UE receiver configurations. 141
Figure 7.4 Optimal BS density for different target minimum harvested power and IoT UE receiver configurations. 142
Figure 7.5 Optimal transmit power for different target minimum harvested power and IoT UE receiver configurations. 143
Figure 7.6 Optimal time splitting factor (for TS) and power splitting factor (for DPS and SPS) for different target minimum harvested power and IoT UE receiver configurations. 144
Figure 7.7 Harvested power as a function of power received by IoT EH user, for a linear (with conversion efficiency of 0.9 and 0.77 respectively) as well as for the nonlinear model (Equation 5.4) with $h_s = 0.064$ mW, and $\chi = 274$. 146
Figure 7.8 Increase in consumed power with respect to linear EH, as a function of user density, for different values of the parameter $\iota$ of the nonlinear EH curve, and for different network setups, in the time splitting configuration. 146
Figure 7.9 Power per $km^2$ consumed by the network at the optimum vs user density, for different BS distributions. 148
Figure 7.10 Optimal BSs densities for different minimum number of vehicular BS and system design. 149

Figure 7.11 Optimal system parameters for different minimum number of vehicular BS and system design. 150
Figure 7.12 Energy Harvested from other UEs vs. user density for different BS distributions. 151
Figure 8.1 Throughput vs $r_{\max}$ for $\lambda = 0.006$ and $\sigma_b = \frac{10\pi}{180}$ for different number of sectors in the disk. 156
Figure 8.2 Throughput vs $r_{\max}$ for $\lambda = 0.06$ and $\sigma_b = \frac{10\pi}{180}$ for different number of sectors in the disk. 157
Figure 8.3 Instantaneous harvestable energy at distance $R_{\max}$ vs $R_{\max}$ for $\lambda = 0.06$ and $\sigma_b = \frac{10\pi}{180}$ for different number of sectors in the disk. 158
Figure 8.4 Energy Harvesting Fraction vs $r_{\max}$ at distance $r_{\max}$ for $\lambda = 0.06$ and $\sigma_b = \frac{10\pi}{180}$ for different number of sectors in the disk. 159
Figure 8.5 Throughput vs $R_{\max}$ for different optimization methodology for $\lambda = 0.006$ 160
Figure 9.1 Optimal AoI at EH-node $(S_2)$ vs. data arrival rate $\lambda$ at node $S_1$, for different energy harvesting rates $\delta \in \{0.1, 0.4, 0.8\}$ and different regimes. Markers represent simulations. 167
Figure 9.2 AoI at the EH-node $S_2$ vs. access probability $q_2$, under both ECR and ESR for a fixed data arrival rate $\lambda = 0.001$ at node $S_1$. Transition between regimes happens at $q_2 = \delta/N$. 168
Figure 9.3 Number of energy units $N$ used per transmission by the EH node $S_2$ at optimal AoI vs. data arrival rate $\lambda$ at node $S_1$, for different energy harvesting rates $\delta \in \{0.1, 0.4, 0.8\}$ in ECR. 169
Figure 9.4 Optimal AoI for fixed values of energy units $N \in \{2, 3, 4\}$ vs. data arrival rate $\lambda$ at node $S_1$, under different energy harvesting rates in ECR. 170

Figure 9.5 Access probability $q_1$ for the grid-powered node $S_1$ at optimal AoI vs. data arrival rate $\lambda$, for various energy harvesting rates $\delta$ at node $S_2$ in ECR. 171
Figure 9.6 Transmit power $P_1$ of node $S_1$ at optimal AoI vs. data arrival rate $\lambda$, for different values of $\delta$ at node $S_2$ in ECR. 172
Figure 9.7 Decomposition of the successful transmission probability $\bar{p}_2$ of the EH-node $S_2$ into interference-free $(p_{2,2})$ and interference-affected $(p_{2,1})$ components, for $\delta = 0.8$ as a function of $\lambda$ in ECR. 173
Figure 9.8 Energy consumed at the optimum vs. densities of users for different BB and IoT target per-bit delays. $\phi = 1$ refers to the baseline configuration where the IoTs cannot manage their duty cycle tuning $\phi_u$ and $\phi_d$. 175
Figure 9.9 Splitting factor at the optimum vs. densities of users. 176
Figure 9.10 Energy consumed at the optimum vs. $\phi_d$ for different users' configurations. 177
Figure 9.11 Optimal shifting strategy for a 24-hour observation window with a time slot duration of 2 hours. The black line represents the considered traffic profile. 178

## LIST OF TABLES

Table 4.1 Main notation used in Section 4.1. 57
Table 4.2 Main notation used in Section 4.2. 73
Table 6.1 Main notation used in Section 6.1. 104

# 1 INTRODUCTION

The Internet was originally intended as a means of interconnecting computers across the world. Over time, this concept became increasingly restrictive, as new categories of devices began transmitting data through the network. Technological progress, particularly the miniaturization of processors, enabled not only people but also everyday objects, such as washing machines, cars, and medical devices, to become part of this digital ecosystem, creating to the so-called Internet of Things (IoT). Today, its pervasiveness extends to nearly every domain, including Industry (IIoT) [22, 132], Medicine (IoMT) [143], and Vehicles (IoV) [66].

The integration of networking capabilities into even minimal sensors provides clear advantages: real-time remote monitoring, cost reduction, and enhanced efficiency. In addition, IoT contributes directly to safety improvements, from fall detection to continuous patient monitoring in hospitals [67].

Such advancements have been made possible thanks to the parallel evolution of communication infrastructures. While 5G networks, with higher data rates, lower latency, and increased capacity represent the most visible face of this evolution, other innovations such as low-power protocols and network softwarization [64] have been equally crucial.

Despite these advances, significant challenges remain due to the extreme resource constraints of IoT devices, many of which are smaller than a coin and therefore equipped with minimal memory and very limited batteries. Perhaps the most pressing challenge is the development of smart algorithms that minimize energy consumption in both computation and communication. Extending device lifetimes is particularly critical in contexts where recharging is impractical, therefore IoT systems are expected to operate for years on tiny batteries [156].

At the hardware level, progress in low-power circuit design has reached incredible levels, with microcircuits capable of operating on the order of milliwatts (mW). While this enables lithium-ion

batteries to last for years, further reductions in circuit power consumption are now marginal.

As a result, attention has shifted toward optimizing communication, which is by far the most energy-intensive operation in IoT [49]. Into this context, Energy harvesting (EH) techniques can be considered as a viable solution for increasing the life of those devices. EH techniques include both environmental sources (e.g., radio frequency, solar, thermal, flow) and external sources (e.g., mechanical, human) [131]. Among these, RF-based energy harvesting has gained particular relevance due to its dual advantage: it not only enables wireless power distribution, where a single transmission can supply energy to multiple nodes, but also aligns naturally with IoT's reliance on radio communications, reusing part of the infrastructure already deployed.

Building upon this, Wireless Power Transfer (WPT) technologies have emerged, using a transmitter coil to generate high-frequency magnetic fields and a receiver coil with an energy management circuit to harvest and regulate power. More recently, research has advanced toward Simultaneous Wireless Information and Power Transfer (SWIPT) [142], a paradigm that unifies energy and data transmission into a single signal. The architecture employed in SWIPT is similar to those used for WPT, with some differences over the antenna used for the transmission. From the point of view of the transmitter, a rectenna is used for transmitting power, and depending on the architecture, it is possible to transmit power and data together on that antenna or it is possible to leverage on a separate antenna. What makes SWIPT a valid solution, is the possibility of delivering power through the same cellular infrastructure used to deliver data, and thus in a potentially more cost-effective manner than alternative approaches. Moreover, the usage of a programmable source for powering up the device, enable the possibility of making those devices available whenever needed, without creating any dependencies on atmospheric condition, such as in the case of solar energy.

As a result among the available technologies for transmitting energy to devices, SWIPT [34, 57, 104, 108, 142] is of particular interest, as it exploits the same cellular infrastructure used to deliver data. This feature makes it easier and more cost-effective to deploy than alternative wireless power delivery approaches.

SWIPT has been demonstrated to be effective both in the band of IoT networks, such as NarrowBand-IoT (NB-IoT) [46], and in cellular networks, such as 5G [9]. The needs for implementing SWIPT systems, are multiple and vary depending on the context in which this solution is deployed:

- **Post-disaster scenario**. Considering the case of post-disaster, where neither connectivity nor power are available; SWIPT is a perfect technology for reaching devices in this emergency context. Unmanned Area Vehicles (UAVs) can be leveraged for offering services in post-disaster scenarios, anyway, concerns about UAV batteries and the mobility of these nodes open new challenges [125] [6].

- **Battery-less devices**. Li-Ion battery use has a significant negative environmental impact [109], which is amplified by the fact that most IoT devices are replaced once the battery dies. By designing circuits that are powered by the energy harvested, SWIPT can significantly minimize the usage of batteries.

- **Continuous sensing**. Real-time applications require the continuous sensing of the environment, which causes the disruption of the battery of those devices. SWIPT can help in those cases by using part of the channel to transfer energy relevant for reducing the impact on the battery.

- **Resilient communication**. SWIPT can be used to increase the resilience of lightweight protocols by transferring additional energy that might be used for an improved version of those protocols. In fact, the greatest power consumption comes from the transmission task, which depend on the protocol implemented.

This technology represents a promising direction for future green networking, particularly within IoT systems where both connectivity and energy autonomy are critical.

## 1.1 CHALLENGES

Differently than traditional single-service cellular networks with no active power transfer, managing SWIPT networks for energy efficiency implies accounting for the interdependence between

the energy consumed by BSs and that consumed by IoT users which, for their ubiquity and rising numbers, are poised to play a key role in determining the overall energy footprint of the network. As in the case of traditional IoT networks, the challenges, such as network instability, hidden terminals, and batteries, makes hard to define a linear function which takes into account all those aspects. Additionally, SWIPT arises another problem, which is related to the co-existence of EH and non-EH devices. In conventional wireless networks, the term Heterogeneous Network (HetNet) often refers to the coexistence of multiple infrastructure layers, such as macro Base Stations (BSs), small cells, and relays, deployed together to improve coverage and capacity. In the context of this thesis, however, heterogeneity acquires a different and more fundamental meaning, one that arises from the energy capabilities of the devices rather than the infrastructure tiers. Non-EH devices are typically powered through stable and reliable sources, such as wired connections or long-lasting batteries. These devices can sustain continuous operation and dedicate their resources to optimizing communication performance without significant concern for energy availability. They usually support advanced communication features, higher transmission rates, and more complex signal processing operations, since their energy supply is not a limiting factor.

Nonetheless, since the considered context is typically populated by thousands of devices, it must handle multiple variables, such as network instability, hidden terminals, devices equipped with small batteries or no battery at all, co-existence interference and signal attenuation, etc. Moreover, the impact of RF signals can be a relevant issue for the health of humans if not properly designed and managed. The transmission of information and power is relatively straightforward in theory; numerous BSs simultaneously transmit information and power to the devices, which are able to collect the supplied energy using specialized modules. Anyway, since power cannot be easily conveyed along with data in this situation and the primary obstacles related to fading, shadowing, and other issues are particularly significant, with significant changes that result from tuning parameters, it is obvious that a correct modelization of the system is crucial for implementing reliable solutions. To make SWIPT a concrete use-case, more effort must be

spent in optimizing the network parameters, while taking into account existing infrastructure and the presence of other categories of devices. Most of the SWIPT use-case are within traditional cellular network, therefore accounting the interplay of end-user is crucial to increase the development of these networks. Despite multiple harvester module are able to convert all the RF-signal they receive into energy, frequencies and bandwidth play crucial roles. Multiple challenges exist considering the huge number of nodes [39], which traditionally involves future networks, and the mobility [29], widely known to be affected by noise and interference. A valid solution to make SWIPT able to work in existing networks is to find the right tradeoffs between performance and power consumption without affecting the QoS of high-end devices.

## 1.2 RESEARCH QUESTIONS

This thesis aims to address different aspects of the wide context of SWIPT network optimization, ranging from network deployment strategies to end-user device policies. The main objective is to identify the optimal design choices that can enhance the overall efficiency of SWIPT heterogeneous networks (HetNets), considering both BS configurations and end-device behavior. To achieve this goal, the thesis is structured around three Research Questions (RQs), which serve as a guiding framework for the remainder of the document. The following description is not intended to be exhaustive, as additional details on the theoretical background and the state of the art are provided in Chapter 2 and Chapter 3, respectively.

**RQ1.** *How do system parameters and deployment configurations influence the trade-offs between energy harvesting and information transfer in SWIPT-enabled HetNet?*

In traditional IoT networks, the network performance are primarly guided by the BSs transmission power, and to the interference generated for the simultaneous transmission of nearest antennae. In SWIPT networks, instead, the network performance are not inversely proportional to the interference generated by the surrounding devices. In fact, interference, as an example, can play

a dual role: it may still disrupt the communication of traditional nodes, but it can also contribute to energy harvesting, potentially becoming beneficial. This paves the way for a non-trivial trade-off between the BSs transmit power and the energy harvested by the devices. Characterizing these behaviours requires the representation of network dynamics, including the energy that might be potentially harvested by the transmission of other devices. As intuitively one can imagine, this is an highly dimensional optimization problem, which lead to a non-convex problem where BS density, transmission power, and harvester sensitivity combines and lead to the presence of multiple optimal point. RQ1 focuses on understanding the fundamental relationships between the aforementioned system parameters and deployment configurations, with the ultimate objective of increasing the performance in a typical cellular SWIPT HetNet. There are two main motivations for addressing RQ1: on the one hand, to provide a clear and quantifiable view of how baseline systems behave under different conditions; on the other hand, to establish a solid analytical foundation for the integration and optimization strategies addressed in the subsequent research questions. As I will elaborate further in this thesis, this phenomenon is influenced not only by network parameters, but also by the location of end devices. Therefore, the deployment strategies and the densities of these devices will also be examined.

**RQ2.** *How can enabling technologies from NextGen networks* (e.g. beamforming) *be exploited to enhance the efficiency of EH in SWIPT-enabled HetNet?*

NextGen wireless systems introduce a variety of enabling mechanisms, such as multiple-input multiple-output (MIMO) antenna arrays, advanced beamforming schemes, and reconfigurable intelligent surfaces (RIS), that can be exploited not only to increase data rates but also to concentrate and direct energy towards energy-constrained nodes. Those techniques add a new level of complexity to the analysis that might be carried out on traditional networks, characterized by the presence of these network features. In fact, these technologies provide spatial degrees of freedom that allow more precise control over the radio environment, enabling stronger energy transfer without significantly degrading informa-

tion decoding. Clearly, those features must be adequately supported and analyzed to understand their behavior and impact for SWIPT networks. RQ2 aims to provide concrete guidelines on the effects of these advanced network features and their impact on SWIPT systems. As will be discussed in this thesis, beamforming can enhance the energy harvesting process by reaching more distant users. However, this introduces a trade-off: while targeting distant users, the total number of users that can be served simultaneously may decrease. The motivation for investigating this area comes from the contrasting characteristics between traditional and SWIPT network environments. In conventional networks, beamforming is more straightforward, as devices can fully utilize the transmitted power and creating narrower beams is typically optimal. Conversely, in SWIPT settings, energy-harvesting modules have a fixed capacity and cannot convert the received power to energy beyond their threshold. Additionally, broader beams can enable multiple devices to harvest energy from a single transmission, as discussed in RQ1. This scenario introduces a new trade-off between beamwidth and network coverage that requires careful consideration. This optimization problem is intrinsically hard to solve exactly. While the disjoint-beam formulation admits a polynomial-time dynamic programming solution, allowing overlapping or adaptive beams leads to a combinatorial explosion of configurations. This last solution, which seems to be counterintuitive in traditional network, can be particularly relevant for SWIPT networks, where multiple UEs belonging to a beam can harvest the energy during the transmission to other UEs in the beam. In fact, since beams can overlap, the problem can be reduced to the classical set coverage problem, which is NP-hard. Hence, RQ2 focuses on developing heuristic and approximate strategies to explore the trade-off between beamwidth and coverage in a computationally feasible way.

**RQ3.** *Which UEs policies can be employed to enhance performance and harvesting process in SWIPT-enabled HetNet?*

Apart from the network parameters, which represent the fundamental components that determine the QoS experienced by end devices, the role of the devices themselves is becoming increasingly relevant. The rise of edge computing is shifting part of the

decision-making process from the BSs to the end devices, enabling diverse operational scenarios depending on user capabilities and priorities. As previously introduced, the users' influence becomes even more evident in highly dense deployments, where small variations in device policies can lead to significant differences in the overall energy harvesting performance of the network. In such contexts, several devices may not need to harvest energy continuously and can either be temporarily deactivated or excluded from power allocation. For instance, a device might decide to perform a duty cycle, thereby reducing its transmission time and, consequently, the environmental energy available for harvesting by nearby UEs. In traditional networks, devices are typically grouped into classes that define their QoS requirements. In SWIPT networks, however, these classes also depend on the devices energy harvesting capabilities, making the optimization problem substantially more complex. RQ3 focuses on the design and evaluation of strategies aimed at improving the performance and energy efficiency of SWIPT-enabled heterogeneous networks from the device perspective. While RQ1 and RQ2 analyze the fundamental trade-offs and integration aspects from the network operator's side, RQ3 shifts the focus toward device-level optimization, seeking to identify methods that dynamically adapt device operation to changing network conditions and data transmission priorities. As will be further elaborated in later chapters, IoT devices can adapt their transmission policies based on environmental factors and autonomously decide when to transmit. However, as highlighted in the previous discussion, such adaptive policies cannot be directly mapped to traditional networks due to the absence of explicit energy modeling, driving the SWIPT networks.

## 1.3 DOCUMENT OUTLINE

The document is structured into four parts, each of them covering a different aspect of the arised research question.

- Part I — Context and State of The Art. This part is structured into two chapters. Chapter 2 provides an overview of the SWIPT architecture and introduces the methodological tools necessary to understand the implementation details discussed in the sub-

sequent chapters. Chapter 3 reviews the current literature on network modeling and NextGen enablers, as well as end-device strategies aimed at maximizing throughput.

- Part II — Approaches for Design and Optimization of SWIPT-enabled HetNet. This part is divided into three chapters: one for each RQ. Chapter 4 discusses the methodology for resolving the RQ1 through the usage of SG. Here I present two works on the usage of SG for modeling the network performance, one on the random planar distribution, and the other one on the vehicular distribution. Chapter 5 discusses the methodology for RQ2 through the usage of a beamforming model and the usage of SG for abstracting the UEs. The chapter also provides a dynamic programming problem to solve the optimal beamforming assignment within polynomial time. Chapter 6 discusses methodologies for RQ3. This chapter discusses two different approaches, the first one focused on the development of algorithm for optimizing the information freshness, relevant in time-sensitive context, and the other one discussing the load shifting algorithm relevant in energy-aware context.

- Part III — Results and Discussion. Having now defined the methodology for all the RQs, this part follows the same division of Part II, with one chapter for each RQ. Chapter 7 discusses the impact of the main network-level parameters on the energy harvesting processes. Chapter 8 discusses the usage of beamforming in SWIPT network, with insights about the spatial distribution and energy harvesting sensitivity. Chapter 9 discusses the optimal end-device policy behavior highlighting pros and cons of each policy.

- Part IV — Conclusion and Future Works. The last part of this thesis is divided into two chapters. Chapter 10 discusses the conclusion of the thesis, outlining the main contribution and discussing the limitation of this thesis, and its practical implementation. Chapter 11 discusses possible extension of the current work, according to existing literature in similar context, and according to the results highlighted by the current thesis.

# Part I

# CONTEXT AND STATE OF THE ART

The first part of this thesis provides the conceptual and methodological foundations necessary to contextualize the research presented. It begins with an overview of the SWIPT architecture, followed by the theoretical frameworks relevant for network analysis, and concludes with a comprehensive discussion of the existing literature.

# 2 THEORETICAL BACKGROUND

This chapter establishes the theoretical framework supporting the analysis and developments presented in the following chapters. It is organized in three sections. Section 2.1 introduces SWIPT architectures, which are central to the system under study. Section 2.2 presents analytical modeling tools based on stochastic geometry for capturing the behavior of wireless networks, supporting the analysis of SWIPT network. Finally, Section 2.3 covers performance modeling frameworks such as queueing theory and Markov chains, necessary to characterize device-level energy dynamics and information freshness.

## 2.1 ENERGY HARVESTING AND SWIPT

EH techniques can extend the life of any device, encompassing those equipped with a huge battery, and those with a supercapacitors. EH can be applied using multiple sources, such as solar, wind, water, and everything able to produce energy. The main difference among them all is the variability and predictability of the source. Let us consider a system of hot water that is only alimented through the usage of a solar (thermal) panel, which works well when the sun it's high in the sky, but what happens if the day is not among the best ones? It is clear that if it is equipped with a big enough tank then the problem can be solved, but if not, how can it be solved?

More in general, we call this as the problem of *prediction lack*, which is recurrent every time we consider the green energy produced through the usage of natural source such as the sun. The usage of those sources introduce an additional problem, which is related to the space needed for the harvester module (e.g. a solar panel, or a turbine).

Let us move on a different perspective of this problem, considering the wireless communication networks. In those environments, without going deeper in the electrical part, the electrical

energy is converted into electromagnetic waves, which propagate into the free space, depending on the direction of the antenna.

On the other side, a receiver can collect such waves and reconstruct the information. Anyway, in the middle between sender and receiver it exist a communication mean, which in this specific case is the air. This signal, rather than be converted into information, might also be used to power up a circuit, similar to the case of NFC.

In fact, NFC is the most evident example of passive energy harvesting device, where the circuit containing the card information is powered-up by an active RF transmitter.

WPT follows the same approach as NFC, harvesting energy from the air and converting it into energy, without an appropriate modeling of data transmission protocol. To overcome WPT limitation, SWIPT can also transmit data. As one can imagine, the transmission of energy cannot happen together with the data transmission.

The growing interest towards the integration of WPT in cellular networks is due to its potential for enabling truly ubiquitous and self-sustained IoT exploiting energy-constrained devices [34, 57, 104, 108, 142]. Indeed, differently from other energy harvesting techniques (e.g., based on solar, or solely on passive RF harvesting) those based on active wireless power transfer have the advantage of being stable and available at any time [127]. Several technical challenges, however, still need to be addressed for the practical viability of SWIPT networks, related to energy-harvesting transceiver and algorithm design, system integration, protocol design, and energy-efficient network planning and operations [32, 103]. To better detail the issues and possible solutions, we start this chapter from the architecture design, where the most typical apporaches to energy and data trade-off are discussed. Once clarified the components involved, and typical architectures, the document discusses about concrete RF-module.

### 2.1.1 *Receiver Architectures and Splitting Strategies*

The antenna architecture used for implementing a SWIPT system is the most important phase when designing a solution. A primary study conducted in [164] investigates the principal antenna

components of SWIPT systems, proposing two approaches: separated and co-located antennae. It is trivial, that by leveraging a separated antenna approaches, the tradeoff between data and energy can be easily acheived, but this is not the most pratical solution to reduced space devices.

Therefore, in the remaining of this documnt we mostly refer to these circuits as an unique antenna device. In fact, in the case of co-located antennae the received signal must be split into two, while in the case of separate antennae, one antenna is used for Energy Harvesting (EH), while the other is for Information Decoding (ID). In the proposed system, a Multiple-Input Multiple-Output (MIMO) architecture has been analyzed with two main co-located antenna approaches: Power Splitting (PS) and Time Switching (TS). In the first one, the power is transmitted together with data at different frequencies, while in the second one, an alternation of the transmission of power to the transmission of data happens. Both the transmissions are modulated using a splitting factor which is responsible for the ratio between power and data transmitted/received. However, a comparison between PS and TS shows an improved performance in the first respect to the second one; making this approach a viable alternative to separated antennae.

MIMO and Multiple-Input Single-Output (MISO) are widely used in the context of SWIPT, considering their ability to send data and energy from a single source with multiple antennae. One of the most interesting point of SWIPT architectures, is the possibility of harvesting energy despite the signal is not intended for them, since the content of the signal is not relevant for powering-up the device. Moreover, MIMO and MISO are recurrent concepts in recent C-RAN such as 5G, thanks to their ability to increase the Signal-to-Noise Ratio (SNR) and extend the coverage in a given direction [45]; which means that far devices can still benefit of network architecture.

To be more technical, integrated antennae are composed of an energy receiver and an information receiver. As depicted in Figure 2.1, the received signal flow in both receivers, with a parameter $\rho$ responsible for tuning the percentage of both [139]. A simple PS system is introduced by Huang et al. [59], which studies the EE optimization problem with PS applied to the IoT devices in

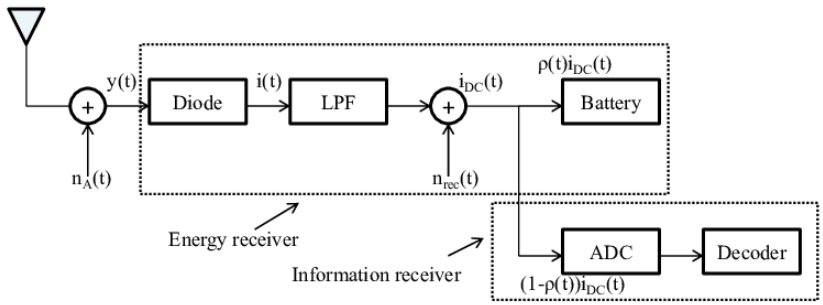


Figure 2.1: Typical PS based Architecture [139]

order to coordinate the ID and EH processes. In the first stage, the authors investigated the case of a single IoT device which is served by multiple Decentralized Antennas (DAS) controlled by a central processor, producing a nonconvex problem. The proposed objective function aims to maximize the EE of DAS while taking into consideration the minimum harvested power for the device and the maximum transmits power for each DA. Configuration of this problem results in a non-concave objective function, where a globally optimal solution has been found by analyzing the Karush-Kuhn-Tucker (KKT) conditions. The proposed model, which does not take into account the quality of the received service, might be seen as a limitation of the proposed strategy, even though it is capable of producing good results and solving the problem in linear time. Further investigation of the EE in the context of DAS has been conducted in [158] and [92], which also consider the problem of Power Allocation (PA) in addition to PS ratio computation. The authors also present a resource allocation schema based on imperfect channel information; where the perfect Channel State Information (CSI) is unfeasible in practice due to channel estimation and quantization errors [105]. They applied an ergodic rate to replace the instantaneous rate proposed in [59]. Also in this case, by applying KKT conditions and the Lambert function the number of valid DA ports and the homologous PA coefficients with closed form are deduced.

In [23], a novel strategy based on game theory has been put out. Non-cooperative games have been developed for three different network scenarios, and each link is portrayed as a strategic

player who seeks to maximize the individual attainable rate. Results have demonstrated that, despite different starting locations, the specified games always produce a singular Nash equilibrium (NE) as a response, achieving good convergence. The same approach has been considered in [147]; where a PS system is defined without the usage of MIMO. Every receiver is connected with a single transmitter creating a single link, but K channels exist and can be used for creating multiple connections but only one single data stream is transmitted. Each one of the K channels is modeled as a strategy player, the game framework is formulated to solve the power allocation problem. Anyway, the problem is still non-convex and non-linear, and an alternating optimization method is employed for the resolution. Results of the proposed approach show less transmit power than traditional approaches. In [97] the authors extended the previous approach to the context of cognitive sensor node considering the SINR and splitting the transmission into three phases: energy harvest, spectrum sensing, and data transmission. The granularization of transmission components led to a convergence in unique NE results that allowed for a significant reduction in energy and time consumption compared to previous algorithms using a similar methodology.

### 2.1.2 *Practical Non-Linear Energy Harvesting*

Despite linear harvesting has been considered in almost all the proposed time-switching and power-splitting systems, this assumption is not feasible in a real context. The performance of a typical RF energy harvester module is defined by power harvesting efficiency, which is typically modeled as a logistic (sigmoidal) function, able to include all the input-output characteristics of the EH circuits. In recent years, practical commercial solutions started to be released within the context of SWIPT for harvesting energy able to power IoT solutions. In an analysis conducted by Meile et al.[93], the performance of Powercast P1110B has been evaluated. Such a commercial solution works at 915MHz and store power in a capacitor, which when collect enough power activate the devices and transfer the necessary energy. Experimental results show 135$\mu$W power achieved at 1.6m and more than 1mW at 1m. A more technical evaluation has been conducted in [86] on

the same harvesting module, where three waveforms were proposed and compared: single-tone, multitone with high and low peak-to-average power ratio (PAPR) levels, random and chaotic signals. The conversion efficiency analysis of introduced waveforms concluded a better efficiency for single-tone with low PAPR. Some other evaluations have been conducted in order to assess the quantity of energy needed from devices in the case of BLE connection [85], system for motion detection equipped with BLE connection [63] and the feasibility of batteryless devices [41]. In [41] the authors harvested the 2.4GHz RF Power in a system able to perform infrared-based motion detection implementing BLE communication without the usage of battery. The power received from this kind of RF system can vary in the range $[+24db, -15db]$, where the smallest value is achievable at a distance of 5 meters. Results show the possibility of implementing a batteryless system, which only uses super-capacitors where a few $\mu$Ws are received from the source and the consumption of the system is $4.3\mu$W when no motion is detected and $6.8\mu$W otherwise. It is notable that harvested energy does not come from the same source of transmission of data so any energy efficiency algorithm has been considered for the modulation. An extended work has been proposed in [154], where a Power Management Unit (PMU) is responsible for generating a stable voltage and an accurate estimation of power harvesting efficiency has been considered. The outcomes of the study highlight the sensitivity of the module at $-17.1dBm$ and the limitations introduced by the parasitic capacitance. Batteryless needs are not limited to the smart city context but can be extended to the medical context, where it is usually unfeasible to equip batteries on biosensors [76], usually used for EEG measurement. Schmickl et al. [128][129] present an approach based on NMOS-transistors for 802.15.4a transmitter powered by a harvester in 180nm CMOS technology. Differently from previous work, the module works at a frequency of 868MHz and is able to produce $5\mu$W which is enough for the transmission of medical data.

To summarize, those circuits cannot harvest the whole amount of energy they receive, therefore once it fulfills the maximum threshold, the energy harvested remain fixed. In addiction, the usage of supercapacitors, limits the total amount of energy which is possible to harvest without consumption. Moreover, it is unfeasible to

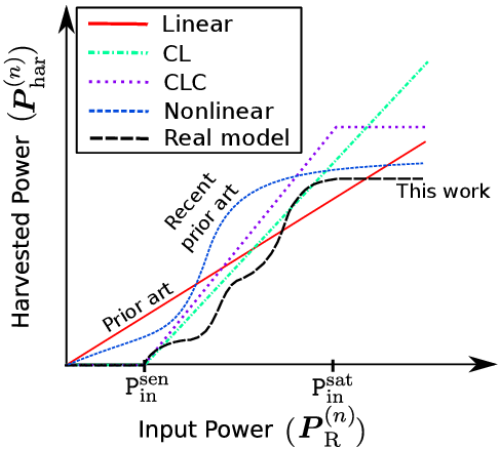


Figure 2.2: Comparison of analytical model for linear vs. nonlinear harvesting in [5]

consider that all the power received will be used for charging the battery since the harvester module introduces additional noise. Existing RF energy harvester modules are charactherized by sensitivity values, under which the harvester will not collect energy and limitations on the maximum power that is possible to harvest using the capacitors. As shown in Figure 2.2, typical linear models overestimate the nonlinear approaches, leading to errors in estimation. Linear-contained approaches, instead, correct these approaches introducing limitations but are still too far from the real devices. Boshkovka et al. [21] firstly considered the practical non-linear energy harvesting model. The proposed model includes a constant denoting the maximum harvested power from the receivers and constants related to the circuit specifications such as resistance and capacitance. An iterative algorithm has been used for solving a non-convex optimization problem with a sum-of-ratios objective function. Results confirm the mismatches between conventional linear EH model and non-linear EH circuits; which can clearly lead to huge problems. In [152] exploitation of the rate-energy region of SWIPT for MIMO broadcasting has been performed by considering both separated and co-located receivers for ID and EH. Results show a reduced region for non-linear EH with respect to the linear one, with a maximum harvested energy of 3.9mW; which completely modifies the behav-

ior of the splitting factor. More details on components are analyzed in [33], where a comparison between nonlinear saturation and nonlinear diode is presented. The saturation nonlinear model originated from the saturation of the output DC power beyond a certain input RF power due to the diode breakdown; while the nonlinear diode is characterized by the relation between the output DC power to the input signal through the diode current-voltage (I-V) characteristics.

Wang et al. [145] proposed a new approach to nonlinear energy harvesting considering multiple properties: (i) if the power harvested is smaller than the harvester's sensitivity threshold, there is no harvested power, (ii) the resulting function is a monotonically increasing function of power received, (iii) when the input power increase, the energy harvesting efficiency increase till a maximum value and then decreases, (iv) when the circuit is saturated, the harvested power will not increase. Such properties include different aspects of the proposed work in the literature, including saturation of the system and harvester sensitivity. The same authors compare this model to a linear one in [146], who emphasize that although linear and nonlinear models produce similar performance when the linear model is tuned with the right parameters, the nonlinear model consumes less power than the linear model when the received powers vary widely. As a result of these considerations and properties analyzed in [145], an interesting formula for including non-linear harvesting in designing a SWIPT-based analytical model is the following:

$$\Theta(h_{in}) = \max\left\{\frac{h_{max}}{e^{-\chi h_s+\iota}}\left(\frac{1+e^{-\chi h_s+\iota}}{1+e^{-\chi h_{in}+\iota}}-1\right),0\right\} \tag{2.1}$$

where $h_{max}$ is the maximum harvested power when the energy harvesting circuit is saturated, $h_s$ is the harvester's sensitivity threshold, which is the minimum amount of energy able to activate the harvesting process. Both $h_{max}$ and $h_s$ are expressed in terms of W. $\chi$ e $\iota$ are parameters that control the steepness of the function. In [5], a primary evaluation of the proposed approach in [145] has been presented by considering both TS and PS. Moreover, unlike the trend in commonly separated receivers, a region has been identified, where TS outperforms PS; anyway, experimental

results have been conducted on passive RFID tags, which are not properly the best user equipment.

### 2.1.3 *Interference*

Interference in SWIPT is a significant challenge that can impact the efficiency and reliability of the system. Considering the huge instability of channels, such as in the case of PS, where transmission of both power and data happens together, and the external interference produced by other devices or blocking objects; more effort must be spent to avoid and mitigate channel interference. Rayleigh fading is usually considered for modeling random variations in signal strength or amplitude that a radio wave experiences as it travels through a wireless communication channel. The inclusion of Rayleigh is required for correctly modeling the system, as reported in [73], a n analysis conducted on High-Power Amplifier (HPA) confirms that the presence of Rayleigh fading significantly reduces the information energy capacity region, which is an important metric for EE measurements. As in traditional networks, NonOrthogonal Multiple Access (NOMA) can be used to enhance the capacity of channels in the SWIPT context. As reported in [117] usage of NOMA in IoT relay systems can be crucial for enhancing the capacity of TS EH.

If by one side, Rayleigh is able to model the capacity of the channel coming from the signal by itself, the noise coming from the environment or thermal noise is another recurrent concern in wireless transmission of new generations of networks such as 5G and more in general the mmWave-based networks. It happens when an obstacle or an environmental condition obstacles the communication between two parties. Usage of directional beams changes the interference behavior, since narrow beams are vulnerable to blockages [102], a more accurate model for the noise modelization is needed. In the case of indoor context is usually caused by walls, while in smart cities context multiple objects can be considered as interferring. Typical approaches are based on the random generation of objects and on the computation of the probability of the presence of obstacles in the path from the transmitter to the receiver. Another study on blockage [112] confirms the benefit of introducing blockage in EE modelization considering the case of

PS, which can be leveraged for adjusting the PS parameter while satisfying outage constraints.

### 2.1.4 *Safety*

Maximum Permissible Exposure (MPE) and Specific Absorption Rate (SAR) are the metrics used for measuring the impact of RF on the human body. Experience Modification Rate (EMR) constraints have been considered as an additional constraint [36] [162] when designing the optimization problem for EE; results show that the inclusion of such a parameter increases the power consumed by the network while limiting the maximum harvesting of devices. SAR instead, defines the maximum level of absorbed power in a unit mass of human tissue, making it a more interesting metric than EMR [113]; with a limitation of 1.6 W/kg imposed by the Federal Communications Commission (FCC). The study provides optimal robust beamforming that complies with these limitations while considering EE challenges, extending what has been proposed in [163].

## 2.2 ANALYTICAL MODELS OF WIRELESS NETWORKS

Considering the expansion of SWIPT networks, and the huge number of paramters involved; the need for modeling tools is a priority. In addiction, the scarse hardware currently available for testing multiple configurations makes the simulations the only option to better understand those networks. Therefore, an important role is the one taken by the tools for modeling networks, including the stochastic geometry. This framework can be used for the computation of really simple scenarios, where only a snapshot of a stationary random model is taken and analyzed in terms of probabilities; or can be used in ergodic models for the computation of key dependencies of the network performance characteristics [14].

### 2.2.1 *Random Variables and Random Processes*

The usage of random variables for the representation of devices in a space is a relevant aspect, able to simulate the randomness of the devices distribution across an area. Before explaining two processes, interesting for the purpose of this thesis, some concepts on random variables and random processes is shared.

**Definition 2.1** (Random Variable)**.** Let $X$ be a random variable defined on a sample space $\Omega$. Then $X$ is a function that maps outcomes $\omega \in \Omega$ to real numbers $x \in \mathbb{R}$.

$$X : \Omega \to \mathbb{R}, X(\omega) = x \tag{2.2}$$

Random variables are important because it is possible to apply probability theory to numbers rather than abstract outcomes. This allows us to compute things like expected values, variances, and probabilities of events. What is fascinating from those kinds of variables is that they can be defined both over a discrete, and a continuous space. It is possible to define the expectation of a random variable $X$, denoted as $\mathbb{E}[X]$, as the average value we can expect over the number of repetition of the experiment. It is a weighted average of all possible values of $X$, where the weights are the probabilities.

**Definition 2.2** (Expectation of a Discrete Random Variable)**.** Let $X$ be a discrete random variable that takes values $x_1, x_2, ..., x_n$ with related probabilities $p_1, p_2, ..., p_n$ then the expectation of $X$ is defined as

$$\mathbb{E}[X] = \sum_i x_i p_i. \tag{2.3}$$

Similarly, if $X$ is distributed over a continuous space, it takes the name as continuous random variable, and its expectation is defined as the integral of its probability density function (pdf) $f_X(x)$ times the value it takes.

**Definition 2.3** (Expectation of a Continuous Random Variable)**.** Let $X$ be a continuous random variable with pdf $f_X(x)$ then the expectation of $X$ is defined as

$$\mathbb{E}[X] = \int_{-\infty}^{\infty} x f_X(x) dx. \tag{2.4}$$

According to those two definitions it is possible to get insights about the average value of a random variable, which can be any stochastic process we are interested in looking at. A random process is an extension of random variable over a space (*e.g.* time or area).

**Definition 2.4** (Random Process)**.** A random process (or stochastic process) is a collection of random variables indexed by a parameter: $\{X(t) : t \in T\}$, where $X(t)$ is a random variable and $T$ is the index set.

Also in this case, it is possible to refer to the expectation, as the average value the process takes over the defined space. Two key properties of a random process are:

- Stationarity: a process is defined stationary if its statistical properties do not change with time
- Ergodicity: a process is ergodic if time averages equal ensemble averages, which allows estimating statistics from a single realization.

Those two properties will be at the basis of the processes discussed in the following subsections, and allows us to derive closed-form expectations for those processes.

### 2.2.2 *Poisson Point Process (PPP)*

The Poisson Point Process (PPP) is a particular type of random process used to model points scattered randomly in space (or time). It generalizes the idea of a Poisson distribution from counts in one dimension to points distributed in continuous space. Formally, a PPP is a random collection of points $\{X_i\}$ in some space that satisfies two properties

1. Poisson counting property: for any bounded region $A$ of the space, the number of points in $A$ denoted by $N(A)$, follows a Poisson distribution:

$$P(N(A) = k) = \frac{(\lambda|A|)^k}{k!} e^{-\lambda|A|} \tag{2.5}$$

2. Independence of disjoint regions: if $A_1, A_2, ..., A_n$ are disjoint sets, then the random variables $N(A_1), N(A_2), ..., N(A_n)$ are independent.

A special case is the case of homogenous PPP, where the intensity of the process $\lambda$ is constant over all the disjoint regions. This lead to a closed form

$$\mathbb{E}[N(A)] = \int_A \lambda(x)dx = \lambda|A|. \tag{2.6}$$

Considering these results in the wireless networks brings interesting considerations and derivations which makes possible the analysis of a network. Let us consider the distribution $\phi$ can as a homogenous PPP in a given real space $\mathbb{R}$, with intensity measure $\lambda$, where $0 < \lambda < \infty$. In the first work within the application of PPP to the wireless networks [10], a cellular network model is composed of such a distribution $\Phi$ of intensity $\lambda$ in the Euclidean plane. What is particularly interesting when modeling a network, is the probability of being associated to the Base Station (BS) with the strongest SINR, where considering the closest one in the space is a good approximation. Therefore, a key quantity is the *empty space probability*, i.e., the probability that a ball of radius $r$ centered at the origin, $B(0, r)$, contains no points of the process:

$$P_0(r) = \mathbb{P}[N(B(0, r)) = 0] = e^{-\lambda\pi r^2}. \tag{2.7}$$

Equivalently, the complementary event corresponds to the situation where all the remaining BSs are located outside the ball of radius $r$. This means that no other BS lies inside the circle, and thus the device is associated with the BS located at the origin.

Using this result it is possible to get the Cumulative Distribution Function (CDF) of the closest BS as:

$$\begin{aligned} F_X(x) &= \mathbb{P}[R \leq r] \\ &= 1 - \mathbb{P}[R > r] \\ &= 1 - \mathbb{P}[N(B(0, r)) = 0] = 1 - e^{-\lambda\pi r^2}. \end{aligned} \tag{2.8}$$

Starting from this definition it is possible to compute the outage probability, which represents the complementary of the probability of receiving a SINR greater than T.

receiving a SINR higher than a fixed threshold T:

$$\begin{aligned} p_c(T,\lambda,\alpha) &= \mathbb{E}_r[\mathbb{P}[SINR > T|r]] \\ &= \int_{r>0} \mathbb{P}[SINR > T|r] f_r(r) dr \end{aligned} \tag{2.9}$$

Baccelli concludes the work in [10] with multiple considerations on the Fading, highlighting a general fading with noise using $\alpha = 4$, and general fading without noise with $\alpha > 2$. The work is a milestone for the downlink cellular network analysis, with possible applications in the C-RANs network composed of micro/pico and femtocells, where user distance and cell size are the most relevant parameters.

### 2.2.3 *Poisson Line Cox Process (PLCP)*

New generation of C-RANs are deployed considering the case of vehicles and high dense context, such as future smart city. These contexts pave the way for more interference generation, which is a perfect prerogative for the deployment of SWIPT networks.

Considering the mobility of vehicles, which are intended to travel on road; a different characterization of the random process must be considered. In fact, PPP put the basis for a completely random process, while when considering roads, a thinning of such a process must be taken into account. This aspect is covered by a different distribution, which takes the name of Poisson Line Cox Process (PLCP). First, a network of roads can be modeled as a stationary Poisson Line Process (PLP) $\Phi_l$ represented by a PPP $\Xi$ on the cylinder set $C = \mathbb{R} \times [0, \pi]$ with intensity $\lambda_l$.

To be more precise, each point of $\Xi$, say $(r, \theta)$, corresponds to a line in the Euclidean space specified by $\{(x, y) \in \mathbb{R}^2 | x cos\theta + y sin\theta = r\}$, where $r$ denotes the distance from the origin to the line and $\theta$ denotes the angle between the positive x-axis and the unit normal vector to the line. Conditionally on the PLP $\phi_l$, it is possible to define a stationary PPP $\psi_v$ with intensity $\mu$. This hierarchical process leads to a distribution of points $\Phi$ in $\mathbb{R}^2$ that

exhibits clustering along random lines, which is suitable to model systems such as roads and vehicles, or streets and base stations.

For the homogenous PLCP, the empty space probability, relevant for the computation of the closest BS, can be expressed as

$$P_0(r) = \exp\Big( -2\lambda_L \int_0^r \Big(1 - e^{-2\mu\sqrt{r^2-u^2}}\Big)\, du\Big), \tag{2.10}$$

where $\lambda_L$ is the line intensity and $\mu$ is the point intensity on each line. The integral accounts for the intersection of each random line with the ball $B(0, r)$ and the probability that no point of the one-dimensional PPP falls within this intersection.

As in the PPP case, the empty space probability can be directly related to the CDF of the nearest-neighbor distance:

$$\begin{aligned} F_R(r) &= \mathbb{P}[R \leq r] \\ &= 1 - P_0(r), \\ &= 1 - \exp\Big( -2\lambda_L \int_0^r \Big(1 - e^{-2\mu\sqrt{r^2-u^2}}\Big)\, du\Big), \end{aligned} \tag{2.11}$$

where $R$ denotes the distance from the origin to the closest point of the process.

Considering these results in wireless networks allows to capture scenarios where nodes are distributed along random lines, such as roads in vehicular networks or streets with linear infrastructure deployments. As depicted in Fig. 2.3, a special case of PLP, is the Manhattan PLP, which is characterized by a limitation on the possible value assumed, and is suitable for context where the displacement of lines is known in advance. In [28], the vehicles are considered activators of IoT devices and can be used for transmitting data. Each vehicle has a coverage risk of radius $r_c$ centered at the vehicle, while IoT devices are distributed according to PPP with a special intensity of $\lambda$. It is possible to consider all the coverage regions as the union of all the disks generated by the vehicle, expressing it as the union $\cup_{X_i \in \phi} B_{X_i}(r_c)$, where $B_x(r_c)$ is the disk of radius $r_c$ centered at $x$ and $X_i$ are the points representing the vehicles. More in particular, by considering the time and the changes in the location of vehicles, it is possible to determine the coverage region of time $t$ as the union of all the $B_{X_i}(r_c)$ where $X_i$ vary depending on the distribution of vehicles at time

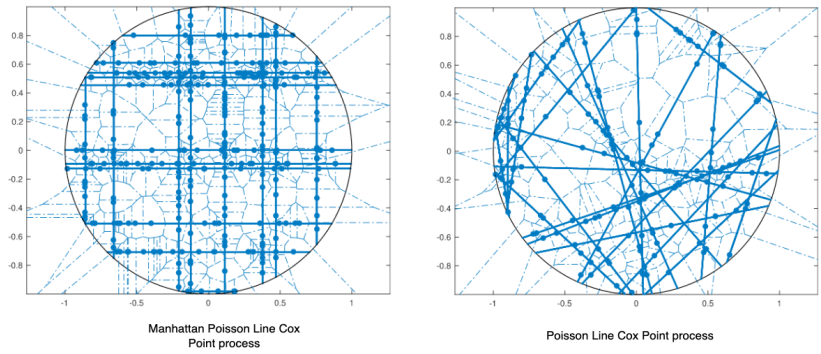


Figure 2.3: Manhattan PLP vs. Classical PLP [29]

$t$. Performance metrics can be computed similarly to the case of PPP by leveraging the formula defined in 2.9 and extending the approach to the Cox Line Point Porcess. The blocking interference can be easily modeled using stochastic geometry approaches, in [3] is considered indoor blocking characterized by walls. The authors modeled the source of power or more generally the BSs using PPP, while a Manatthan Poisson Line Process is used for modeling the walls. Considering the case of dense context, the results show an important impact of walls while there is no effect on the maximum achievable information rate by tuning the power splitting ratio.

Analysis of the literature underscores the widespread adoption of SG as a powerful tool for modeling and analyzing networks, particularly in wireless communication scenarios. Therefore, this creates a perfect tool for analyzing performance in SWIPT networks. In fact, this thesis aims to leverage SG-based approach tailored for SWIPT-enabled vehicular networks, to offers insights into performance metrics specific to these scenarios.

## 2.3 PERFORMANCE MODELING TOOLS

Once clarified the anaylitical tools for modeling the network itself, it is necessary to give a short introduction to the performance modeling tools which are mostly based on some concept introduced in the previous subsection. Beyond accurate network modeling, it is crucial to optimize the network from an individual

user's perspective, creating a so-called user-centric approach to network management.

Random processes can be applied to space for defining the position of users in the network, as well as to time to define the probability of generation of a data packet. In the following sections, an introduction on queue theory and Markov chains is given, as fundamental tools for modeling statistics from the user perspective. The relevance of those processes is mostly due to the randomness and to the charactheristics of the system, where batteries might be depicted as a Markov process.

### 2.3.1 *Queue Theory*

To begin the discussion on queue theory, let's consider a simple, yet insightful example. People reach the supermarket with a given intensity, which vary during the peak hours (e.g. at the end of the work day, or in weekend), and this causes the cashier to have more people waiting for paying. The fact of having ten people waiting for pay is function of various dynamics, where two of them are immediate: (1) the intensity of the arrival of people in the store, (2) the number and effectiveness of the cashier. Despite guessing how much people enter the store in a precise time is hard to compute; their average at the end of the day is a well-known data (see Section 2.2.1). Similarly, estimating the mean service time can be modeled as an alternative random process.

Queue theory study these interactions and give a fundamental tool for modeling queue dynamics, providing valuable insights into various metrics (e.g. financial, performance, network). At its core, as seen in the supermarket example, a queueing system can be characterized by three main components: the arrival process, the service process, and the queue discipline. The arrival process models how requests (or customers, packets, tasks) enter the system, while the service process models how requests leave the system. Those processes are often described as deterministic (when the source is known), or exponential (when the source is random) processes. The service mechanism specifies how servers handle requests, typically through exponentially distributed or general service times. The queue discipline defines the order in which requests are served, with common examples in-

cluding First-Come-First-Served (FCFS), Last-Come-First-Served (LCFS), and priority-based policies.

Standard notation for queueing models was introduced by Kendall, expressed in the form $A/S/c$, where $A$ denotes the interarrival distribution, $S$ the service-time distribution, and $c$ the number of servers.

For example, the M/M/1 queue represents a system with a single server, Markovian arrivals, and exponentially (Markovian) distributed service times. Despite its simplicity, this model yields fundamental performance measures such as average queue length, waiting time, and system utilization. Formula for deriving the average waiting time, and the number of user in the system are consequences of the distribution of random variables. In particular, rather than looking the system in one of the initial moment, it is possible to look the system in a *steady state*, in other words, the system not change or changes only slightly over time. This state is reached as time approaches to $\infty$. This state is important because through this assumption one can predict the system performance and having (or not) stability. Let's consider a system composed of one server, with $\lambda$ users coming at each second, Poisson distributed, and $\mu$ representing the reciprocal of the service time per each user, exponential distribued. It is possible to define the traffic intensity (or utilization) as:

$$\rho = \frac{\lambda}{\mu} \tag{2.12}$$

An important condition to analyze the queue is the *stability*. A system is stable if and only if its utilization is below 1 (e.g. $\rho < 1$). In fact, if this is not the case, the arrivals exceed the service capacity, and the queue grows without any bound. A central focus of queueing theory is the derivation of performance metrics that quantify system efficiency and user experience. These include average waiting time, average number of customers in the system, probability of delay, and system throughput.In a M/M/1 stable queue, a set of known results, known under the name of Little's Law can be applied.

- Long-term average number of users in the system

$$L = \lambda W \tag{2.13}$$

- Average Waiting Time

$$W = \frac{1}{\mu - \lambda} \tag{2.14}$$

- Average Waiting Time in Queue

$$W_q = \frac{W}{\mu} \tag{2.15}$$

Queueing theory also accounts for cases where arrivals follow distributions other than the Poisson process, or for scenarios with preemptive queues, in which a low-priority task may be interrupted by a high-priority one. Another important model is the tandem queue, which represents a sequence of service stages that customers or tasks must pass through in order. For the purposes of this thesis, however, a fundamental understanding of what a queue is and how the associated processes work will be sufficient.

In the context of SWIPT networks, queue theory can be particularly useful for representing both the energy harvesting process and the information freshness analysis at the nodes. Specifically, IoT devices in such networks can only transmit data packets if sufficient energy is available at the time of transmission or when a packet is generated, creating a dependence between the arrival process and the energy consumption process, which is function of the service rate (as expected, a device consume more if it needs to transmit for a longer time).

Nevertheless, queueing theory alone is not sufficient to capture certain processes, such as the dynamics of a battery. An IoT device, for instance, cannot keep harvesting energy once the battery is fully charged, nor can it transmit when the stored energy is below a required threshold. In addition, each transmission resets the energy queue to zero, which makes it difficult to model the system using standard formulations such as M/M/1 or according to well-known distributions. The next subsection introduces a powerful mathematical framework for accurately modeling such cases.

### 2.3.2 *Markov Chains*

Markov Chains are a useful framework to models the status of a system and the evolution over the time. What is most interesting of these chains is their memory-less property (or Markov property). In fact, each event depends only on the state immediately before it, not on the full history of past states.

**Definition 2.5.** A Markov chain is a stochastic process $\{X_t\}_{t\geq 0}$ defined on a countable state space $S = \{s_1, s_2, \dots\}$, such that for all $t \geq 0$ and all states $i, j \in S$:

$$\mathbb{P}(X_{t+1} = j \mid X_t = i, X_{t-1} = i_{t-1}, \dots, X_0 = i_0) = \mathbb{P}(X_{t+1} = j \mid X_t = i) = P_{ij}.$$

The matrix $P = [P_{ij}]$ is called the *transition matrix*, where

$$P_{ij} = \mathbb{P}(X_{t+1} = j \mid X_t = i), \qquad \sum_{j\in S} P_{ij} = 1 \quad \forall i \in S.$$

The distribution of the initial state is given by a vector $\pi^{(0)}$, where

$$\pi_i^{(0)} = \mathbb{P}(X_0 = i).$$

The distribution at time $t$ evolves as

$$\pi^{(t)} = \pi^{(0)} P^t.$$

To put Markov Chains in relation with queue theory, let's consider the birth-death process. It is a special class of continuous-time Markov chains that describes systems in which the state variable evolves through increments (*e.g. births*) or decrements (*e.g. deaths*) of one unit at a time; similarly to what happens in queue theory. The states are usually represented as non-negative integers, where state $n$ corresponds to having $n$ entities in the system. In fact, transitions occur only between neighboring states: from $n$ to $n + 1$ with rate $\lambda$ (birth rate), and from $n + 1$ to $n$ with rate $\mu$ (death rate).

It is worth noting that Markov chains can be defined both in discrete time (DTMC) and in continuous time (CTMC). In the

discrete-time case, the system evolves at fixed time steps according to the transition matrix $P$, while continuous-time chains are governed by a *generator matrix* $Q = [q_{ij}]$, where

$$q_{ij} = \lim_{\Delta t \to 0} \frac{\mathbb{P}(X_{t+\Delta t} = j \mid X_t = i)}{\Delta t}, \quad i \neq j,$$

and $q_{ii} = -\sum_{j \neq i} q_{ij}$. The generator matrix characterizes the Kolmogorov forward equations, which describe the temporal evolution of the probability distribution.

An important property of Markov chains is the existence of a *stationary distribution* $\pi$, which satisfies

$$\pi = \pi P, \qquad \sum_{i \in S} \pi_i = 1.$$

If the chain is irreducible and positive recurrent, such a distribution is unique and represents the long-term behavior of the system, regardless of the initial state. In queueing systems or in energy harvesting models, this allows to compute meaningful steady-state performance metrics, such as the average queue length, the probability that the battery is empty, or the expected Age of Information (AoI).

While frequent queueing models, such as the M/M/1 and M/M/c queues, can be expressed as birth-death processes, where the *births* represent arrivals and the *deaths* represent service completions; representing an example of continuous-time Markov chain, many systems require more general models. In particular, when modeling the dynamics of a finite-capacity battery, transitions may occur between non-adjacent states. For example, an energy arrival event could increase the battery level by multiple units, leading to a jump from state $i$ to state $i + k$. These processes extend the birth—death paradigm and are often referred to as *generalized birth—death processes* or *skip-free chains*.

As a simple illustrative example, consider a device with battery capacity $B$, whose Markov chain is represented in Fig. 2.4. At each slot, the device harvests one energy unit with probability $\lambda$, and consumes one unit with probability $\mu$. The system can be modeled as a Markov chain with states $S = \{0, 1, \dots, B\}$, where transitions occur according to the harvesting and consumption probabilities. The stationary distribution of this chain provides

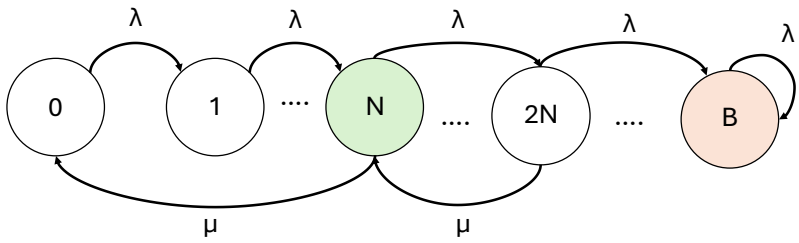


Figure 2.4: Battery Markov chain with non-adjacent transitions. Rates $\lambda$ (harvest jumps) and $\mu$ (consumption jumps) illustrate generalized dynamics.

the long-term probability that the device is in each energy state, and thus the likelihood of being able to transmit at a given time.

# 3 STATE OF THE ART

Chapter 2 discussed the theoretical background. Buildings on this knowledge, this chapter provides a comprehensive overview of the most relevant approaches and findings in the literature. It also aims to identify open challenges and research gaps that better motivate the contributions of this thesis. Section 3.1 surveys analytical framework used for network modeling, including typical deployment strategies and optimal configurations. Section 3.2 focuses on NextGen enablers for SWIPT network, with a concrete discussion on which elements might contribute to the enhancement of the harvesting process, and which characteristics cannot be leveraged. Finally, Section 3.3 reviews device-side protocols for energy efficiency, splitting the discussion between the time-sensitive applications (*e.g. information freshness*) and non-critical ones (*e.g. load shifting*).

## 3.1 SYSTEM-LEVEL TRADE-OFFS IN SWIPT NETWORKS

Spatial structure of the surrounding environment is a fundamental aspect when deploying a network. It typically requires that the BSs are placed following the best strategies to maximize the QoS perceived by the UEs, while reducing the energy consumption for covering the network. In traditional networks, this problem is associated with the maximization of the capacity achieved by the average worst case user [96], or the max-avg, corresponding to the maximum capacity achieved by the average (typical) user [11], under minimization of network resources.

This problem, already hard by nature, cannot be directly applied to SWIPT, since networks features differs due to device-side energy constraints. In fact, as an example, the max-min problem needs to take into account the worst case user from the energy perspective, which might be different from the one considered in a traditional network. As a consequence, the design of the network and end-user capabilities, need to take into account also aspects

that may influence the energy harvesting process; such as antenna design and power consumption, among the others.

### 3.1.1 *Deployment Strategies and Configurations*

Initial works on energy efficiency in SWIPT networks considered scenarios composed of a BS and non-EH UEs with several remote radio heads, and a population of EH devices. These works aim to optimize the system configuration in terms of energy efficiency [60, 90, 169]. Among these, [169] characterizes the data rate vs. energy trade-off in a single SWIPT BS scenario. For the same setting, [60] proposes an approach for optimizing transmit power allocation to each user. [90] elaborates a Markov chain model to derive the joint power and connectivity outage probability. [140] investigates strategies for transmit-power-efficient resource allocation. All of these works provide a first insight into the basic performance patterns of a SWIPT system. However, they are based on single BS configurations, which are not representative of the average performance of a whole SWIPT network, and they do not account for the impact of the statistics of BS and user distribution. In particular, they lack accurate modelling of the effects of co-channel interference and passive RF power transfer from BSs other than the serving one, as well as from users associated with them.

To represent the SWIPT network as a whole, therefore considering the effects of the distribution of devices, results from a network operator point of view might be considered (e.g. those focusing on a given set of BS and a given spatial layout of BS and of users). Interesting energy-optimal configurations, for networks with CoMP [137], in NOMA networks [135], in full duplex settings [160], as well as in scenarios with two-way relays [81] have been already investigated in the literature. Among these, [89] considered the specific case of IoT device and proposes an algorithm to minimize the total energy consumption of a set of BSs able to deliver both energy and data to a population of EH device, over sub-carrier and transmit power allocation. However, the strategies proposed in these works focus on deriving the optimal configuration for a sample BS deployment, with a specific layout and with a given user spatial distribution. Being tied to a

specific setup, they do not allow drawing general considerations on the overall potential of these schemes for energy-saving.

To overcome those limitations, I will introduce in the next subsection a series of work focusing on Stochastic Geometry (SG), which can be a really useful tool in this context.

### 3.1.2 *Stochastic Geometry Approaches*

Recently, SG [13, 31, 43, 79] has emerged as an effective modelling approach for a stochastic characterization of the performance patterns in a wireless network. SG allows focusing on the average behavior of the system over many realization of the process of UE and BS spatial distributions.

In [82], considerations on macro cell demonstrate the PPP is not usable in the context where BSs are deployed close to each other and possible usage of the Determinantal Point Process (DPP) can be leveraged. Anyway, new generation C-RAN leveraging micro, pico, and femtocells enables the analysis of those network using the SG.

To this end, reuse of spectrum near the cells is usually deployed in terrestrial wireless networks; where Area Spectral Efficiency (ASE) can be defined as the sum of the maximum data rate per unit area per unit bandwidth [7]. AlAmmouri et al. [4] considered the case of ASE within the context of ultra-dense context deployed according to PPP, trying to understand the scalability of ASE starting from the Shannon rate definition. Results show that the average ASE saturates to a constant when the BS density is large, while constrained ASE and the average potential throughput both collapse to zero. These insights confirm the poor relevance of ASE in really dense contexts, which are those subjects of our research.

Shadowing is another concern of wireless communication and must be taken into consideration when deploying wireless networks; the presence of obstacles or usage of high-level frequency can lead to blocking communications. In an analysis conducted in [80], two PPP-based networks have been considered: in the first one the nodes are in the same cell of some random shadowing tesselation (spatially correlation); while in the second the nodes share a common point in some cluster process which share

the same shadow (independent shadowing). Simulation results show that coverage probability under correlated shadowing is higher than in independent cases, leading to a pessimistic evaluation of coverage probability when ignoring the spatial correlations of shadowing.

The shadowing can be reduced by considering the Line-of-Sight (LOS), which increases the availability of the network. In [75], the LOS probability is evaluated in urban microcells, characteristics of new generation urban C-RANs. By using PPP it is possible to model the shadowing produced by urban objects such as pedestrians, trees, or buildings; results show that shadowing objects rather than buildings can have a huge effect on LOS probability.

In SWIPT networks, SG has been used to characterize several performance aspects, such as the data rate vs. energy trade-off [43], or the optimization of the D2D successful transmission rate [31]. In [106], a multi-tier heterogeneous downlink network has been discussed. The authors used PPP to analyze two-tier BSs distribution, and to study the outage probability associated with such a scenario. Results show the analytical tractability of the problem, and the exact approximation offered by PPP. In [78], the authors modeled a MIMO SWIPT network with Access Points (APs) modeled according to a homogeneous PPP. Also in this case the research outlined the impact of the transmission power and the analysis of the outage probability. In [2], the authors used SG to models the randomness of the energy arrival process, highlighting the power of this tool also in analyzing the harvested power. On the same path, [83] leveraged PPP to model the energy received by cluster of devices randomly distributed in the space, characterizing the energy allocation algorithm as function of the BS downlink process. Finally, [141] evaluated a SWIPT-enabled cellular network, with BSs and UEs distributed according to two different PPP and modeling the path-loss and PS harvesting protocol. Preliminary results show the effect of user density on the ASE and outage probability.

### 3.1.3 *Research Gaps*

The discussed work provide a strong background for validating the usage of PPP in SWIPT networks, both for the charachteri-

zation of energy, and performance. Still, these works, often for the sake of analytical tractability, do not account for the effects of resource allocation and scheduling among users ( *e.g. the statistics of the sharing of BS time across all associated users*) which are key metrics for accurate stochastic modelling SWIPT networks. Thus, they leave ample room for investigating the more general problem of identifying the most effective QoS-aware dimensioning and tuning strategies to achieve system-level energy proportionality in a SWIPT network, as a function of the main system parameters. Crucially, however, none of these results account for the effects of resource scheduling among users on user-perceived performance, nor do they address the key issue of characterizing energy-optimal strategies for QoS-aware (for both power and information delivery) dynamic network provisioning, as a function of traffic and energy demand. Therefore, it is still unclear what is the actual potential for energy efficiency of strategies which dynamically tune the configuration of SWIPT networks, and what is the impact of optimizing the main system parameters on the energy consumed by IoT users and BSs.

With RQ1, this thesis aims to address these issues by proposing two SG modeling frameworks which captures the relationship between energy consumption, user-perceived performance, and the main system parameters in SWIPT cellular networks. The frameworks allow characterizing in a scenario-independent manner the potential for QoS-aware energy efficiency in these networks, as well as the main trade-offs between user-perceived performance in the communication and power delivery services, resource utilization, and overall energy consumption of the network. In doing so, this thesis aim to give an initial characterization of the performance-energy tradeoffs in SWIPT cellular networks, providing the instruments for evaluating the impact of UE population density and QoS targets on the sum of the energy consumption of the network.

## 3.2 NEXT-GENERATION COMMUNICATION ENABLERS FOR SWIPT NETWORKS

NextGen networks are paving the way for faster connectivity, reduced latency and continuous data transmission. Under this scenario, SWIPT networks can surely benefit of the novel features introduced by those networks. As outlined in Section 2.1, the harvester sensitivity of SWIPT networks is an important aspect to take into account, and those features can speed up the overall harvesting process. While modeling the network geometry is an important part of the analysis, another huge impact is taken by the modelization of BSs features. To begin with the optimization of a particular feature, this section gives a complete overview of the most interesting features and respective limitations in the context of NextGen enablers for SWIPT networks.

### 3.2.1 *Antenna Directivity and Array-Based Energy Focusing*

As introduced in [25], path loss in energy-aware networks becomes more significant than in traditional networks, mainly because the energy impact is directly proportional to the distance, rather than following a logarithmic relationship, as in the data receiving. To this end, the authors proposed the use of large-scale MIMO, and the results show that this approach can effectively overcome path loss in long-distance WPT, achieving satisfactory energy harvesting performance despite the increased distance. Numerical results highlight the significant performance gains and antenna-scaling benefits, emphasizing the importance of directional transmission. The problem of spatial switching has been considered in [136] including the multiple antenna at the receiver side. This approach characterizes the best configuration for the receiver, highlighting how the distance keep impacting in logarithmic way the energy harvesting process. Results also show the saturation of circuit when the number of receiver antenna is too high ($> 8$); making antenna design a complex choice that must take into account harvester saturation. The criticality of this approach and the one discussed in [155] is the presence of multiple antenna on the devices side, making it not practical for IoT devices, and in general, on devices with not enough space on the board.

Focusing on single-antenna receivers, [153] evaluated the problem of antenna directivity and power allocation for each element

of the MISO antenna. Their results show the logarithmic deterioration of harvested energy with respect to the SINR constraint, making it equivalent to the data downlink. Despite providing useful insights, both works focused on characterizing the power harvested by the devices, without considering other benefits coming from equipping BS with multiple antennae. As outlined [54], through the usage of interference management mechanisms, 5G networks presents opportunities to exploit the spatial diversity gains in enhancing system performances through collaboration between network nodes. In fact, antennae while transmitting to a destination might be leveraged to harvest the energy by all the other nodes under the coverage area of that signal. This is mostly possible through algorithms which takes into account the location of end-devices, and deliver power accordingly.

### 3.2.2 *Spatial Scheduling*

The spatial scheduling is the ability of the BS to schedule users on the basis of their position, with the aim of optimizing a given network performance. Han et al. [53] considered the problem of finding the minimum path energy efficiency cost, putting it in relationship with the routing policy, that can be approached with Djikstra algorithm. Results demonstrate the importance of selecting the best path for delivering energy to a node, and this path can be expressed through a graph with devices representing the nodes. Along the same path, [138] defined a power allocation problem with a two-step optimization problem, seeking to firstly optimize the location of antennae and then defining the optimal energy allocation strategy considering the user locations. Their analysis demonstrates that this is a quasi-concave function, leading to a NP-hard problem. Zhang et al. [166] investigated a mixed near- and far-field channels. In this case, the authors demonstrate that in a scenario where Information Decoding (ID) devices are placed further away with respect to the EH devices it is possible to enhance the energy efficiency of the network. In fact, results underline the capacity of the latter benefit from the channel transmission to the first. Clearly, this is only possible in a network which enable directional antenna, to accomplish the coverage of far away users. However, in realistic settings, devices might

be very distant from the antenna, therefore making the findings of [166] not valid. Problem of spatial scheduling are typically reduced to set coverage problem, known to be NP-hard. Approximation algorithms for this problem have been proposed in the literature, but none of them directly approach the case of SWIPT networks.

### 3.2.3 *Research Gaps*

Antenna directivity, spatial scheduling and dynamic beam management are all key enablers for SWIPT networks, as they enable efficient power delivery to distant users and improve overall network coverage. However, several aspects have not been properly addressed. The adoption of low-power communication protocols, such as NB-IoT, is essential to ensure that these approaches remain realistic, therefore excluding all the mmWave-based approaches. Non-linear characteristics of harvester, including both sensitivity and saturation thresholds, must be taken into account when designing the energy harvesting function. Results indicate that beam definitions should depend on the spatial distribution of devices within the network, and maximizing these configurations as a function of user positions becomes a key design objective. Generally, spatial scheduling problems in SWIPT networks are often abstracted as set coverage problems, which are well-known to be NP-hard. While several approximation algorithms exist for generic set coverage formulations, few directly address the specific constraints and objectives unique to SWIPT-enabled communication networks. This indicates a gap in current research and opens the door for developing tailored heuristics and approximation strategies that incorporate spatial energy efficiency considerations. In particular, RQ2 will investigate the interrelation between spatial scheduling, antenna directivity, and user distribution. The aim is to develop a concrete strategy that dynamically defines antenna directivity as a function of user location, thereby maximizing energy and information transmission efficiency in NextGen SWIPT-enabled networks. To this end, the proposed framework will integrate a dynamic programming approach to solve the spatial scheduling problem. This method will capture the combinatorial complexity inherent in user positioning, directional beam-

forming, and energy allocation, offering insight into the computational and structural challenges of operating such networks in real-time conditions.

## 3.3 DEVICE-SIDE OPTIMIZATION POLICIES

The previous sections discussed communication enablers for SWIPT networks from the network perspective. Equally critical, however, are the strategies adopted by end-devices to conserve energy and enhance QoS. In conventional networks, such strategies are typically driven by policies that restrict channel access to reduce interference. In SWIPT systems, by contrast, they are primarily driven by energy considerations. While higher cell occupancy can support device powering, it also increases waiting times. This section reviews research in two key areas: energy harvesting protocols and load shifting. Although distinct, these approaches represent complementary strategies for optimizing device access with respect to both energy availability and data demand. On the one hand, information freshness requires more frequent updates, which is a characteristic of real-time systems; on the other hand, load shifting offers a suitable alternative for non-critical systems, where IoT devices can delay transmissions to more convenient moments.

### 3.3.1 *Information Freshness Strategies*

It is clear that when a device wants to transmit data, it must hold enough energy for supporting the transmission; therefore creating a trade-off between achievable throughput and energy harvested, but it is not clear weather the impact of transmission leveraging more power can enhance the probability of successful packets delivery. As a matter of fact, the first requirement for a EH protocol is the guarantee of holding enough energy for the transmission, but depending on the final objective different approaches arises.

For this purpose, a metric that investigates this problem is the Age of Information (AoI), tied to the intra-update time. AoI has emerged as a performance metric in communication networks where data freshness is essential, such as in real-time monitor-

ing, UAV-based communication [61, 165] and autonomous systems [42]. For the problem of EH trade-off, AoI is a relevant metric due to the measure of timeliness, while taking into account the energy consumption. Moreover, in EH-enabled networks, the stochastic nature of energy arrivals introduces intricate dynamics that significantly affect the AoI [27].

Two widely known protocols affecting the AoI are presented in [107]: *Transmit Without Waiting* (*TWW*) and *Wait Until Charged* (*WUC*). Under the TWW policy, transmission occurs immediately once there is sufficient power, whereas the WUC policy requires the user to accumulate enough energy before transmission begins. This simple, yet powerful, tradeoff determines an interesting metric which guides the need of timely information delivery in EH-enabled networks. Since energy availability is inherently intermittent, devices must balance the time devoted to harvesting energy with the need to transmit data. This balance creates a fundamental design challenge: strategies that maximize transmission opportunities may quickly exhaust available resources.

Several works have analyzed AoI in communication networks, often relying on queueing-theoretic models to characterize its behavior under different configurations. Perera et al. [107] demonstrated that higher transmission power and shorter packet sizes can improve the long-time average AoI in RF-powered networks. Basnayaka et al. [17] examined a decode-and-forward two-way relay system with EH assistance, contrasting two different approaches. Their analysis revealed an important aspect: reducing block length decreases latency but does not guarantee better intra-transmission performance, particularly in low-SINR regimes where rapid transmissions may still deliver outdated or less reliable information.

Therefore an interesting fact is that transmitting with less power is not always the best choice for information freshness. In fact, despite considering always the same packet length, if this packet is delivered using a reduced power it affects the final decoding of the packet itself. This aspect has been further investigated in [55], where a multi-agent deep reinforcement learning framework for resource allocation in RF-powered NOMA cognitive radio networks is presented, jointly optimizing information timeliness and energy sustainability. Similarly, in [56, 87] resource scheduling algorithms for optimizing information timeliness have been pro-

posed. As highlighted in [91], queue theory serves as a powerful framework capable of providing precise statistical insights into the performance of such SWIPT networks, offering essential tools for evaluating network dynamics under various operational policies.

AoI evaluation through the usage of SG has been proposed in [161], where a characterization of the optimization of AoI for bipolar and cellular network has been investigates.

In [37, 38], the complementary problem is addressed. Specifically, the authors investigate the Peak Age of Information (PAoI) in the context of data downlink, always leveraging the SG characterization of the network. They analyze the scenario in which a packet cannot be successfully decoded if the receiver lacks sufficient energy, and accordingly, they characterize an optimization framework for this metric in the downlink process. Their results highlight the importance of jointly optimizing both energy availability and data transmission in order to minimize the downlink time and achieve optimal performance.

Underlying energy dynamics of EH nodes remain largely underexplored. Some progress has been made in [35] and [15] incorporated queuing dynamics into their analyses, but these efforts did not extend to heterogeneous settings. More recently, Zhao et al. [167] investigated AoI performance under different battery capacities and packet lengths, offering useful insights but still within relatively homogeneous environments.

Subsequent works have broadened the scope, such as the stochastic packet-generation modeling in [69] and the integration of EH considerations into AoI evaluations in [167]. Nonetheless, a critical gap persists: the absence of comprehensive models that capture the full dynamics of heterogeneous networks—scenarios that closely reflect practical deployments.

### 3.3.2 *Energy Efficient Strategies*

While critical systems such as industrial automation or medical monitoring applications must minimize the AoI to guarantee strict QoS requirements, there exist other classes of systems where timing is not the main concern [65]. In massive IoT deployments, for instance, the paradigms shift: what matters is not necessarily

the real-time data delivery but rather the long-term sustainability of devices with limited resources [51]. Applications such as smart metering, or environmental sensing can tolerate moderate transmission delays without significantly affecting the reliability of the service. In these contexts, the main priorities become the energy budget of battery-powered devices and the tight memory constraints imposed by low-cost hardware. Consequently, strategies such as energy-aware scheduling, adaptive duty cycling, and task offloading to more capable nodes are far more relevant than minimizing AoI [8].

Unlike traditional WSN, where more users typically demand more BS resources, and strategies aim to reduce the interference, SWIPT networks exhibit a counterintuitive trend: within specific user density ranges, the optimal number of active BSs, and consequently, energy consumption, decreases as user density increases [150]. Clearly, this is only possible in scenario where data transmission might be retarded to favorable network conditions. The concept of load shifting is the most immediate in achieving this task, and while this apporach has been successfully applied in computational energy management [120], its application to transmission scheduling in SWIPT remains underexplored. If passive charging from user transmissions can be efficiently leveraged—and considering that higher transmission activity may reduce energy costs at certain densities, there is significant potential to reduce total network energy consumption [159].

The problem of defining a greedy approach to load shifting strongly depends by the aim. As outlined in [24], the opportunistic scheduling in wireless network, and in particular in WSN [115], need to reduce the scheduling of devices which do not hold any data to transmit, or as in the case of SWIPT, no not hold enough energy to support the transmission. Load shifting, opportunistic scheduling and demand-side management are well-established concepts [148] in traditional networks. [144, 170] evaluated the impact of sending packets of different size through multiple channels to maximize the system throughput, and designing optimal policy for downlink channel, respectively.

Greedy approaches to load shifting in SWIPT need to take into account the interference generated in the system, to use it as a source for the energy harvesting to support the transmission. The

concept of interference alignment has been investigated in [118, 168], where an opportunistic scheduling which takes advantage of other devices transmission has been presented, both in traditional, and in MIMO scenario. Anyway they misses a clear impact of the system user density on the transmission capabilities, since they only evaluate the energy collected by those devices.

For example, [151] addressed joint scheduling and power control for offloading delay-tolerant traffic in dual-connectivity networks, showing significant energy savings through coordinated decisions. [133] advances policy-driven load balancing and traffic steering in O-RAN, leveraging two-tiered optimization to meet diverse traffic demands while reducing handovers and resource waste. [77] shows that adaptive on/off switching and data shift strategies can reduce macro BS power usage by up to 30% per hour, especially for delay-tolerant services.

### 3.3.3 *Research Gaps*

Both in the case of critical context, the usage of optimal AoI policies, can directly lead to the best achievable policy; but a relevant gap exist in the characterization of this performance metric in SWIPT HetNet. In fact, those networks have distinct service requirements and energy profiles coexist and interfere with one another, leading to nontrivial interactions.

Complementary, strategies used in non-critical context such as load shifting and opportunistic scheduling have been extensively studied in traditional wireless networks, but their adaptation to SWIPT scenarios introduces new trade-offs between user density, interference, and energy harvesting. This gap motivates the development of density-aware scheduling strategies, which will be addressed in the following section.

In the first case, transmission of non-EH devices might deteriorate the successful delivery of packets at EH node; and excessive aggressive update at EH devices might decrease the quality of delivered packets, incurring into decoding errors.

In the second case, the defintion of a load shifting protocol is not trivial, because of the interference existing in the network. In fact, differently from traditional network it might be the case that

devices prefer to transmit when other devices exist in the network thanks to the energy harvesting mechanisms put in place.

In both cases, the current literature does not consider the heterogeneous scenario, as a relevant one, but limit its research to single-class scenario, which does not give enough insights about HetNet. To capture these dynamics, this thesis introduces two different optimization frameworks characterizing the problem of AoI and load shifting in HetNet, respectively.

These approaches are further motivated by the realistic coexistence of EH and non-EH devices in modern infrastructures, where such heterogeneous interactions are increasingly. Central to this differentiation is the diversity in IoT device behavior, broadly categorized as always-active (e.g., continuous sensors) and event-driven (e.g., activity-triggered sensors) devices. While both sense and compute, not all their tasks are time-sensitive. For example, transmitting historical logs or update on non-sensitive context can be postponed to energy-favorable periods without affecting performance. This aligns with DSM principles: shifting non-urgent tasks to periods with lower energy costs or higher passive energy availability; while guarantee a low AoI for critical context. Through intelligent scheduling and load shifting, SWIPT networks can realize substantial EE gains, reinforcing their potential as a sustainable and cost-effective foundation for 6G communication systems.

# Part II

# APPROACHES FOR DESIGN AND OPTIMIZATION OF SWIPT-ENABLED HETEROGENEOUS NETWORKS

This part presents the methodological framework developed to address the defined research questions. Each chapter is dedicated to a specific research question, detailing the network models, analytical characterization, and related optimization problems. The objective is to provide concrete frameworks for answering the research questions posed and to investigate the role of heterogeneous SWIPT network parameters and their impact on system performance.

# 4 SYSTEM-LEVEL DESIGN OF SWIPT HETNETS

This chapter introduces both the system modeling and work conducted on these modeling to obtain interesting insights about the main network parameters. The discussion is divided into two distinct works: the first one consider a generic device layout, random distributed across an area, while the second one introduce a more realistic system, where BSs are distributed along lines, which might represents the street in a city. This separation has been made to investigate the role of system parameters, and how they fundamentally change between two different system models.

## 4.1 PLANAR DEPLOYMENT MODEL

The first contribution of this thesis regards the definition of an analytical framework for characterizing SWIPT networks. As introduced below, this is needed to evaluate the performance of SWIPT network under randomness of user distribution.

### 4.1.1 *Problem Statement and Motivation*

The advent of real-time IoT applications has impacted the energy consumption of those devices, and as consequences the energy requested to Radio Access Networks (RAN) [116] operators. Another interesting behavior in this network is the exponential increase in the number of connected devices and in the amount of data generated and exchanged[111]. Section 2.1.3 introduced the concept of harvesting from interference, and broadband devices are one of the greatest contribution in producing interference in a cellular network.

This impact is further amplified when the cellular network does not only deliver connectivity to all its users but also power to IoT devices.

To better understand the impact of interference, this work considers scenarios in which IoT devices harvest RF energy from the environment (*passive energy harvesting* - EH) as well as from the signal transmitted by their serving base station (*active EH*) [127]. Such configurations are interesting as they allow for overcoming the power budget constraints that limit the potential of battery-operated IoT devices in many application domains. Indeed, these limitations often imply tight constraints on the amount of sensing, computing, and actuation that IoT devices can perform, negatively affecting their availability.

As discussed in Section 3.1.2, a tool for representing User Equipments (UEs) random position in the network is the SG, which allows focusing on the average behavior of the system over many realizations of the process of UEs and BS spatial distributions, making it possible to analyze the trade-offs between different potential objectives such as maximizing coverage, maximizing throughput, and maximizing energy harvesting, in ways that would otherwise be very difficult or way less accurate.

As the system performance will be mostly driven by the interference this contribution explicitly seek to give an answer to which is the impact of interference in those HetNet. The framework allows characterizing in a scenario-independent manner the potential for QoS-aware energy efficiency in these networks, as well as the main trade-offs between user-perceived performance in the communication and power delivery services, resource utilization, and overall energy consumption of the network. A concise list of contributions is as follows:

- Derivation of a set of analytical results for the key statistics of the main performance indicators of a SWIPT network, which account for resource scheduling among broadband and IoT EH users, and allow modeling the impact of the main system parameters on network energy consumption;

- Formulating an optimization problem to determine the potential energy savings achievable by tuning the main network parameters while guaranteeing a target user-perceived performance for both information transfer (in downlink and uplink) and wireless power delivery.

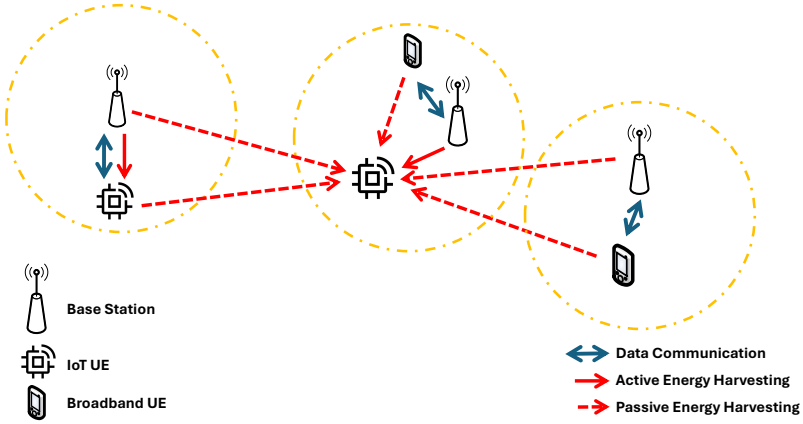


Figure 4.1: Outline of the system model for the SWIPT wireless network considered in this work.

- Proposing a Genetic Algorithm (GA) approach to derive energy-efficient SWIPT network configurations which achieve the target QoS levels;
- Numerical validation of the proposed approach, shedding light on several aspects of the tradeoff between user-perceived performance and resource efficiency in a SWIPT network. Our analysis allows observing some unexpected and rather surprising effects such as, in some cases, a decrease in the optimal density of BSs required to serve an increasingly dense population of UEs, and the irrelevance of active power delivery for very dense populations of IoT devices.

### 4.1.2 *Methodological Approach*

I assume that BSs are distributed in space according to a homogeneous planar PPP with a density equal to $\lambda_b$ BSs per $km^2$. UEs are distributed in space according to a different homogeneous PPP with an intensity equal to $\lambda_u$ UEs per $km^2$. UEs are either broadband (BB) terminals, or IoT devices. I assume the latter are a fraction $\gamma$ of the total number of UEs.

As depicted in Fig. 4.1, I considered the case in which IoT devices harvest the energy necessary for their own operation, while BB users don't. To this end, each IoT device is equipped with two separate receivers, one for information and another for energy, and it is capable of exploiting downlink signals for decoding its intended information, as well as downlink and uplink signals from both BSs and UEs for charging its battery. The receiver operating modes considered are [100]:

- **Time Switching (TS)**, by which a fraction $\eta$ (the *time switch ratio*, with $0 \leq \eta \leq 1$) of the time dedicated by a BS to serve an associated IoT device in downlink is devoted to active power transfer, i.e., it is used by the UE for harvesting energy from the signal received from the BS. The rest of that time is used for receiving information.

- **Static Power Splitting (SPS)**. In this operating mode, the receiver antenna at every IoT device is followed by a splitter, which sends a fraction $\nu$ (the *power split ratio*, with $0 \leq \nu \leq 1$) of the total signal power received at any time instant to the RF harvesting electronics. The rest of the received signal power is instead used for decoding information.

- **Dynamic Power Splitting (DPS)**. As depicted in Fig. 4.2, in this operating mode, at every IoT user the power split ratio is $\nu$ when the serving base station is serving that user, and it is equal to one for the rest of the time. That is, when an IoT node is not receiving data from its serving base station, all the received power (from any RF source, including all BSs and users) is fed to the RF harvesting electronics.

The splitting factors $\eta$ and $\nu$ are the same for all devices.

Thus, IoT devices harvest energy not only from their serving BS (*active charging*), but also from the signal received from all of the other BSs, as well as from uplink transmissions from both IoT and BB UEs (*passive charging*).

I assume that BSs use a generalized processor sharing (GPS) mechanism to divide BS time among all the connected UEs. As represented in Fig. 4.3, in downlink, the GPS weights are 1 for IoT UEs, and $w_d$ for BB UEs. The time spent by the BS without transmitting is modeled as a user with a GPS weight $\beta_d$. As for

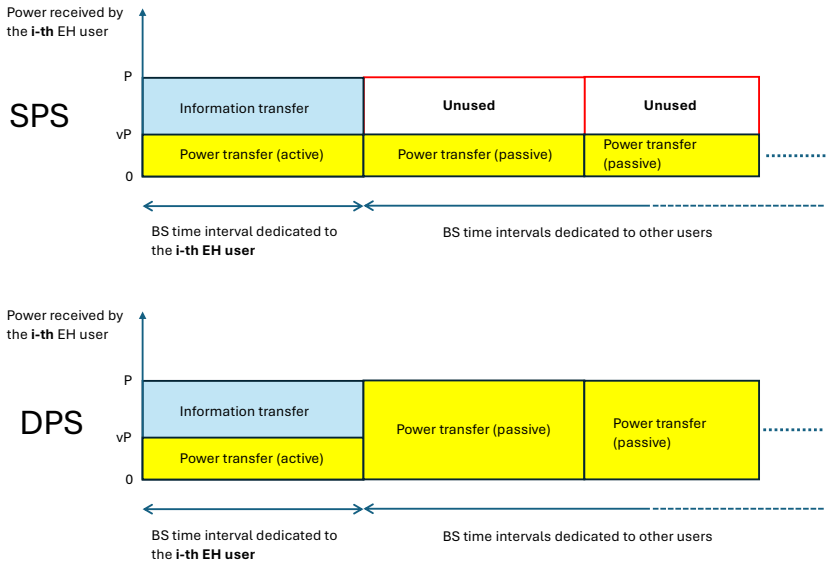


Figure 4.2: Difference in the harvesting process between SPS and DPS receiver operating modes.

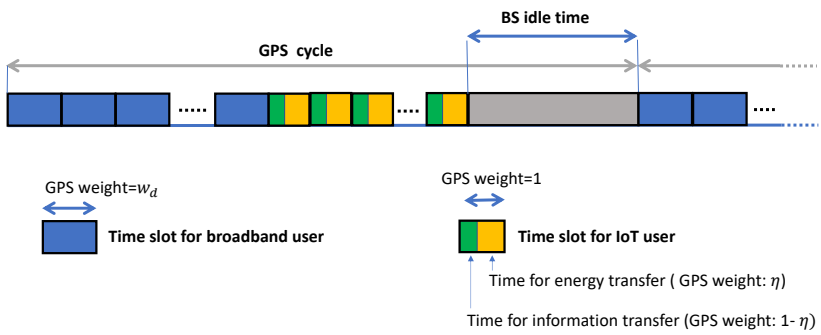


Figure 4.3: Downlink time scheduling scheme for a SWIPT BS, for a network with time switching EH receiver architecture, with GPS weights.

uplink, in all configurations, the GPS weights are 1 for IoT UEs, $\delta_u$ for BB UEs, and $\beta_u$ for the uplink BS time not assigned to any UE. IoT UEs periodically cycle between two operational states. During the *active state*, they send and receive data, plus possibly they perform some other task, such as sensing, while harvesting energy from active and passive sources. In the *low power* state, IoT devices only harvest energy. IoT devices are disconnected from the

power grid, and possesses an ideal battery (i.e., with efficiency equal to one) with enough capacity to compensate for the fluctuations in the energy consumed and harvested. Note however that our approach can be easily extended to consider battery nonidealities and limitations due to finite battery capacity. $\phi$ denotes the fraction of time spent by an IoT device in the active state. BB users are instead assumed to always be in the active state.

It is assumed that the system is in saturation, i.e., BSs have always data to send to users, and users in the active state have always data to transmit. A key aspect of the EH process is the function $h = \Theta(h_{in})$ that maps the received power $h_{in}$ to the harvested power $h$ for EH IoT devices. $\Theta$ models the effect of several technological factors affecting the efficiency of the energy harvesting process, ranging from receiver antenna gain to exposure of the specific IoT device, to receiver architecture, among others. In this work, I considered two different models:

- a linear model, by which $\Theta(h_{in}) = \xi h_{in}$, with $\xi \leq 1$; and
- a nonlinear model, where the mapping function is a normalized sigmoid [145], given by

$$\Theta(h_{in}) = \max\left\{\frac{h_{max}}{e^{-\chi h_s+\iota}}\left(\frac{1+e^{-\chi h_s+\iota}}{1+e^{-\chi h_{in}+\iota}}-1\right),0\right\} \tag{4.1}$$

  $h_{max}$ is the maximum harvested power when the energy harvesting circuit is saturated, while $h_s$ is the harvester's sensitivity threshold, i.e. the minimum amount of power able to activate the harvesting process. $\chi$ and $\iota$ are parameters that control the steepness of the sigmoid.

Note however that our approach extends easily to other EH models.

Given that the cellular RAN delivers two classes of services to two different types of UE, the performance metrics are defined as follows:

- **Information transfer**: For all UEs, the end-user performance metric is the *per-bit delay* $\tau$ of data transfers. It is the time required to transfer a single bit, and it is thus the inverse of the short-term throughput, i.e., of the rate at which data is transferred.

Table 4.1: Main notation used in Section 4.1.

| Name | Description |
|---|---|
| $\bar{\tau}_j, j = d, u$ | Mean ideal per-bit delay in downlink/uplink ($s^{-1}$) |
| $\tau_j, j = d, u$ | Per-bit delay in downlink/uplink ($s^{-1}$) |
| $\tau_j^0, j = d, u$ | Target per-bit delay in downlink/uplink ($s^{-1}$) |
| $\xi$ | EH conversion efficiency ratio (linear model) |
| $h_0$ | Minimum harvested power required by each IoT device ($W$) |
| $\mu$ | Maximum acceptable ratio of IoT users which harvest less than $h_0$ W |
| $\phi$ | Fraction of time in which IoT devices are active |
| $\lambda_b$ | Mean BS density ($m^{-2}$) |
| $\lambda_u$ | Mean density of user terminals ($m^{-2}$) |
| $\gamma$ | Fraction of user terminals which are IoT devices |
| $\eta$ | Fraction of the time dedicated by a BS to serve an IoT device in downlink used for harvesting energy from the signal received from the base station |
| $\nu$ | Fraction of the power received at any time instant by an IoT device which is used for energy harvesting |
| $\beta_j, j = d, u$ | GPS weight of the amount of time spent by a BS in idle mode in downlink/uplink |
| $w_d$ | Ratio between the amount of time dedicated to serving a BB UE and the one dedicated to serving an IoT user in downlink |
| $\delta_j, j = d, u$ | Ratio between the BS time dedicated to a BB user, and the base station time dedicated to an IoT user for data transfer in downlink/uplink |
| $k$ | Frequency reuse factor |
| $\alpha$ | Path loss exponent |
| $P$ | BS transmit power ($W$) |
| $G$ | BS antenna gain |
| $L$ | BS antenna loss (out of beam) |

- **Power transfer**: The performance parameter is the amount of power harvested by an IoT device, denoted with $h$.

As a result of the scheduling strategy (both in downlink and uplink), the amount of harvested energy may vary substantially across the various devices. These metrics must be considered relative to the corresponding application demands. As an example, the energy harvested by each device during a complete on-off cycle (and therefore the value of the parameter $h$) must be sufficient to compensate for the energy consumed during the cycle by such tasks as sensing, processing, storing, and distributing data, while

accounting for battery efficiency and for fluctuations in consumption patterns due to changes in the operational state of IoT devices. Accordingly, the target performance for information transfer is related to application-specific requirements.

#### 4.1.2.1 *Channel and Service Model*

Our channel model only takes into account distance-dependent path loss. Incorporating the effects of fading and shadowing would not alter our approach, and is left for future consideration. I assume that *random frequency reuse* is in place, with reuse factor $k$. That is, every BS is assigned one out of $k$ frequency bands with equal probability. I assume that UEs are associated with the BS that provides the largest SINR at the user location. I considered urban scenarios, where the high capacity demand justifies strategies for energy-efficient network planning and management, and where the assumption of high attenuation (with exponent $\alpha \geq 3$) typically holds. In these settings, as no fading is considered and all BSs use the same transmit power, assuming that users associate to the closest BS is a reasonable approximation [13].

BS antennas use beamforming, whose beamforming gain is denoted by $G$ and side lobes attenuation $L$. Considering with $a$ the aperture of the main lobe (in degrees), the relationship between $G$ and $L$ is given by

$$L = 1 - (G - 1)\frac{a}{360 - a}$$

Since users are assumed to be distributed uniformly in space, and base station time is supposed to be shared in equal parts across users of the same type, the mean power received by a user while it is not being served from the base station to which it is associated (located at a distance $r$) is $PL_g r^{-\alpha}$, with $L_g = \frac{Ga+L(360-a)}{360}$. Thus $L_g r^{-\alpha}$ is the mean attenuation with which the power transmitted by the serving base station is received by a user when it is not being served. Denote by $S(x)$ the location of the BS that is closest to a UE located at $x$. I denote the capacity of a user located at a distance $r$ from the BS by $C(r, P, G, I)$ bit/s per Hertz, where $P$ is the BS transmit power, and $I$ the total received interfering power. The capacity $C(r, P, G, I)$ is modeled using Shannon's capacity law. Thus,

$$C(r, P, G, I) = \frac{B}{k} \log_2 \left( 1 + \frac{PGr^{-\alpha}}{N_0 + I(r, k)} \right) \tag{4.2}$$

where $\alpha$ is the attenuation coefficient, $N_0$ the power spectral density of the additive white Gaussian noise, and $k$ the reuse factor.

#### 4.1.2.2 *Base Station and UE Energy Consumption Model*

The power consumed by a BS depends on several factors, which vary according to the BS type (e.g. macro, micro, femto) and the implementation technology (e.g. standalone vs cloud-RAN), among others. In what follows, I adopted a very flexible BS energy model, first proposed in [40, 98], by which the power consumed by a BS, denoted as $P_{BS}$, is given by the following expression:

$$P_{BS} = q_1 + U_d[q_2 + q_3(P - P_{min})] \tag{4.3}$$

In this model, the power consumed is thus given by the sum of three contributions.

- A first contribution, given by $q_1$, is constant, and depends only on the specific type of BS considered (e.g. macro, micro, femto, cloud). It models the power consumed when the BS is not carrying any traffic to/from users. As such, it does not depend on utilization or transmit power, and it is due to the power consumed by, e.g., part of the cooling function, by power amplifier consumption in idle state, and by all those functions which keep the BS in an operational (i.e. non standby) state.

- The second component $q_2 U_d$, in which $U_d$ is the downlink BS utilization, models that fraction of consumed power which depends on BS utilization (and it is thus proportional to the amount of traffic served), but not on transmit power. It models the power consumed by such functions as baseband processing and RF signal processing.

- Finally, the third component $q_3 U_d(P - P_{min})$ (where and $P$ is its transmit power, which it is assumed to vary within the interval $[P_{min}, P_{max}]$) models the fraction of consumed power due to the power amplifier which depends, at the same time, on the

transmit power $P$ and on the fraction of time that the BS is busy transmitting (given by $U_d$).

This energy model is very flexible and suited for accounting not only for implementations with different degrees of load proportionality, but also for cloud RAN configurations.

#### 4.1.2.3 *Base station service model*

I defined the utilization $U(S(x))$ of the BS serving a UE at location $x$ as the average fraction of time in which the BS is busy transmitting (in downlink – $U(S_d(x))$) or receiving (in uplink – $U(S_u(x))$), respectively. Thus, the expression of the utilization of the BS is given by the fraction of BS time dedicated to all active users:

$$U_d(S(x)) = \frac{N_{iot}(S(x)) + w_d N_{bb}(S(x))}{N_{iot}(S(x)) + w_d N_{bb}(S(x)) + \beta_d} \tag{4.4}$$

$$U_u(S(x)) = \frac{N_{iot}(S(x)) + \delta_u N_{bb}(S(x))}{N_{iot}(S(x)) + \delta_u N_{bb}(S(x)) + \beta_u} \tag{4.5}$$

where $N_{iot}(S(x))$ and $N_{bb}(S(x))$ denote respectively the number of broadband and IoT users in the *active* state, and associated with the same BS as the UE at location $x$. Note that, as IoT users cycle between active and inactive states, on average only a fraction $\phi$ of them is active at any point in time. Given $w_d$ and $\delta_u$, by tuning $\beta_j$ it is possible to vary the mean amount of service received by UEs for both communication and energy transfer, and the overall BS utilization, both in downlink and in uplink.

**Definition.** The ideal per-bit delay perceived by a UE is the per bit delay which a UE would perceive if the BS with which the UE is associated had utilization equal to 1.

Note that the above definition does not assume that *all* of the BSs have utilization equal to one, but only the BS serving the considered UE. From expressions (4.4), (4.5) and the above definition, for a UE at $x$, the relationship between the ideal per bit delay $\tau_j^{id}$, $j \in \ d, u$ and the actual per bit delay, both in uplink and in downlink, is $U_j(S(x))\tau_j(S(x)) = \tau_j^{id}(S(x))$, with $j \in \ d, u$. Indeed,

from the expression of the utilization, the ratio between the ideal and the actual per-bit delay is equal to the fraction of time the BS is active.

For each UE type, and for both uplink and downlink, a notion of target minimum quality of service (QoS) is defined. Namely, UEs are said to perceive satisfactory performance if the average per-bit delay experienced by a *typical* BB user (resp. IoT device)[1] are less than their respective predefined target values. In what follows, for a given $\eta$, I assumed each BS adopts the values of $\beta_j, j \in d, u$ (and thus of utilization in downlink and uplink) which achieve the target QoS for communications. This makes the average of the actual per bit delays (over all the users associated to that BS) coincide with the target values.

#### 4.1.2.4 *Modeling User-Level Performance*

In this section characterizes the main performance parameters, i.e., the per-bit delay and the harvested power of a typical user who is just beginning service[2] , as well as the mean harvested power, as a function of the main system parameters. The expression of the power harvested by a user at $x$ is given by the following result.

**Lemma 4.1.** Let $K(x) = [N_{iot}(S(x)) + w_d N_{bb}(S(x))]^{-1}$. Then the power harvested by a user at $x$ is $h(x) = \Theta(h_{in}(x))$, where the received power $h_{in}(x)$ is given by:

- **TS**:

$$\begin{aligned} h_{in}(x) = PD(x)^{-\alpha} U_d(S(x)) \left[ G\eta K(x) + L_g(1 - K(x)) \right] \\ + \left[ 1 - K(x) U_d(S(x))(1 - \eta) \right] (I(x) + O(x)) \end{aligned} \tag{4.6}$$

1 The definition of the typical user in the system is provided by classical Palm theory [134].

2 This assumption is standard in stochastic geometry, and it is one of the possible ways of choosing the point of view from which to carry out the analysis. Indeed, there is no difference in terms of performance with respect of the case in which users have been in the system for a while.

- **SPS**:

$$h_{in}(x) = \nu PD(x)^{-\alpha} U_d(S(x)) \left[ GK(x) + L_g(1 - K(x)) \right] + \nu(I(x) + O(x)) \tag{4.7}$$

- **DPS**:

$$h_{in}(x) = PD(x)^{-\alpha} U_d(S(x)) \left[ G\nu K(x) + L_g(1 - K(x)) \right] + I(x) + O(x) \tag{4.8}$$

$I(x)$ is the total power harvested by the user at $x$ from BSs other than the one with which it is associated. $O(x)$ is the power harvested from UE transmissions, averaged over time, and $U_d(S(x))$ is the downlink utilization of the BS with which the user at $x$ is associated.

*Proof of Lemma 4.1.* I derived the expression of $h_{in}$ only for the TS case, as the SPS and DPS cases are a minor variation of the former. The power the user receives at $x$ by its serving BS is $PD(x)^{-\alpha}$. $K^{-1}(x) = N_{iot}(S(x)) + w_d(1 - \eta)N_{bb}(S(x))$ is the sum of the GPS weights of all users served by the base station serving the user at $x$. Given that $\eta$ is the GPS weight for the fraction of BS time dedicated to *active* power transfer (to distinguish it from *passive* power transfer, i.e. from power harvested by ambient radiation) to an IoT user, and as the GPS weight of IoT users is 1, $\eta U_d(S(x))K(x)$ is the fraction of total base station time dedicated to actively charging the user at $x$. Thus, the amount of active transfer energy received by the user at $x$ is $PD(x)^{-\alpha}\eta U_d(S(x))GK(x)$. This implies that the expression for the fraction of total base station time dedicated to transmitting information to the IoT user at $x$ is $(1-\eta)U_d(S(x))K(x)$, and that the BS time dedicated to serving other users is $(1-K(x))U_d(S(x))$. During this BS time, the BS charges also passively the given user, though it transmits to it with gain $L_g$.
From the above, it follows also that $[1 - (1 - \eta)U_d(S(x))K(x)]$ is the fraction of BS time during which the user at $x$ can harvest energy (from both active and passive transfers) because this is the fraction of time during which it is not receiving information, and $[1 - (1 - \eta)U_d(S(x))K(x)]\,(I(x) + O(x))$ the received power due to passive power transfer from BSs other than the serving one,

and from any transmitting user. Putting all together, we have Eq. 4.6.

□

From its definition and from the service model description, it derives that in downlink, the ideal per-bit delay perceived by a BB UE at $x$ is given by

$$\tau_d^{id}(x) = \frac{N_{iot}(S(x)) + w_d N_{bb}(S(x))}{w_d C(x, P, G, I)} \tag{4.9}$$

For IoT users, in the TS receiver mode, the ideal per-bit delay is given by:

$$\tau_{d,I,TS}^{id}(x) = \frac{N_{iot}(S(x)) + w_d N_{bb}(S(x))}{(1-\eta) C(x, P, G, I)} \tag{4.10}$$

while, in both the power split modes, the ideal per-bit delay is

$$\tau_{d,I,PS}^{id}(x) = \frac{N_{iot}(S(x)) + w_d N_{bb}(S(x))}{C(x, (1-\nu)P, G, (1-\nu)I)} \tag{4.11}$$

For the uplink instead, for broadband users

$$\tau_u^{id}(x) = \frac{N_{iot}(S(x)) + \delta_u N_{bb}(S(x))}{\delta_u C(x, P_I, 1, 0)} \tag{4.12}$$

For IoT users, the ideal per-bit delay perceived in uplink is $\tau_{u,I}^{id}(x) = \delta_u \tau_u^{id}(x)$.

$\bar{\tau}_j$ $(\bar{\tau}_{j,I})$, $j = d, u$ denotes the average per-bit delay perceived in downlink (resp. in uplink) by broadband and IoT users, respectively. By leveraging stochastic geometry, it is possible to derive the main analytical results, in terms of probabilistic expressions for user-perceived performance metrics, which account for the random spatial patterns of both BSs and UEs. The following result derives an expression for the average per-bit delay perceived by the typical user (BB or IoT) which is just beginning service.

**Theorem 4.1.** The mean ideal per-bit delays in downlink and uplink, and the mean ideal per-Joule delay perceived by a typical best-effort user joining the system are given by:

$$\bar{\tau}_d = H(w_d, w_d, C(r, P, G, \bar{I})) \tag{4.13}$$

$$\bar{\tau}_{d,I,TS} = \bar{\tau}_d \frac{w_d}{(1-\eta)} \tag{4.14}$$

$$\bar{\tau}_{d,I,PS} = H(w_d, 1, C(r, (1-\nu)P, G, (1-\nu)\bar{I})) \tag{4.15}$$

$$\bar{\tau}_u = H\left(\delta_u, \delta_u, C(r, P_I, 1, 0)\right) \tag{4.16}$$

$$\bar{\tau}_{u,I} = \delta_u \bar{\tau}_u \tag{4.17}$$

Where:

$$H(y, z, g(r)) = \int_0^\infty \frac{f(r,y) e^{-\lambda_b \pi r^2} \lambda_b 2\pi r}{z g(r)} \, \mathrm{d}r, \tag{4.18}$$

with

$$f(r,y) = \lambda_u \left[y + \gamma\left(\phi - y\right)\right] \int_0^\infty \int_0^{2\pi} e^{-\lambda_b A(r,x,\theta)} x d\theta dx, \tag{4.19}$$

and

$$\begin{aligned} A(r,x,\theta) = \pi x^2 - \Bigg[ & r^2 \arccos\left(\frac{r + x\sin(\theta)}{d(r,x,\theta)}\right) \\ & + x^2 \arccos\left(\frac{x + r\sin(\theta)}{d(r,x,\theta)}\right) \\ & - \frac{1}{2}\sqrt{[r^2 - (d(r,x,\theta) - x)^2][(d(r,x,\theta) + x)^2 - r^2]}\Bigg]. \end{aligned} \tag{4.20}$$

$d(r,x,\theta)$ denotes the euclidean distance between $(x,\theta)$ and $(0,-r)$. $C(r,P,G,\bar{I})$ is given by Equation 4.2, with the interference term $\bar{I}$ given by:

$$\bar{I}(r,k) = \frac{P L_g \lambda_b 2\pi r^{2-\alpha}}{k(\alpha - 2)} \frac{\bar{\tau}_d}{\tau_d^0}. \tag{4.21}$$

*Proof of Theorem 4.1.* To prove Theorem 4.1 I considered the user at zero, but dropping this indication in what follows for ease of notation (i.e. $S(0)$ becomes $S$, and $D(0)$ becomes $D$). To derive $\bar{\tau}_d$,

let us start by computing the Palm expectation of $\tau_d^{id}(x)$ (dropping the dependence on P and G for notation ease):

$$\begin{aligned}
\bar{\tau}_d &= E^0\Big[\frac{N_{iot}(S) + w_d N_{bb}(S)}{w_d C(D,I)}\Big] \\
&= \int_0^\infty E^0\Big[\frac{N_{iot}(S,D) + w_d N_{bb}(S,D)}{w_d C(D,I)} | r \le D \le r + dr\Big] \times \\
&\times P(r \le D \le r + dr) \\
&\approx \int_0^\infty \frac{E^0[N_{iot}(S,D) + w_d N_{bb}(S,D) | r \le D \le r + dr]}{w_d C(r, \bar{I}(r,k))} \times \\
&\times P(B(0,r) = \phi)\lambda_b 2\pi r dr
\end{aligned}$$

where $\bar{I}(r,k)$ is the average interfering power for the typical user at $r$, given by $\bar{I}(r,k) = \frac{PL\lambda_b 2\pi r^{2-\alpha}}{k(\alpha-2)} \frac{\bar{\tau}_d}{\tau_d^0}$ [121]. The notation $N_{iot}(S,D)$, $N_{bb}(S,D)$ puts in evidence the fact that this case considers a BS located at $S$, serving the user at zero at a distance $D$.

$P(B(0,r) = \phi)$ is the probability that a ball of radius $r$ centered at the origin is empty, equal to $e^{-\lambda_b \pi r^2}$. If $N_{tot}(S,D) = N_{bb}(S,D) + N_{iot}(S,D)$, then $N_{iot}(S,D) + w_d N_{bb}(S,D) = Q N_{tot}(S,D)$, with $Q = w_d + \gamma(\phi - w_d)$. The palm expectation at the numerator becomes $Q E^0[N_{tot}(S,D) | r \le D \le r + dr]$. The random variable $N_{tot}(S,D)$ is the total number of users present in the same cell as the user at the origin, when his distance from its serving base station is $D$. As users are distributed according to a PPP with intensity $\lambda_u$, $N_{tot}(S,D)$ is Poisson, with an intensity given by the conditional Palm expectation inside the integral. Using Campbell's formula [134], this expectation becomes

$$\begin{aligned}
&E^0\Big[\int_0^\infty \int_0^{2\pi} \mathbf{1}_{(S(x,\theta)=S | r \le D \le r+dr)} \lambda_u d\theta x dx\Big] \\
&= \int_0^\infty \int_0^{2\pi} \lambda_u P(S(x,\theta) = S | r \le D \le r + dr) d\theta x dx.
\end{aligned}$$

The conditional probability within the integral is given by the CDF the nearest point of PPP: $\int_0^\infty \int_0^{2\pi} \lambda_u e^{-\lambda_b A(r,x,\theta)} d\theta x dx$, where $A(r,x,\theta)$ is the area of the circle centered at $(x,\theta)$ with radius $x$ that is not overlapped by the circle centered at $(0,-r)$ with radius $r$ [119]. By substituting, the expression for $\bar{\tau}_d$ can be obtained. The derivation of $\bar{\tau}_u$ follows along the same lines. Expressions (4.13), (4.14) and (4.15) are implicit in the per bit delays. That is, they

are a function of the per-bit delays themselves, via the expression for the interference. Thus each constitutes a fixed point problem. However it is easy to see that the mapping operator associated with each of these fixed points is contractive, and thus the problem admits a unique solution. Specifically, to prove the existence and uniqueness of the fixed point for Eq. 4.13, I prove that the operator $T(\bar{\tau}_d)$, whose expression is given by the right member of Equation 4.13, is a contraction. To this end, one can verify that Blackwell's sufficient conditions for a contraction [18] hold for $T$. The monotonicity of $T$ is straightforward, because increasing $\bar{\tau}_d$ increases the mean BS utilization, and hence the mean interference level. This translates into an increase in per-bit delays (i.e. a decrease in mean throughput). For the discounting property, one can prove that $\exists \beta \in (0,1)$ such that $T(\bar{\tau}_d + a) \leq T(\bar{\tau}_d) + \beta a$, $\forall a \geq 0$ and for all system parameter values for which $\bar{\tau}_d$ is defined. This is done by upper bounding $\bar{I}(\bar{\tau}_d + a)$ as the sum of two terms, one function of $\bar{\tau}_d$ and the other of $a$. Substituting into Equation 4.13, it follows that integrand in Equation 4.13 can be upper bounded as the sum of two terms, and after some algebraic steps this allows proving the discounting property. □

The considered system is in the *dense IoT regime* when the density of IoT users is such that the probability of having a cell without IoT users is negligible. This assumption is coherent with many current projections on expected IoT deployments in 6G, in which the expected device densities are of the order of 10 million devices per km$^2$ and more [16, 50, 101, 114].

**Theorem 4.2.** In the dense IoT regime, the cumulative distribution function $CDF_h^i$, $i \in \{TS, SPS, DPS\}$ of the power harvested by an IoT user who is just beginning service is $CDF_h^i(h_0) = CDF_r(g_i^{-1}(h_0))$ for all $h_0 \geq 0$. $CDF_r$ is the cumulative distribution function of the distance of the user to its serving BS:

$$CDF_r(r) = \int_0^r e^{-\lambda_b \pi y^2} \lambda_b 2\pi y dy$$

where $g_i(r) = \Theta\left(F_i(r) + \frac{Z_i(r)}{f(r, w_d)}\right)$, and $f(r, w_d)$ given by Theorem 4.1. As for $F_i(r)$ and $Z_i(r)$:

- *TS configuration*:

$$F_{TS}(r) = Pr^{-\alpha}L_g\frac{\bar{\tau}_d}{\tau_d^0} + k\bar{I}(r,k) + \bar{O}$$
$$Z_{TS}(r) = \frac{\bar{\tau}_d}{\tau_d^0}\Big[Pr^{-\alpha}(G\eta - L_g) - (1-\eta)(k\bar{I}(r,k) + \bar{O})\Big]$$
$$\bar{O} = \frac{(1-\gamma)\delta_u P_{bb} + \phi\gamma P_I}{(1-\gamma)\delta_u + \phi\gamma}\frac{\lambda_b \pi\alpha}{\alpha - 2}\frac{\bar{\tau}_u}{\tau_u^0}$$

- *SPS configuration*: $F_{SPS}(r) = \nu F_{TS}(r)$, and $Z_{SPS}(r) = \nu Pr^{-\alpha}\frac{\bar{\tau}_d}{\tau_d^0}(G - L_g)$.
- *DPS configuration*: $F_{DPS}(r) = F_{TS}(r)$, and $Z_{DPS}(r) = Pr^{-\alpha}\frac{\bar{\tau}_d}{\tau_d^0}(\nu G - L_g)$.

*Proof of Theorem 4.2.* The transmit power from a user (averaging between IoT and BB users) is $\frac{(1-\gamma)\delta_u P_{bb}+\gamma\phi P_I}{(1-\gamma)\delta_u+\gamma\phi}$. Let $\chi(j)$ is the set of users served by the $j$−th BS, and $x_i'(t), i \in \chi(j)$ be the position of the $i$-th user served by BS $j$ at time t. Let $d(x, x_i'(t))$ denote the distance between the two users considered, and $u(x_i'(t))$ the probability that the given user is transmitting at time $t$. Then

$$O(x,t) = \sum_j \sum_{i\in\chi(j)} \frac{(1-\gamma)\delta_u P_{bb} + \gamma\phi P_I}{(1-\gamma)\delta_u + \gamma\phi} d(x, x_i'(t))^{-\alpha} u(x_i'(t)) \tag{4.22}$$

As I assumed the base station has utilization $\frac{\bar{\tau}_u}{\tau_u^0}$ in the uplink, $u(x_i'(t)) = \frac{1}{\lambda_u A_j}\frac{\bar{\tau}_u}{\tau_u^0}$, where $A_j$ is the area of the Voronoi cell of BS j. Given that users are uniformly distributed in the plane, the Palm expectation of Equation 4.22 is well approximated by

$$\frac{(1-\gamma)\delta_u P_{bb} + \gamma\phi P_I}{(1-\gamma)\delta_u + \gamma\phi} E\left[\sum_j \frac{\int_{x'\in A_j} d(x,x')^{-\alpha}dx'}{\lambda_u A_j}\right]\frac{\bar{\tau}_u}{\tau_u^0}$$

. As $A_j$ is statistically independent on $d(x, x')$, the approximated formula becomes

$$\bar{O} = \frac{(1-\gamma)\delta_u P_{bb} + \gamma\phi P_I}{(1-\gamma)\delta_u + \gamma\phi}\frac{\int_0^{+\infty}\lambda_u min(1, s^{-\alpha})2\pi s ds}{\lambda_u \bar{A}}\frac{\bar{\tau}_u}{\tau_u^0} \tag{4.23}$$

where $\bar{A} = \lambda_b^{-1}$ is the mean area of a Voronoi cell for a BS density of $\lambda_b$. The final expression of $\bar{O}$ is derived from the high attenuation assumption ($\alpha > 2$). □

$P_{bb}$ and $P_I$ denote the transmit power of BB and IoT UEs, respectively.

**Theorem 4.3. (Maximally fair GPS weights).** The values of the GPS weight $w_d$ which maximize fairness among users are given by $w_d = \delta_d(1-\eta)$ for the time split (TS) mode, and

$$w_d = \delta_d \frac{\log_2\left(1 + \frac{(1-\nu)PG\bar{r}^{-\alpha}}{N_0+(1-\nu)\bar{I}(\bar{r},k)}\right)}{\log_2\left(1 + \frac{PG\bar{r}^{-\alpha}}{N_0+\bar{I}(\bar{r},k)}\right)}$$

for the power split modes. $\bar{r}$ is the mean distance of UEs from the serving base station, and $\bar{I}(\bar{r},k)$ is given by Theorem 4.1.

*Proof.* In our GPS scheduler, $w_d$ is the ratio between the amount of time dedicated to serving a BB UE and the one dedicated to serving an IoT user (for both information transfer and power transfer). Sytem needs to ensure fairness in resource scheduling for information transfer between BB and IoT users (as for power transfer, only IoT users are involved). This is implemented by having the ratio between the (mean) amount of bits received by a BB user and an IoT user be equal to $\delta_d$, i.e. to the ratio between the target values of throughput of the two user classes. Thus, for the TS case, in any location at a distance $r$ from the serving base station,

$$\delta_d = \frac{w_d R(r)}{(1-\eta)R(r)}$$

where $R(r)$ denotes the amount of bits received by the user at $r$ during the time that its serving bases station dedicates to it. By recalling that $(1-\eta)$ is the GPS weight dedicated to information transfer to an IoT UE, this brings to $w_d = \delta_d(1-\eta)$. For the PS cases, it is possible to proceed in the same manner. The ratio between the amount of bits received from the serving base station, using the Shannon capacity formula, is given by:

$$\frac{w_d \log_2\left(1 + \frac{PGr^{-\alpha}}{N_0+I(r,k)}\right)}{\log_2\left(1 + \frac{(1-\nu)PGr^{-\alpha}}{N_0+(1-\nu)I(r,k)}\right)}$$

However such a ratio is a function of $r$, and of the interference experienced by the specific considered user. Thus, it is possible

to consider the mean user, and set $w_d$ in such a way as to satisfy the equality

$$\delta_d = \frac{w_d \log_2\left(1 + \frac{PG\bar{r}^{-\alpha}}{N_0 + \bar{I}(\bar{r},k)}\right)}{\log_2\left(1 + \frac{(1-\nu)PG\bar{r}^{-\alpha}}{N_0 + (1-\nu)\bar{I}(\bar{r},k)}\right)}$$

where I approximated the mean interference perceived by the user with the expression in Theorem 4.1. □

### 4.1.3 *Optimization Problem*

One of the main open issues in SWIPT networks is to determine, as a function of the main system characteristics as well as of the energy and traffic demands, how the main network parameters should be tuned in order to optimize the energy consumed by the system. To this end, this section elaborates the formulation of the optimization problem which provides, for a given BS energy model, as well as for a given user mean density, the energy optimal BS transmit power, the optimal density of active BSs, as well as the optimal amount of BS time dedicated to power transfer, which satisfy the specified performance constraints.
The objective function is given by the mean power per unit surface consumed by the network, as a function of the BS density, of the BS transmit power, and of the time/power switch ratio. It is thus derived as the product of the power consumed by a BS (expressed in Equation Equation 6.56) and of the mean BS density. Note that, by the definition of per bit delay, $U_d = \frac{\bar{\tau}_d}{\tau_d^0}$. The optimization problem that can be formulated with such an objective function depends also on the EH operating mode. In the TS case, we have the following optimization problem formulation:

**Problem 4.1.** (**TS operating mode**)

$$\underset{P,\lambda_b,\eta}{\text{minimize}}\ \lambda_b \left[ q_1 + \frac{\bar{\tau}_d}{\tau_d^0}\left(q_2 + q_3(P - P_{min})\right)\right] \tag{4.24}$$

Subject to:

$$\text{(C1)} \quad \frac{\bar{\tau}_d}{\tau_d^0} \leq 1, \quad \frac{\bar{\tau}_u}{\tau_u^0} \leq 1$$

$$\text{(C2)} \quad P_{\min} \leq P \leq P_{\max}$$

$$\text{(C3)} \quad 0 \leq \eta \leq 1$$

$$\text{(C4)} \quad CDF_h^{TS}(h_0, \eta, P) \leq \mu$$

$$\text{(C5)} \quad 0 \leq \lambda_b \leq \lambda_{b,\max}$$

Constraints C1 requires the mean BS utilization in downlink and uplink to be smaller than one. The expression of the ideal per-bit delay is the one from Theorem 4.1. Constraints C2 and C3 define the range of acceptable values for the BS transmit power and the time split ratio, respectively. Constraint C4 requires that the probability for an IoT device to harvest less power than the minimum required to operate (denoted as $h_0$, and accounting for the amount of energy required by the device during a whole on-off cycle) be less than a given maximum acceptable value $\mu$. The expression of the cumulative distribution function is the one derived in Theorem 4.2. Finally, constraint C5 derives from practical limitations to the maximum density of BS deployments in realistic urban settings, which in any realistic scenario cannot exceed a maximum value.

In the power splitting EH operating modes (both static and dynamic), the resulting optimization problem takes a very similar structure. In both SPS and DPS, the objective function is the same, and decision variables are $P$,$\lambda_b$ and $\nu$. Moreover, constraint C3 is replaced by

$$\text{(C3a)} \qquad 0 \leq \nu \leq 1 \tag{4.25}$$

For SPS, constraint C4 becomes

$$\text{(C4a)} \qquad CDF_h^{SPS}(h_0, \nu, P) \leq \mu \tag{4.26}$$

For DPS, constraint C4 is substituted by

$$\text{(C4b)} \qquad CDF_h^{DPS}(h_0, \nu, P) \leq \mu \tag{4.27}$$

with $CDF_h^{TS}$, $CDF_h^{SPS}$ and $CDF_h^{DPS}$ given by Theorem 2. The other constraints and the objective function remain the same. In all formulations, however, the optimization problem is non-convex and

nonlinear, and it cannot be solved efficiently. This is since $\bar{\tau}_d$ (which appears in the expression of both the objective function and in constraints C1) is a nonlinear and non-convex function of the optimization variables. Similar consideration holds also for the expression of $CDF_h(h_0, \eta, P)$ from Theorem 4.2, which is nonlinear and non-convex in the three optimization variables.

As for the time complexity of the proposed GA, in the worst case scenario, if $n$ iterations are required per each population of $m$ chromosomes, and $T_{sim}$ denotes the time to compute the value of the function modeled by the chromosome and to perform the estimation of the fitness value, then the time complexity of the algorithm is $O(mnT_{sim})$.

### 4.1.4 *Limitations*

Despite providing a strong framework for the analysis of SWIPT HetNet; the current work does not take into account a realistic BS distribution. In fact, in a realistic network realization of smart city, or even in more sparse scenario, BSs are distributed according to a determined pattern. These patterns can be modeled through the SG, by modifying the underlying process, and related intensities. The next section extends the presented model to a vehicular network, as an example of smart city.

## 4.2 VEHICULAR DEPLOYMENT MODEL

Given the limitation outlined in Subsection 4.1.4, a more deterministic layout is needed to take into account the context. In this second contribution, two BS layout will be discussed. The introduction of a second BS layout changes the approach, leading to a different characterization of the system.

### 4.2.1 *Problem Statement and Motivation*

The advent of the automotive industry, 5G and future 6G drastically increased the number of devices [39] leading to new opportunities within the context of smart devices and network mod-

eling. Through this new paradigm, it is possible to imagine different ways of communicating with devices. Antennas placed on flying devices, such as UAVs (Unmanned Aerial Vehicles) can be used to power up IoT devices in post-disaster scenarios [44]. It is possible to imagine a context where devices are not directly connected to the Internet but can leverage vehicle connections for sending information, enabling the so-called backhauling, where end-devices leverage other infrastructures to deliver data. If by one side, the PPP is a well-defined framework in network coverage and analysis [12], as also demonstrated in the previous section, this cannot fully represent the concrete SWIPT system due to missing accuracy. Placing BSs on roads, rather than on the plan according to a PPP, some differences will be introduced on statistics and performance perceived by the users.

Driven by these motivations, this work present a different model aimed at evaluating vehicular SWIPT networks. The main contributions of this work can be summarized as follows:

- Development of a two-tier analytical model for SWIPT networks, where BSs are placed along lines following a Poisson Line Cox Process (PLCP), and UEs are distributed according to a PPP
- Formulation of an optimization problem targeting power consumption minimization by fine-tuning key architectural parameters of the network
- Comparative evaluation of the proposed model against a planar PPP-based SWIPT network, to assess the impact of the new characterization and to highlight its advantages and limitations.

### 4.2.2 *Methodological Approach*

#### 4.2.2.1 *Modeling Vehicular Networks with Poisson Line Cox Processes (PLCP)*

As represented in Fig. 4.4, let us consider a two-virtual-tier network containing two different distributions of BSs:

**Planar BS (PBS)**. In the first tier, the BSs are distributed according to an independent 2D homogeneous PPP $\Phi_b$ with a density $\lambda_b$.

**Vehicular BS (VBS)**. In the second tier, a road system is modeled by an independent Poisson Line Process (PLP) $\Phi_l \in R^2$ produced by a homogeneous PPP $\Xi$ on the cylinder $C := R \times [0, \pi)$ with an intensity $\lambda_l$. More precisely, a point of $\Xi$, denoted by $(r_i, \theta_i)$, describes the line $l_i \in R^2$ of equation

$$l(r_i, \theta_i) = \{(x, y) \in R^2 | xcos(\theta_i) + ysin(\theta_i) = r_i\} \tag{4.28}$$

where the parameters $r$ and $\theta$ correspond to the shortest distance from the origin to the line and the angle between the positive $x$-axis and the line $l$, respectively. Conditionally on the lines, BSs are modeled by independent 1-D homogenous PPP with intensity $\mu_b$, so the distance between two consecutive points on the same line hence follows the exponential distribution with parameter $\mu_b$. The result is a *Poisson Line Cox Point Process* $\Psi_b$ with spatial intensity which can be expressed as

$$\Lambda(A) = \mathbb{E}[N_p(A)|\Psi_b] = \mu_b \sum_{l_i \in \Psi_b} v_1(l_i \cap A) = \mu_b \pi \lambda_l \tag{4.29}$$

Most of the UEs notation is the same as the previous system model. UEs are distributed in space according to Poisson Point Process (PPP) with a density $\lambda_u$. UEs are either BB terminals, or IoT (Internet of Things) devices. Let us assume the latter are a fraction $\gamma$ of the total number of UEs.

Table 4.2: Main notation used in Section 4.2.

| Name | Description |
|---|---|
| $\Phi_b$, $\Phi_u$ | Planar BSs and Planar UEs distribution |
| $\lambda_b, \lambda_u$ | Planar BSs and Planar UEs density |
| $\Psi_b$ | Vehicular BSs distribution |
| $\lambda_l \mu_b$ | Vehicular BSs density |
| $\eta$ | Splitting Factor |

#### 4.2.2.2 *Analytical Characterization*

As presented in [11], the analytical characterization will be structured into three main steps, which correspond to find: (1) Rele-

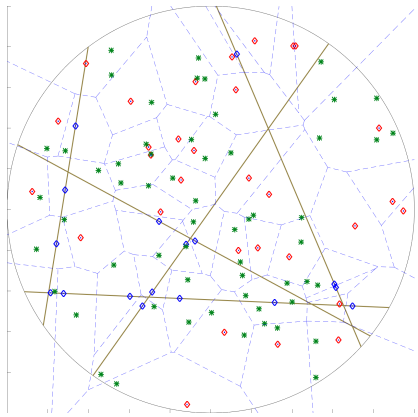

Figure 4.4: Two tiers proposed architecture composed by UE (green), vehicular BS (blue) placed on roads (yellow), and planar BS (red).

vant distance distribution, (2) Association probabilities, (3) Serving BS distance distribution. Once clarified which is the serving BS distance distribution, this section introduces the relevant performance metrics.

*Step 1: Relevant distance distributions*. The key distributions that are of interest for our analysis are the CDF and PDF of the distances between UE and the candidate serving BS from Tier 1 or Tier 2. Let us denote these distances with typical BS on Tier 1 with $x_1$ and with the typical BS on Tier 2 with $x_2$, which are driven by the random variable $R_1$ and $R_2$, respectively. As $\phi_b$ is an 2D homogeneous PPP, the CDF and PDF of $R_1$ are given (similarly to the previous section) by:

$$F_{R_1}(r_i) = 1 - \exp(-\lambda_b \pi r_i^2)$$

$$f_{R_1}(r_i) = 2\pi\lambda_b r_i \exp(-\lambda_b \pi r_i^2)$$

While in the Tier 2, since BS are distributed according to a PLCP $\Psi_b$, the CDF and PDF are given by:

$$F_{R_2}(r_i) = 1 - \exp\Big[ -2\pi\lambda_l \int_0^{r_i} \Big(1 - \exp(-2\mu_b\sqrt{r_i^2 - \rho^2})\Big)\, \mathrm{d}\rho \Big]$$

$$f_{R_2}(r_i) = \Big[ 2\pi\lambda_l \int_0^{r_i} \frac{2\mu_b r_i}{\sqrt{r_i^2 - u^2}} \exp(-2\mu_b\sqrt{r_i^2 - u^2})\, \mathrm{d}u \Big] \times$$

$$\times \exp\Big[ -2\pi\lambda_l \int_0^{r_i} \Big(1 - \exp(-2\mu_b\sqrt{r_i^2 - \rho^2})\Big)\, \mathrm{d}\rho\Big]$$

*Step 2: Association probabilities.* To derive the coverage probability it is necessary to define the association probabilities to one of the BSs belonging to the two tiers. Let us define $E_1$ the event in which the user is associated with a BS on the Tier 1, and with $E_2$ the event in which the user is associated with a BS on the Tier 2. The event $E_1$ occur when the distance from the nearest BS on the Tier 2 is greater than the distance of the BS on the Tier 1, so the probability of occurrence of the event $E_1$ can be computed as:

$$\begin{aligned}
\mathbb{P}(E_1) &= \mathbb{P}(R_1 < R_2) \\
&= \mathbb{E}_{R_1}\Big[\mathbb{P}(R_2 > r_1 | R_1)\Big] \\
&= \int_0^\infty \Big(1 - F_{R_2}(r_1)\Big) f_{R_1}(r_1)\, \mathrm{d}r_1 \\
&= \int_0^\infty 2\pi\lambda_b r_1 e^{-\lambda_b \pi r_1^2 - 2\pi\lambda_l \int_0^{r_1} 1 - e^{-2\mu_b\sqrt{r_1^2-\rho^2}}\, \mathrm{d}\rho}\, \mathrm{d}r_1
\end{aligned} \tag{4.30}$$

While, the probability of being associated with a BS on the Tier 2 will be $\mathbb{P}(E_2) = 1 - \mathbb{P}(E_1)$. It is possible to notice that these probabilities also correspond to the probability to be associated to one of the two distribution, so $\mathbb{P}(X \in \phi_b) = \mathbb{P}(E_1)$.

*Step 3: Serving BS distance distribution.* After computing the association probability to one among vehicular or planar BS, it is now possible to compute the distance from the serving BS. As introduced, $R_1$ and $R_2$ are two independent random variable (since the processes are independent), so the resulting minimum is a new random variable $U = \min\{R_1, R_2\}$ whose CDF can be computed as follows.

**Lemma 4.2.** Let $R_1$ and $R_2$ be two independent random variables denoting the distance to the nearest planar and vehicular BS, respectively. Define the serving distance as $U = \min\{R_1, R_2\}$. Then the CDF of $U$ is

$$\begin{aligned}
F_U(r) &= 1 - (1 - F_{R_1}(r))(1 - F_{R_2}(r)) \\
&= 1 - \exp\Big( -\lambda_b \pi r^2 - 2\pi\lambda_l \int_0^r (1 - \exp(-2\mu_b\sqrt{r^2 - \rho^2}))\, \mathrm{d}\rho\Big).
\end{aligned} \tag{4.31}$$

Moreover, the PDF is obtained by differentiation as

$$\begin{aligned} f_U(r) = {} & 2\pi\lambda_b r\, e^{-\pi\lambda_b r^2 - 2\pi\lambda_l \int_0^r \left(1 - e^{-2\mu_b\sqrt{r^2-t^2}}\right) \mathrm{d}t} \\ & + e^{-\lambda_b \pi r^2 - 2\pi\lambda_l \int_0^r (1 - e^{-2\mu_b\sqrt{r^2-\rho^2}})\, \mathrm{d}\rho} \\ & \times \int_0^r \frac{4\pi\lambda_l\mu_b r\, e^{-2\mu_b\sqrt{r^2-u^2}}}{\sqrt{r^2-u^2}}\, \mathrm{d}u. \end{aligned} \tag{4.32}$$

*Proof of Lemma 4.31.* Since $U = \min\{R_1, R_2\}$ and $R_1, R_2$ are independent,

$$F_U(r) = 1 - \mathbb{P}(R_1 > r)\, \mathbb{P}(R_2 > r).$$

For the planar PPP, $\mathbb{P}(R_1 > r) = e^{-\lambda_b \pi r^2}$. For the vehicular PLCP,

$$\mathbb{P}(R_2 > r) = \exp\left(-2\pi\lambda_l \int_0^r \left(1 - e^{-2\mu_b\sqrt{r^2-\rho^2}}\right) \mathrm{d}\rho\right).$$

Multiplying the two terms gives the expression in (4.31). The PDF follows by differentiation,

$$f_U(r) = \frac{\mathrm{d}}{\mathrm{d}r} F_U(r) = e^{-\lambda_b \pi r^2 - B(r)} \left(2\pi\lambda_b r + B'(r)\right),$$

where $B(r) = 2\pi\lambda_l \int_0^r (1 - e^{-2\mu_b\sqrt{r^2-\rho^2}})\, \mathrm{d}\rho$. Applying Leibniz' rule yields $B'(r)$ as in (4.32), which completes the proof. □

#### 4.2.2.3 *Base station Model and User Model*

The BS energy model, by which the power consumed by a BS, denoted as $P_{BS}$, is given by the expression presented in the previous section. The same expression is applied to both planar and vehicular BSs, aiming at demonstrating the impact of the deployment of one of the two, independently of the costs that each of them leverage on. The capacity of the channel is expressed by the Shannon's law introduced in (4.2).

This section characterizes the main performance parameters as a function of the main system parameters and the expression derived in the coverage analysis section.

**Theorem 4.4.** The mean ideal per-bit delays in downlink and uplink, and the mean ideal per-Joule delay perceived by a typical best-effort user joining the system are given by:

$$\bar{\tau}_d = H(w_d, w_d, C(r, P, G, \bar{I})) \tag{4.33}$$

$$\bar{\tau}_{d,I,TS} = \bar{\tau}_d \frac{w_d}{(1-\eta)} \tag{4.34}$$

$$\bar{\tau}_{d,I,PS} = H(w_d, 1, C(r, (1-\nu)P, G, (1-\nu)\bar{I})) \tag{4.35}$$

$$\bar{\tau}_u = H\left(\delta_u, \delta_u, C(r, P_I, 1, 0)\right) \tag{4.36}$$

$$\bar{\tau}_{u,I} = \delta_u \bar{\tau}_u \tag{4.37}$$

Where:

$$H(y, z, g(r)) = \int_0^\infty \frac{f(r,y)k(r)}{zg(r)} \, \mathrm{d}r. \tag{4.38}$$

with

$$f(r,y) = \lambda_u \left[y + \gamma\left(\phi - y\right)\right] \times$$

$$\times \int_0^\infty \int_0^{2\pi} e^{-\lambda_b A(r,x,\theta) - 2\pi\lambda_l \int_0^\rho 1 - e^{-2\mu_b \sqrt{\rho^2 - t^2}\,\mathrm{d}t}} x \, \mathrm{d}\theta \, \mathrm{d}x$$

$A(r, x, \theta)$ is the area of the circle centered at $(x, \theta)$ with radius $x$ that is not overlapped by the circle centered at $(0, -r)$ with radius $r$. $\rho$ is the radius of a circle with the same area $A(r, x, \theta)$. $C(r, P, G, \bar{I})$ is given by Equation 4.2, with the interference term $\bar{I}$ given by

$$\bar{I}(r,k) = \frac{PL_g(\lambda_b + \lambda_l \mu_b) 2\pi r^{2-\alpha}}{k(\alpha - 2)} \frac{\bar{\tau}_d}{\tau_d^0} \tag{4.39}$$

*Proof of Theorem 4.4.* Following the same path as Theorem 4.1, by substituting the CDF of PPP with the CDF of the nearest point of a joint distribution presented in Equation 4.31. □

Anyway, since the network under consideration belong to a SWIPT network, it is important to model the energy received from a typical IoT device, can be harvested both from other UEs, and from other BSs, as well as from the connected BS.

**Theorem 4.5.** In the dense IoT regime, the cumulative distribution function $CDF_h$ of the power harvested by an IoT user who is just beginning service is

$$CDF_h(h_0) = CDF_r(g^{-1}(h_0))$$

for all $h_0 \geq 0$, where $CDF_r$ is the cumulative distribution function of the distance of the user to its serving BS:

$$CDF_r(r) = \int_0^r 2\pi\lambda_b r e^{-\lambda_b \pi r^2 - 2\pi\lambda_l \int_0^r (1-a(r,u))\,\mathrm{d}u}$$

$$+ e^{-\lambda_b \pi r^2 - 2\pi\lambda_l \int_0^r (1-a(r,u))\,\mathrm{d}u}$$

$$\times \int_0^r \frac{4\lambda_l \pi \mu_b r a(r,u)}{\sqrt{r^2 - u^2}}\,\mathrm{d}u\,\mathrm{d}r,$$

where

$$a(r,u) = e^{-2\mu_b \sqrt{r^2-u^2}}$$

$$g(r) = \Theta\left(F_{TS}(r) + \frac{Z_{TS}(r)}{f(r,w_d)}\right)$$

with $F_{TS}$ representing the energy harvested from the connected BS, and $Z_{TS}$ representing the energy harvested from all the other BSs, as well as from the other UEs near the UE. These can be computed as follows, while $f(r,w_d)$ is given by Theorem 4.1.

$$F_{TS}(r) = Pr^{-\alpha} L_g \frac{\bar{\tau}_d}{\tau_d^0} + k\bar{I}(r,k) + \bar{O}$$

$$Z_{TS}(r) = \frac{\bar{\tau}_d}{\tau_d^0}\left[Pr^{-\alpha}(G\eta - L_g) - (1-\eta)(k\bar{I}(r,k) + \bar{O})\right]$$

$$\bar{O} = \frac{(1-\gamma)\delta_u P_{bb} + \phi\gamma P_I}{(1-\gamma)\delta_u + \phi\gamma} \frac{(\lambda_b + \lambda_l \mu_b)\pi\alpha}{\alpha - 2} \frac{\bar{\tau}_u}{\tau_u^0}$$

*Proof of Theorem 4.5.* Following the same path as Theorem 4.2, by substituting the CDF of PPP with the CDF of the nearest point of a joint distribution presented in Equation 4.31. □

### 4.2.3 *Optimization Problem*

Typically, in SWIPT networks it is hard to establish a unique setting for the main system parameters. This is because multiple configurations can achieve the same result. To determine the best configuration, let me introduce here an optimization problem, which aims at reducing the total network power consumption in terms of transmitting power $P$, PBS density $\lambda_b$, VBS density $\mu_b$ and splitting factor for a given user density $\lambda_u$.

**Problem 4.2.**

$$min_{P,\lambda_b,\mu_b,\eta} \;\; \lambda_b + \pi\lambda_l\mu_b\Big[q_1 + \frac{\bar{\tau}_d(\eta,P,\lambda_b,\mu_b)}{\tau_d^0}\times$$

$$\times\,(q_2 + q_3(P - P_{min}))\Big]$$

Subject to:

$$\frac{\bar{\tau}_d(\eta,P,\lambda_b)}{\tau_d^0} \leq 1, \quad \frac{\bar{\tau}_u(\eta,P,\lambda_b)}{\tau_u^0} \leq 1 \tag{4.40}$$

$$P_{min} \leq P \leq P_{max} \tag{4.41}$$

$$0 \leq \eta \leq 1 \tag{4.42}$$

$$CDF_h(h_0,\eta,P) \leq \mu \tag{4.43}$$

$$0 \leq \lambda_b \leq \lambda_{b,max} \tag{4.44}$$

$$\pi\lambda_l\mu_b > \varpi\lambda_b \tag{4.45}$$

where $h_0$ in constraint ((C2)) is the minimum harvested power required by each IoT device to operate, computed based on the amount of energy required by the device during a whole on-off cycle. $\mu$ is the maximum acceptable ratio of IoT users which harvest less than $h_0$ Joules per second. $\bar{\tau}_d$, $\bar{\tau}_u$ are given by Theorem 4.1. $\lambda_{b,max}$ derives from practical constraints to BS deployments in urban settings. Finally, it has been considered a constraint on vehicular BSs in (4.45), which forces the optimization problem to consider a minimum amount of vehicular BSs. This constraint has been considered due to the generally better performance of PPP, with respect to PLCP.

To efficiently solve the proposed problem, considering the complexity of the interdependency of network parameters, and the strength in avoiding local minima by working with a population

of potential solutions, I leveraged a Genetic Algorithm (GA)-based approach, described in Algorithm 1. I executed the GA by selecting the dominant chromosome (i.e., the one with the highest fitness value on the problem). The algorithm then generates a new population through appropriate genetic operators, namely mutation and crossover. The mutation used in the proposed algorithm is the default one, namely the Gaussian mutation, while the crossover employed by the proposed algorithm returns a child that lies on the line containing the two parents, a small distance away from the parent with the better fitness value in the direction away from the parent with the worse fitness value. Through MATLAB it is possible to set the distance for which goes, which in our case has been set to 1.9. The application of two operations generates a new population which is evaluated against a fitness function according to the objective function of Problem 6.4. This process is repeated over 150 generations or until the termination condition is met, which is defined as no improvement over 10 consecutive generations. Through this approach, guided by the fitness function, the GA performs a random exploration of the solution space, driven by the outcomes of the evolutionary operators.

**Algorithm 1** Genetic Algorithm used for the resolution of Problem 1

1: Initialize population $W$ with $n$ random chromosomes $C_i = (P, \lambda_b, \mu_b, \eta)$
2: **repeat**
3: Evaluate fitness of each chromosome in $W$
4: Archive best solutions from $W$ in an archive
5: Evaluate solutions in the archive and remove low-quality ones
6: Select parents from $W$ based on fitness (e.g., roulette wheel selection)
7: Apply genetic operators (e.g., crossover and mutation) to produce offspring
8: Replace least fit individuals in $W$ with offspring to have a new generation
9: **until** Any improvement in 10 generations

To enhance the convergence of GA, the fitness function is constructed using the penalty method. In this method, a penalty term proportional to the degree of violation of constraints ((C1)) (downlink and uplink) and ((C2)) is added to the objective function of 6.4. Constraints (4.41), ((C7)), (4.44) and (4.45) are considered in the nature of chromosome. This ensures that the algorithm can explore values near the boundary of the feasible region of Problem 1.

## 4.3 CONCLUSION

This chapter introduced a system-level framework for SWIPT HetNets and examined two representative deployment geometries. Under a planar PPP model, a non-convex optimization problem, and a related heuristic using GA has been presented. The problem takes into account performance metrics that expose the coupled role of base-station density, transmit power, and receiver-side splitting in determining the energy—information trade-off, causing it to be non-convex by nature due to the dependency coming into the definition of per-bit delay. A second setup proposes a vehicular PLCP model. The introduction of this second scenario support the extension of the results of the first system model, in a more realistic and concrete model, thus addressing the limitations highlighted in Section 4.1.4. Also in this case, the high level of interdependence between parameters lead to a non-convex optimization problem solved thorugh the usage of a GA-based heuristic. Numerical evaluations of the problem is discussed in Chapter 7, together with experimental set-up and major findings.

# 5 NEXT-GEN ENABLERS FOR SWIPT

According to the findings presented in Section 3.2, antenna directivity and beam management emerge as key enablers for SWIPT networks. This section introduces a novel framework for modeling SWIPT systems accounting for the randomness in UEs distribution. In particular, this chapter formalizes the concept of the worst user in Next-Gen SWIPT networks, which fundamentally differs from the traditional definition. Building on this concept, the chapter proposes a new analytical framework to study the effects of beamforming and its intrinsic limitations on energy harvesting performance. Finally, a dynamic programming approach solves the problem of defining the optimal beam definition by taking into account the single UEs distribution.

## 5.1 ANALYSIS AND OPTIMIZATION OF ENERGY-EFFICIENT BEAMFORMING FOR SWIPT NETWORKS

### 5.1.1 *Problem Statement and Motivation*

IoT devices are typically constrained by limited battery capacity, and energy harvesting techniques are paving the way toward more sustainable and reliable communication for such resource-limited systems. At the same time, networks are continuously evolving to support real-time, ultra-low-latency communication. Among the key enablers driving this evolution, beamforming is one of the most significant. However, while beamforming directs power in a specific sector of the coverage area, it does so at the expense of reduced coverage in other parts of the network. When combined with strategic time-switching mechanisms, this technique can become highly effective in next-generation networks, enhancing overall performance. In fact, beamforming is well known to improve the SINR for selected UEs, depending on the beamwidth. Narrow beams provide higher SINR compared to wider beams, despite reduced coverage. Although this trade-off has been exten-

sively studied in communication-centric systems, its implications for SWIPT networks remain largely underexplored.

As introduced in Chapter 4, the spatial distribution, and interference generated by devices existing in the area can be exploited in SWIPT systems. Beamforming, among the others is one of the most relevant, able to increase the coverage area and the power allocated to downlink process, as outlined in Section 3.2. Anyway, despite energy harvesting from beamforming has been proven to be effective, there is no clear indication on how to effective improve the power harvested and how the spatial distribution can affect this process. Wide beams can deliver few power to a greater number of UEs at the same time, while narrowed beam can deliver more power to far users, reducing the coverage area. An important aspect is that device under the beam can harvest the whole power transmitted by the antenna, therefore this lead to non-trivial characterization of the scheduling process.

In this research, I exploit the beamforming capabilities of 5G networks, combined with the NB-IoT protocol, as a means to simultaneously receive information and transmit power to IoT devices. In order to obtain tractable insights, we propose a two-layer framework for energy-efficient SWIPT beamforming: (i) a SG layer capturing spatial uncertainty and identifying robust operating points; (ii) a dynamic programming (DP) layer enabling optimal beam scheduling and resource allocation per frame realization. This analysis reveals that, under realistic densities, the system performance is largely dominated by the worst-case user, whose operating point closely approximates the network average, and that will be used to conduct the analysis under both the assumptions. Overall, this chapter provides a basis for the adaptation in a specific context, with an analysis of the proposed framework from a generic perspective, to enable the system to be implemented in a system where UEs distribution is not known a priori.

The key contributions of this manuscript are:

- Characterization of the worst-case user in a beamforming SWIPT network, and analytical justification, through stochastic geometry, that its performance closely represents the network average.

- Derivation of closed-form expressions for the power-splitting factor required by the worst-case user, establishing the main energy–rate trade-off.
- Design of a dynamic programming framework to optimize beam assignment and resource allocation over time. The non-overlapping case is solved optimally, while a heuristic is proposed for the overlapping NP-hard scenario.

### 5.1.2 *Methodological Approach*

We consider a SWIPT network composed of IoT devices able to harvest RF energy from the downlink signal of a single Base Station (BS). BS leverages beamforming and uses a set of directional beams, scheduling their activation over a frame of duration $\tau$.

The BS covers an area of radius $r_{\max}$, and each user is located at least a distance $r_{\min}$ from the center. For each frame, a set of sectors $\mathcal{S} = \{S_1, ..., S_m\}$ is active. Each active sector has two parameters identifying it $S_i = (\sigma_i, \theta_i)$, where $\sigma_i$ is the sector width and $\theta_i$ is the boresight direction.

IoT devices are distributed across the active sectors of the BS according to a homogeneous PPP $\Phi$ with intensity $\lambda$. The set of IoT devices is denoted by $\mathcal{U} = \{X_1, ..., X_n\}$, with $X_u = (D_u, \Theta_u)$ denoting the distance from the BS, and the azimuth, respectively.

Let us denote the set of users in the sector $b$ as $\mathcal{U}_b = S_b \cap \Phi$, whose cardinality is denoted by $|\mathcal{U}_b|$.

#### 5.1.2.1 *Device-Beam Association Model*

Depending on the sector's size, and their overlapping, one device might be in one or more sectors. Let us denote $\mathcal{B}_u$ the sets of beams covering the device $X_u$, while $S_u$ denotes the beam accepting uplink transmission from device $u$. For analytical tractability, we adopt the classical sectored antenna model [149], which captures the main features relevant to beamforming: directivity gain, half-power beamwidth, and side-lobe leakage. In this model, the antenna gain is constant within the main lobe and equal to a re-

duced constant $z$ in the side lobes. The gain of the antenna for the sector $S_b$, towards the device $X_u$ is:

$$g(S_b, X_u) = \begin{cases} \dfrac{2\pi - (2\pi - \sigma_b)z}{\sigma_b}, & |\theta_b - \theta_u| \leq \frac{\sigma_b}{2}, \\ z, & \text{otherwise.} \end{cases} \tag{5.1}$$

#### 5.1.2.2 *Channel and Energy Harvesting Model*

Transmit power is equal among all the IoT devices, denoted by $p^{up}$, while the BS transmits at transmit power $p^d$. Thermal noise is modeled as AWGN with power spectral density $N_0$ [W/Hz]. The capacity of the uplink channel between device $X_u$ and the BS is given by:

$$C_u = W \log_2(1 + \frac{p^{up} D^{-\alpha}}{N_0}), \tag{5.2}$$

with $W$ denoting the bandwidth.

Regarding the downlink, the received power $P_u$ perceived by the device $X_u$ from the beam $S_i$:

$$P_u \;=\; p^d \, g(S_i, X_u) \, D_u^{-\alpha}, \tag{5.3}$$

with $\alpha$ denoting the path-loss exponent, and $S_i \in \mathcal{B}_u$.

For EH, we adopt the practical sigmoidal model of [21], which captures both the sensitivity, which is the minimal amount of power to activate the EH circuit, and the saturation, which is the maximum amount of RF power that is possible to harvest:

$$h(y) = \max\left\{ \frac{h_{\max}}{e^{-\chi h_s + \iota}} \left( \frac{1 + e^{-\chi h_s + \iota}}{1 + e^{-\chi y + \iota}} - 1 \right), 0 \right\}, \tag{5.4}$$

where $h_{\max}$ is the saturation threshold, $h_s$ the sensitivity threshold, and $\chi, \iota$ are shaping parameters. The power harvested by the device $X_u$ is denoted by $H_u = h(P_u)$.

#### 5.1.2.3 *Resource Allocation Model*

Each device is associated with a beam, depending on the association policy implemented, and will be associated for a total time

$(\gamma_u + \delta_u)$. The device will perceive a total uplink time of $\gamma_u$, while a time $\delta_u$ is devoted to energy harvesting.

The uplink throughput of device $X_u$ is then

$$R_u = \frac{\gamma_u}{\tau} W \log_2(1 + \frac{p^{up} D^{-\alpha}}{N_0}) \tag{5.5}$$

Similarly, assuming that a device can harvest energy for the whole duration of activity of a beam in downlink, both from the one serving the device, plus all the others serving other users but covering its sector, the harvested energy of device $X_u$ in the frame of duration $\tau$ is

$$E_u^{harv} = (\sum_{Z \in S_u \setminus X_u} \delta_z + \delta_u) \frac{H_{u,S_u}}{\tau} + (\sum_{S_i \in \mathcal{B}_u} \sum_{Z \in S_i \setminus S_u} \delta'_u \frac{H_{u,S_i}}{\tau}), \tag{5.6}$$

and the uplink energy consumption is

$$E_u^{cons} = \frac{\gamma_u}{\tau} p^{up}. \tag{5.7}$$

#### 5.1.2.4 *Optimization Problem*

Considering that this work aims to give guidelines on the deployment of beamforming in a SWIPT network, in this section, we provide a problem aiming at optimizing the fairness among the uplink throughput of each user of the network under the energy constraint.

**Problem 5.1.**

$$\max_{\{\sigma_b, \theta_b\}_{b=1}^{B}, A, \gamma_u, \delta_u} \quad \sum_{u \in \mathcal{U}} \log(R_u) \tag{5.8}$$

$$\text{s.t.} \quad E_u^{\text{harv}} \geq E_u^{\text{cons}}, \qquad \forall u \in \mathcal{U}, \tag{5.9}$$

$$\sum_{i=1}^{N} \gamma_u + \delta_u = \tau, \tag{5.10}$$

$$\sum_{i=1}^{N} A_{i*} = 1, \tag{5.11}$$

where $A \in \mathbb{R}^{N \times B}$ denotes the association matrix between users and beams. Constraint (5.22) guarantee that each user has enough energy to support the transmission. Constraint (5.10) guarantees

that the total beams-user association time sum to the total activation time. Constraint (5.24) guarantees that each user is assigned exactly to one beam.

Considering the complexity of the presented problem, it is hard to find an optimal heuristic solving the problem, since the pairs $(\sigma_b, \theta_b)$ can be defined in multiple way, possible evaluating overlapping between beam. To reduce the complexity of the problem I start by evaluating the optimally condition, which may hopefully lead to a reduction of the complexity of the problem.

After eliminating the variables related to the association of users to the beam and postponing this problem, Constraint (5.10) and Constraint(5.24) are equivalent (up to constants independent of the decision variables) to the convex program

$$\max_{\gamma \geq 0,\ \delta \geq 0} \quad \sum_{u \in \mathcal{U}} \log(\gamma_u) \tag{5.12}$$

$$\text{s.t.} \quad \gamma \leq D\,B\,\delta, \tag{5.13}$$

$$\mathbf{1}^\top(\gamma + \delta) = T. \tag{5.14}$$

The objective follows from $\log(R_u) = \log C_u + \log \gamma_u - \log T$ and we drop constants $\sum_u \log C_u - U \log T$.

COMPLEXITY REDUCTION STUDY USING KKT. Let $\lambda \geq 0$ be the multiplier of the energy constraint $\gamma \leq DB\delta$, $\alpha \geq 0$ for $-\gamma \leq 0$, $\beta \geq 0$ for $-\delta \leq 0$, and $\theta \in \mathbb{R}$ for the time budget $\mathbf{1}^\top(\gamma + \delta) = T$. The Lagrangian reads

$$\begin{aligned}\mathcal{L}(\gamma, \delta; \lambda, \alpha, \beta, \theta) = \sum_u \log \gamma_u - \lambda^\top(\gamma - DB\delta) - \alpha^\top(-\gamma) \\ - \beta^\top(-\delta) - \theta(\mathbf{1}^\top(\gamma + \delta) - T).\end{aligned}$$

Stationarity conditions are

$$\partial_\gamma : \quad \frac{1}{\gamma} - \lambda + \alpha - \theta\mathbf{1} = 0 \quad \Longrightarrow \quad \gamma_u = \frac{1}{\lambda_u - \alpha_u + \theta}, \tag{5.15}$$

$$\partial_\delta : \quad -B^\top D\lambda + \beta - \theta\mathbf{1} = 0 \quad \Longrightarrow \quad B^\top D\lambda = \theta\mathbf{1} - \beta. \tag{5.16}$$

Complementary slackness requires

$$\lambda^\top(\gamma - DB\delta) = 0, \qquad \alpha^\top\gamma = 0, \qquad \beta^\top\delta = 0.$$

Because $\log(\gamma_u)$ is strictly increasing, any user whose energy constraint is not tight ($\gamma_u < [DB\delta]_u$) could increase $\gamma_u$ to improve the objective. Hence, at the optimum, the energy constraint is active for those users with $\lambda_u > 0$, while others (with $\lambda_u = 0$) are time-limited. When all users are active (i.e., $\lambda_u > 0$ for every $u$), then $\alpha = 0$ (since $\gamma_u > 0$) and (5.15) simplifies to

$$\gamma_u = \frac{1}{\lambda_u + \theta}, \quad \forall u.$$

Whenever $\delta_b > 0$, $\beta_b = 0$, and (5.16) becomes

$$B^\top D\lambda = \theta \mathbf{1}, \qquad \text{(for active } b\text{)}. \tag{5.17}$$

These relations are consistent with $\lambda > 0$ and $\gamma = DB\delta$ via complementary slackness. In light of these reduction, the system admits a pure reduction in $\delta$ only when the energy constraint is active for every user, i.e.,

$$[DB\,\delta^\star]_u \leq \frac{1}{\theta^\star} \quad \forall u \iff \lambda_u^\star > 0.$$

In this regime, it is possible to substitute $\gamma = DB\,\delta$ in the primal formulation and obtain a single-variable problem:

$$\max_{\delta \geq 0} \quad \sum_{u \in \mathcal{U}} \log((DB\delta)_u), \tag{5.18}$$

$$\text{s.t.} \quad \mathbf{1}^\top((I + DB)\delta) = T. \tag{5.19}$$

Problem (5.18)–(5.19) is strictly concave and has a unique optimum $\delta^\star$ (up to symmetry). The optimal transmission allocation is then $\gamma^\star = DB\,\delta^\star$.

Empirical evaluation with $R_{\max}$ varying between 20 m and 80 m shows that the TDMA equal-time allocation achieves almost identical performance to the optimized $\gamma_u$ obtained from ((5.18)–(5.19)). This behavior arises because, in short-distance regimes typical of SWIPT networks, the harvested energy of the farthest user is comparable to that of nearby users due to harvester saturation effects, which limit energy differentials. Therefore, in what follows, we adopt the TDMA equal-time configuration, which reduces the problem dimensionality by one variable while preserving near-optimal fairness and throughput performance. In particular, we assume a common harvesting duration $\delta_u = \delta$ for

all users, thereby enhancing fairness by improving the minimum harvested energy across users.

**Lemma 5.1.** In a system where the harvesting ratio $\delta_u$ must be the same among all the devices, the optimal $\delta^*$ maximizing the minimum throughput is the one that resolves:

$$\delta^* = \max_{u \in \mathcal{U}} \frac{p^{up}}{p^{up} + E_u^{harv}} \tag{5.20}$$

*Proof of Lemma 5.1.* Because $\delta_u$ is inversely proportional to the achievable throughput and all devices must adopt a common value of $\delta$, the system performance is ultimately constrained by the device that requires the largest value of $\delta_u$ to satisfy its energy neutrality condition. Therefore, maximizing the minimum throughput is equivalent to minimizing the $\delta_u$ corresponding to the device with the highest one. This can be equivalently expressed as:

$$\begin{aligned} &\max_{u \in \mathcal{U}} \quad \min \delta_u \\ &\text{s.t.} \quad E_u^{\text{harv}} \geq E_u^{\text{cons}}, \quad \forall u \in \mathcal{U}. \end{aligned}$$

Assuming that $\delta_u$ is identical across all devices, Equation (5.6) can be simplified as:

$$E_u^{\text{harv}} = \frac{\delta_u |\mathcal{B}_u|}{\tau} H_u.$$

Considering the Constraint (5.22), and recalling that increasing $\delta_u$ leads to a decrease in throughput, we can identify the worst-case $\delta_u$ as the highest value among all the devices that satisfies the equality (minimum satisfying the inequality) in Constraint (5.22). Consequently, the optimal (common) value of $\delta$ for the entire set of devices is given by:

$$\delta^* = \max_{u \in \mathcal{U}} \frac{p^{\text{up}}}{p^{\text{up}} + E_u^{harv}}.$$

□

By combining those results, it is possible now to present the final problem as sole function of the beam width and user allocation.

**Problem 5.2.**

$$\min_{\{\sigma_b,\theta_b\}_{b=1}^{B},A} \quad \max_{u\in\mathcal{U}} \frac{p^{up}}{p^{up}+E_u^{harv}} \tag{5.21}$$

$$\text{s.t.} \quad E_u^{\text{harv}} \geq E_u^{\text{cons}}, \qquad \forall u \in \mathcal{U}, \tag{5.22}$$

$$\tag{5.23}$$

$$\sum_{i=1}^{N} A_{i*} = 1, \tag{5.24}$$

### 5.1.3 *Dynamic Optimization Framework*

An effective way to solve the optimization problem proposed in the previous section is to consider a dynamic programming-based approach. First, it is needed to order the users by their angular coordinate, by cutting the circle in a given $\theta_u$, $\theta_1 < \theta_2 < \cdots < \theta_n$ and seek a partition of $\{1,\dots,n\}$ into at most $K$ contiguous blocks, each block served by a single non-overlapping beam. Let $w(i,j)$ denote the cost of covering users $i,\dots,j$ with one beam, considering the order starting in $\theta_u$:

$$w(\theta_u,i,j) = \max_{u_i,u_{i+1},\cdots,u_j\in\mathcal{U}(\theta_u)} \delta_u, \tag{5.25}$$

and

$$w(i,j) = \min_{u\in\mathcal{U}} w(\theta_u,i,j), \forall i,j \in |\mathcal{U}|. \tag{5.26}$$

For a given number of beams $K$, the goal is to minimize the cost for covering all the users using at maximum $K$ beams. Let us define $F(t,m)$ as the optimal objective value for covering the first $t$ users with exactly $m$ contiguous blocks. The dynamic program is:

$$F(t,1) = w(1,t), \qquad 1 \leq t \leq n, \tag{5.27}$$

$$F(t,m) = \min_{m-1\leq j<t}\{F(j,m-1)+w(j+1,t)\}, \qquad 2 \leq m \leq K,\ m \leq t \leq n. \tag{5.28}$$

The optimal value with up to $K$ beams is

$$V^* = \min_{1\leq m\leq K} F(n,m). \tag{5.29}$$

We keep back-pointers $J(t,m)$ achieving the minimum in (5.28) to reconstruct the partition.

**Lemma 5.2** (Optimality)**.** For all $t$ and $m \geq 1$, the recursion (5.27)–(5.28) yields the optimal partition of $\{1, \dots, t\}$ into $m$ contiguous blocks minimizing the maximum block cost.

*Sketch.* Induction on $(t, m)$. The base case $m = 1$ is trivial: one block must cover all $1{:}t$ users with cost $w(1, t)$. For the inductive step, consider an optimal $m$-block solution whose last block is $[j + 1, t]$. By optimal substructure, the prefix $\{1, \dots, j\}$ must be an optimal $(m-1)$-block solution, hence $F(j, m-1)$. Minimizing over all admissible cut points $j$ gives (5.28). □

#### 5.1.3.1 *Complexity and Implementation*

The DP can be computed in $O(n^2K)$ time and $O(nK)$ memory. If $w(i, j)$ admits $O(1)$ evaluation from prefix summaries (e.g., maxima/averages of per-user quantities), the overall complexity remains $O(n^2K)$. *Optional speedups.* If $w$ satisfies monotone-queue or quadrangle inequalities, divide-and-conquer or SMAWK optimizations can reduce runtime; this is problem-dependent and omitted here for brevity.

#### 5.1.3.2 *Heuristic Extension to Overlapping Beams*

The provided optimization problem is hard to solve in a overlapping scenario (*e.g.* when beams overlaps over the same region) for multiple motivations, where one of those is the association policy. In fact, a UE may be covered by multiple beam, but it is not clear weather such a user is going to associate, hence, to transmit, when one or the other beam is active. This creates an NP-hard problem, and a practical heuristic is to compute the non-overlapping optimum via the DP above, then iteratively insert auxiliary beams around the largest inter-block boundaries (angular bisectors) where $w(j, j{+}1)$ is high, re-evaluating costs locally. This improves robustness near boundaries while keeping the computational load modest. An analysis of this heuristic is provided in the results section.

### 5.1.4 *Analytical Modeling*

Despite providing the optimal solution, the proposed formulation does not account for the randomness of the UE distribution, which is the typical case in practical scenarios where the network operator must deploy a BS without any a priori knowledge of the environment—except for the expected UE density. To analyze the randomness of the space, and characterize system-level performance let me consider a scenario where UEs are distributed according to a homogeneous PPP of intensity $\lambda_u$ over a circular coverage area with inner radius $r_{\min}$ and outer radius $r_{\max}$. Therefore, the average number of UEs in an active beam is:

$$\Lambda = \lambda_u \frac{\sigma_b}{2} (r_{\max}^2 - r_{\min}^2). \tag{5.30}$$

According to the system model, $m$ beams of equal width $\sigma_b$ are active for performing both energy transmission and data receiving from the node. A fraction of beam time denoted as $\delta$, equal for all the beams, is used for energy transmission. Time is split among devices using a TDMA equal-time approach; hence, each device has equal data transmission and energy receiving time. The aim of this work is to characterize the performance perceived by a typical user under the energy constraints of the whole system. We define this expectation as

$$\mathbb{E}[C_{avg}] = \int_{r_{\min}}^{r_{\max}} f_D(d)\, \mathbb{E}[C \mid D = d]\, \mathrm{d}d, \tag{5.31}$$

where $f_D(d)$ is the PDF of the distance of the typical UE from the center of the disk, which is:

$$f_D(d) = \frac{2d}{r_{max}^2 - r_{min}^2}. \tag{5.32}$$

By Slivnyak's theorem, conditioning on a typical UE at distance $d$ does not affect the distribution of the other UEs. Let $N \sim \text{Poisson}(m\Lambda)$ be the number of other UEs in the system; then the total number in the system, including the typical one is $1 + N$. The expected uplink throughput of the typical UE can then be expressed as

$$\mathbb{E}[C \mid D = d] = \mathbb{E}\left[\frac{1-\delta^*}{N+1}\right] W \log_2\Big(1 + \frac{P_{IoT} d^{-\alpha}}{N_0}\Big), \tag{5.33}$$

where $\delta^*$ is the fraction of time devoted to energy transfer, determined by the worst-case user in the system.

$$\mathbb{E}\left[\frac{1-\delta^*}{N+1}\right] \approx (1-\mathbb{E}[\delta^*])\,\mathbb{E}\left[\frac{1}{N+1}\right], \tag{5.34}$$

with

$$\mathbb{E}\left[\frac{1}{N+1}\right] = \frac{1-e^{-m\Lambda}}{m\Lambda}. \tag{5.35}$$

The definition of the worst user, which determines the value of $\delta^*$ must take into account two aspects: (1) the user furthest away in the radius, as in traditional systems, and (2) number of users in the beam. This second aspect, positively impact the energy harvested by a device, since we are considering the case in which devices can harvest energy for the whole duration of beam activity for energy transmission.

**Lemma 5.3.** The ratio $\delta^*$ denoting the fraction of time spent by the worst-case user in harvesting energy in a beamforming BS is given by the following expectation. In what follows I refer to $\delta^*$ as:

$$\delta^* = f(y) = \frac{P_{\text{IoT}}}{P_{\text{IoT}} + y}, \tag{5.36}$$

where $y(u,b) = N_b(u)\Theta(P_b(r_u, \theta_u, \theta_b, \sigma_b))$ and $N_b(\cdot)$ indicates the number of users in the same beam as the device $u$, which is a random variable, resulting from the PPP. The the derivation of $\mathbb{E}[\delta^*]$ is presented in Equation (5.37),

with

$$p = 1 - e^{-\Lambda}, \tag{5.38}$$

denoting the probability of having at least one user in the beam (which follows from the definition of active beam), and $\Theta^{-1}(\cdot)$ denotes the inverse of the sigmoidal function of energy harvested, used to determine at which distance corresponds the amount of energy harvested.

*Derivation of Lemma 5.3.* We aim to evaluate the expected value of $\delta$ for the worst case device, $\mathbb{E}[\delta^*] = \mathbb{E}[\max_{u\in U} \delta_u]$, where $\delta_u =$

$$
\begin{aligned}
\mathbb{E}[\delta^*] &= \mathbb{E}[\max_{u \in ll} \delta_u] \\
&= 1 - \int_0^\infty \frac{P_{IoT}}{(P_{IoT}+y)^2} P(Y > y) dy \\
&= 1 - \int_0^\infty \frac{P_{IoT}}{(P_{IoT}+y)^2} \times \\
&\times \sum_{k=1}^{m} \mathbb{P}(K = k) \mathbb{P}(N_b(u)\Theta_{b,u} > y | K = k) dy \\
&= 1 - \int_0^\infty \frac{P_{IoT}}{(P_{IoT}+y)^2} \sum_{k=1}^{m} \binom{m}{k} p^k (1-p)^{m-k} \times \\
&[\sum_{n=1}^{\infty} \mathbb{P}(N_b(u) = n) \mathbb{P}(\Theta_{b,u} > \frac{y}{n} | N_b(u) = n)]^k dy \\
&= 1 - \int_0^\infty \frac{P_{IoT}}{(P_{IoT}+y)^2} \sum_{k=1}^{m} \binom{m}{k} p^k (1-p)^{m-k} \\
&\left[ \sum_{n=1}^{\infty} \frac{e^{-\Lambda} \Lambda^n}{n!} [F_D(\Theta_{b,u}^{-1}(\frac{y}{n})]^n \right]^k dy
\end{aligned}
\tag{5.37}
$$

$\frac{P_{\text{IoT}}}{P_{\text{IoT}}+Y_u}$ and $Y_u = N_b(u)\Theta(P_b(r_u, \theta_u, \theta_b, \sigma_b))$ represents the power harvested for device $u$.

A useful approach to compute the expectation of a function of a non-negative random variable is through the identity:

$$\mathbb{E}[g(Y_{\min})] = g(0) + \int_0^\infty g'(y) \mathbb{P}(Y > y) dy.$$

Applying this to $g(y) = \frac{P_{\text{IoT}}}{P_{\text{IoT}}+y}$, with $g(0) = 1$ and $g'(y) = -\frac{P_{\text{IoT}}}{(P_{\text{IoT}}+y)^2}$, we obtain:

$$\mathbb{E}[\delta^*] = 1 - \int_0^\infty \frac{P_{\text{IoT}}}{(P_{\text{IoT}}+y)^2} \mathbb{P}(Y > y) dy,$$

which justifies the first step.

The event $\{Y > y\}$ corresponds to the event that all the users in all the active beam receive sufficient energy, i.e., the threshold $y$ is exceeded in every active beam (note that if the beam does not contain any user, then it is denoted as non-active). Let $K$ denote

the number of active beams, where a beam is active if it contains at least one user. Since users are distributed according to a PPP with intensity $\Lambda$ for each beam, the probability that a beam is active is $p = \mathbb{P}(n_b \geq 1) = 1 - e^{-\Lambda}$. Thus, the probability of a user in being in a beam is binomial, therefore $K \sim \text{Binomial}(m, p)$.

By the law of total probability, we condition on the number of active beams $K$:

$$\mathbb{P}(Y > y) = \sum_{k=1}^{m} \mathbb{P}(K = k)\mathbb{P}(Y > y \mid K = k).$$

Given $K = k$, the event $\{Y > y\}$ requires that the energy harvested condition holds in all the users in all the $k$ active beams. Assuming independence across beams, this probability becomes $[\mathbb{P}(n_b\Theta_b > y]^k$. Therefore,

$$\mathbb{P}(Y > y) = \sum_{k=1}^{m} \binom{m}{k} p^k (1-p)^{m-k} [\mathbb{P}(n_b\Theta_b > y)]^k.$$

We now analyze $\mathbb{P}(n_b\Theta_b > y)$. Considering that all users in the beam must satisfy the energy harvesting condition, and by applying the law of total probability, we have:

$$\mathbb{P}(n_b\Theta_b > y) = \sum_{n=1}^{\infty} \mathbb{P}(N_b = n) \times \mathbb{P}(n_b\Theta_b > y \mid N_b = n).$$

Since $N_b \sim \text{Poisson}(\Lambda)$, and given $N_b = n$, the condition $n_b(u)\Theta_b > y$ requires that $\Theta_b > \frac{y}{n_b(u)}$ for all $n$ users.

Since the only varying factor in $\Theta(\cdot)$ is the distance of the user from the BS, and since users' locations are independent under the PPP assumption, the probability is

$$\mathbb{P}(n_b\Theta_b > y \mid N_b = n) = [F_D\Big(\Theta^{-1}\Big(\tfrac{y}{n_b(u)}\Big)\Big)]^n,$$

where $F_D(\cdot)$ is the cumulative distribution function of the user distance.

Substituting this expression back into the decomposition of $\mathbb{P}(n_b\Theta_b > y)$, and then into the expansion of $\mathbb{P}(Y > y)$, we obtain a closed characterization of the survival function in terms of the spatial

distribution of users. Finally, plugging this into the integral representation of $\mathbb{E}[\delta^*]$ yields the desired expression, which concludes the proof.

□

## 5.2 CONCLUSION

This chapter presented a two-level approach for the characterization of the typical user performance under the constraint of worst-case satisfactory energy harvesting. The strength of this contribution lies in its ability to capture both an optimal scheduling algorithm for beamforming, adapted to a specific realization of the UE spatial distribution, and a more general analytical framework that supports the random distribution of UEs. The first part of the chapter introduced the general optimization problem, involving five optimization variables related to beamforming design and allocation policies. By applying the KKT optimality conditions, the problem was reduced to a simplified form depending only on three variables, associated with the beamforming design and the user–beam association. This reduction enabled the evaluation of each network realization with a computational complexity of $O(n^2K)$, providing an optimal solution to the non-overlapping beamforming case. To address the randomness of UE locations, the second major contribution, the chapter further modeled the stochastic nature of the user spatial distribution, deriving a closed-form expression for the expected worst-case user performance. Together, these two approaches establish a framework for the design and optimization of beamforming in SWIPT networks. Numerical evaluations of the proposed approach, along with the experimental setup and main findings, are discussed in Chapter 8.

# 6 OPTIMIZING USER TRANSMISSION POLICIES IN SWIPT NETWORKS

According to gap found in the literature, this chapter discusses potential device-side policies to enhance the efficacy of EH process. In particular, acknowledging the impact of energy drained for data transmission, this chapter discusses two different policies, function of the context where SWIPT is deployed. The first contribution is relevant for real-time systems, where information freshness is a challenge, therefore trying to reduce AoI while adopting strategic policy in a two node network. The second contribution is relevant for non-critical systems, where information freshness is not relevant. In particular, an energy optimitazion problem is formulated, taking into account the load shifting policies on the device-side. Both first and second contributions reveal non-trivial patterns on which is the best policy in both context, while taking into account the existence of other class of non-EH nodes.

## 6.1 THE OPTIMAL AGE OF INFORMATION POLICY

This first contribution considers a two-node network, representative of an heterogeneous network, where IoT devices are interested in reducing AoI, while non-EH nodes are interested in mantaining a decent QoS, as function of their queue stability. Results reveal an interesting pattern on the best strategy to adopt.

### 6.1.1 *Problem Statement and Motivation*

Data sensing is expanding its use case thanks to the adoption of EH into wireless communication and through the usage of low-power communication protocols [130]. EH-enabled infrastructures are able to deliver the power devices need for the transmission, increasing the lifespan of these off-grid device deployments [1, 72].

EH also makes possible the deployment of scenarios where battery replacement is impractical [52]. The usage of EH techniques is subject to a trade-off between information transmission reliability and energy consumption since low-power transmission significantly reduces the probability of successful data delivery due to interference. This directly correlate with two effects: waste of harvested energy without accomplishing effective communication, and an exponential increase in time elapsed between two consecutive successful transmissions.

In real-time systems, these effects are much more critical, just thinking to medical devices, or real-time actuators. When extending the discussion to heterogeneous networks, the situation becomes even more complex due to the coexistence of diverse device types (*e.g., EH vs. non-EH nodes*), each with distinct QoS requirements. To investigate these dynamics and the optimal transmission strategies adopted, an investigation on the role of two classes of devices in a typical EH-enabled heterogeneous network is proposed. The effect of this two-node network, competing over a shared wireless medium and affected by interference, directly impacts the best parameter choices. The key contributions are:

- Development of a system model comprising two heterogeneous devices with variable transmission power levels. The model characterizes the probability of successful transmission as a function of the activation state of the other node, thereby capturing the mutual interference and dynamic interaction between the devices.

- Formulation of a constrained optimization problem to minimize the long-term average AoI at the EH-node, subject to queue stability at the energy-supply node by highlighting the dependence between the transmission power of the non-EH node and different operating regimes.

- Analysis of emergent phenomena, such as flat regions in optimal transmit power, which provide new insights for practical network design.

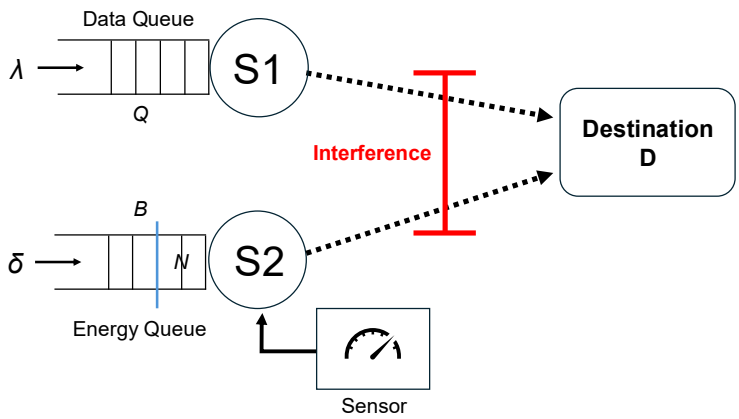


Figure 6.1: System model characterized by a grid-powered device $S_1$ with a data queue $Q(t)$, and an energy-harvesting device $S_2$ equipped with an energy buffer $B(t)$. Interference arises when both nodes transmit simultaneously to the destination $D$.

### 6.1.2 *Methodological Approach*

#### 6.1.2.1 *Preliminary Analysis*

Let us consider a system composed of two nodes, as depicted in Fig. 6.1, denoted as $S_1$ and $S_2$, both communicating with a common destination node $D$.

The first node, $S_1$, is a grid-powered device with an unlimited energy supply. Data packets arrive at $S_1$ in each time slot $t$, following a Bernoulli process $a_1(t)$, and are stored in an infinite-capacity data queue. The second class, $S_2$, consists of battery-constrained devices equipped with an EH module, capable of harvesting energy from ambient RF, whose harvesting rate can be represented by a Bernoulli process $a_2(t)$. $S_2$ can store energy in a battery of capacity $B_{\max}$, with battery state denoted by $B(t)$ at time $t$. Node $S_2$ follows a *generate-at-will* policy, namely, it waits for the accumulation of $N$ energy units and then tries to access the channel with a given probability. For each packet transmission, at least $N$ energy

units are needed; hence, each transmission consumes exactly $N$ energy units, independently of the success of that transmission.

#### 6.1.2.2 *Transmission and Queue Modeling*

Both $S_1$ and $S_2$ follow a decentralized, probabilistic channel access model. Each node makes transmission decisions independently, on the basis of its internal state. Time is slotted and synchronized across all nodes. Device $S_1$ is equipped with a data queue, while device $S_2$ is equipped with an energy queue. The data queue at $S_1$ evolves as:

$$Q(t+1) = \max[Q(t) - b_1(t), 0] + a_1(t), \tag{6.1}$$

where $b_1(t) = 1$ if the packet transmitted by $S_1$ in time slot $t$ is successfully received, and $b_1(t) = 0$ otherwise. The system adopts an instantaneous ACK feedback from the destination at the end of each slot, hence causing the retransmission of a packet in case of a negative ACK.

Considering the particular behaviour of energy storage at node $S_2$, where states do not follow a traditional birth-death process, a Markov chain which captures the state transitions is needed. Let us consider a Discrete-Time Markov Chain (DTMC) with state space $\beta = \{0, 1, 2, ..., B\}$. Denoting by $\kappa$ the state of the energy buffer, and with $\delta$ the energy arrival probability, and $q_2$ the channel access probability; then the buffer state has the following transitions:

- If $\kappa \in [0, N-1]$, the energy storage cannot support any transmission, and so only two possible state transitions are avaialble:
  1. $\kappa \to \kappa + 1$: If there is an energy arrival, which happens with probability $\delta$
  2. $\kappa \to \kappa$: If there is no energy arrival, which happens with probability $1 - \delta$
- If $\kappa \in [N, B-1]$, there are four possible transitions:
  1. $\kappa \to \kappa$: If the device does not perform a data update and no energy arrives; this is done with probability $(1-\delta)(1-q_2)$.
  2. $\kappa \to \kappa + 1$: If the device does not perform a data update but receives energy; this is done with probability $\delta(1-q_2)$.

3. $\kappa \to \kappa - N$: If the device does not receive energy but performs a data update; this is done with probability $(1 - \delta)q_2$.
4. $\kappa \to \kappa - N + 1$: If the device both receives energy and performs a data update; this is done with probability $\delta q_2$.

- If $\kappa = B$, there are three possible transitions:
  1. $\kappa \to \kappa$: If the device does not perform energy update, independently by the energy arrival; this happens with probability $(1 - q_2)$.
  2. $\kappa \to \kappa - N$: If the device does not receive energy but performs a data update; this is done with probability $(1 - \delta)q_2$.
  3. $\kappa \to \kappa - N + 1$: If the device both receives energy and performs a data update; this is done with probability $\delta q_2$.

Considering the complexity of this DTMC, which leads to complicate derivation, already investigated in [167], let us consider the case of an infinite energy buffer ($B \to \infty$). This abstraction, also adopted in prior works such as [26, 167], is justified for a variety of practical IoT scenarios in which EH nodes transmit short packets at a low rate and the energy per transmission is negligible compared to the storage capacity of modern supercapacitors or high-density microbatteries. In such contexts, the risk of energy overflow is minimal, and the system is primarily constrained by energy arrival and access policies, not by buffer size. Therefore, the energy queue of node $S_2$ evolves according to:

$$B(t+1) = \max\left[B(t) - N \cdot u_2(t), 0\right] + a_2(t), \tag{6.2}$$

where $a_2(t) \in \{0, 1\}$ denotes the harvested energy units in time slot $t$, and $u_2(t) \in \{0, 1\}$ denotes transmit attempts of a status update in time slot $t$ from node $S_2$. The respective expected values of queues are denoted by $\lambda = \mathbb{E}[a_1(t)]$ and $\delta = \mathbb{E}[a_2(t)]$.

Table 6.1: Main notation used in Section 6.1.

| Symbol | Description |
|---|---|
| $q_i$ | Access probability of node $S_i$ |
| $P_i$ | Transmit power of node $S_i$ |
| $N$ | Energy units consumed per transmission by $S_2$ |
| $\lambda$ | Packet arrival rate at node $S_1$ |
| $\delta$ | Energy arrival rate at node $S_2$ |
| $\mu$ | Service rate of node $S_1$ |
| $\mathbb{P}[B(t) \geq N]$ | Probability $S_2$ has enough energy to transmit |
| $p_{i,i}$ | Success probability of $S_i$ without interference |
| $p_{i,j}$ | Success probability of $S_i$ under interference from $S_j$ |
| $\bar{p}_2$ | Average success probability of $S_2$ |
| $\bar{\Delta}$ | Average Age of Information at $S_2$ |
| $\mathbb{E}[T]$ | Mean inter-update time of $S_2$ |
| $\mathbb{E}[T^2]$ | Second moment of inter-update time |
| $T_E$ | Time to accumulate enough energy for supporting a transmission |
| $T_A$ | Time to attempt access |
| $R_t$ | Target rate for decoding |
| $c_N$ | Blocklength (bits) used by $S_2$ |
| $\varepsilon$ | Block decoding error probability |

Additionally, the interference from node $S_1$ creates a coupling effect that indirectly influences battery usage efficiency through governing parameters $(\delta, N)$, since more energy is needed for a successful transmission under interference environments.

To this end, two different regimes are considered: Energy-Constrained Regime (ECR) where $q_2 N > \delta$, hence, the energy consumption

rate exceeds the harvesting rate, leading to potential energy outages that affect transmission opportunities; and Energy-Sufficient Regime (ESR) where $q_2 N \leq \delta$, and energy is sufficient for starting the transmission. Distinguishing between ECR and ESR is needed to capture the impact of energy availability on system performance. Such a distinction is key to understanding how energy dynamics affect information freshness and to identifying the optimal transmission strategies under varying interference and traffic scenarios.

An important metric, that will be leveraged later on in this section, it the probability of holding enough energy. As outlined in Equation 6.12, which exhibit the same formula presented in [167], this can be simplified for scenario where $B \to \infty$.

$$\begin{aligned}\mathbb{P}[B(t) \geq N] = \rho(N, q_2, \delta, B) &= \sum_{i=N}^{B} \frac{\delta(1-z)z^{i-N}}{Nq_2} \\ &= \frac{\delta(1-z)(1-z^{B-N+1})}{Nq_2(1-z)} = \frac{\delta}{Nq_2}, \end{aligned} \tag{6.3}$$

with

$$(1-\delta)q_2 z^{N+1} + \delta q_2 z^N - (1-(1-\delta)(1-q_2))z + \delta(1-q_2) = 0,$$

By taking only the root in the region $z \in \{0, 1\}$, which are the only valid solutions.

#### 6.1.2.3 *Physical Model*

Both nodes transmit to a common destination node $D$ that supports multi-packet reception (MPR). That is, $D$ can successfully decode multiple simultaneous transmissions, provided their received SINR exceeds a certain threshold. Considering different battery setup, two different transmit power habe been considered, denoted by $P_1$, and $P_2$ respectively for node $S_1$ and node $S_2$.

Since node $S_2$ is the energy harvesting node, and its power consumption is $N$ if the node tries to access the channel, then $P_2 = Ne_{\min}$, where $e_{\min}$ represent the minimal amount of energy consumed for transmission. By setting it to 1mW (typical for IoT context), a minimal transmit power for node will be $S_2 = 0$dBm.

A block-fading channel model is adopted: channel gains remain constant over one time slot and change independently across slots. The received SINR for the node $S_i$ is given by

$$\mathrm{SINR}_{S_i} = \frac{|h_i|^2 \beta_i P_i}{1 + \sum_{j \in \mathcal{A} \setminus \{i\}} |h_j|^2 \beta_j P_j}, \tag{6.4}$$

where:

- $\mathcal{A}$ is the set of active transmitters,
- $|h_i|^2 \sim \mathrm{Exp}(1)$ is the small-scale fading (Rayleigh) for user $i$,
- $\beta_i$ is the large-scale fading coefficient for user $i$,
- Noise is normalized
- $P_i$ is the transmit power of node $i$

$p_{i,i}$ denotes the success probability for $S_i$ when it transmits alone, and $p_{i,j}$ when both $S_i$ and $S_j$ transmit simultaneously. Denoting the SINR threshold for successful decoding at the destination from the transmission of node $S_1$ as $\theta_1$, then success transmission probabilities can be expressed as:

$$p_{1,1} = \mathbb{P}\{\mathrm{SNR}_1 \geq \theta_1\} = \exp\left(-\frac{\theta_1}{\beta_1 P_1}\right), \tag{6.5}$$

$$p_{1,2} = \mathbb{P}\{\mathrm{SINR}_1 \geq \theta_1\} = \frac{\exp\left(-\frac{\theta_1}{\beta_1 P_1}\right)}{1 + \theta_1 \cdot \frac{\beta_2 P_2}{\beta_1 P_1}}. \tag{6.6}$$

These probabilities are valid for node $S_1$, which is always able to guarantee a satisfying coding rate, while they cannot be used for energy-constrained devices. For this reason the concept of finite blocklength is used for nodes $S_2$; thus characterizing the nature of shortcode transmission in RAN. Every codeword is constructed of $k$-bit information batches, and the information coding rate is a function of code length $c_N = Nk$ and a frame error rate of $\epsilon$. If the packet transmission of node $S_2$ is stipulated with a block length $c_N$, each source node encodes its data packet in a

codeword of length $c_N$, consuming $N$ units of energy for the transmission. On the receiver side, if the codeword exceeds a constant target rate $R_t$, the codeword is decoded correctly with probability larger or equal to $\epsilon$, otherwise the transmission fails. For this reason, the success transmission probabilities have been adapt to $p_{2,2}$ and $p_{2,1}$ as follow:

$$p_{2,2} = \mathbb{P}\{\mathrm{SNR}_2 \geq \theta_{N,\epsilon}\} = (1-\epsilon)\exp(-\frac{\theta_{N,\epsilon}}{\beta_2 P_2}), \tag{6.7}$$

$$p_{2,1} = \mathbb{P}\{\mathrm{SINR}_2 \geq \theta_{N,\epsilon}\} = (1-\epsilon)\frac{\exp(-\frac{\theta_{N,\epsilon}}{\beta_2 P_2})}{1+\theta_{N,\epsilon}\cdot\frac{\beta_1 P_1}{\beta_2 P_2}}, \tag{6.8}$$

with

$$\log_2(1+\theta_{N,\epsilon}) + \frac{\log_2(c_N)}{2c_N} - \frac{\log_2(e)Q^{-1}(\epsilon)}{\sqrt{c_N}}\times$$
$$\times\sqrt{\frac{(1+\theta_{N,\epsilon})^2-1}{(1+\theta_{N,\epsilon})^2}} = R_t, \tag{6.9}$$

derived from the definition of maximum coding length in the finite blocklength regime [110].

#### 6.1.2.4 *System Model*

In this section, I provide the definitions that describe the behavior of the heterogeneous nodes, their interactions, and the key performance metrics of interest. Analytical expressions derived from these definitions will be presented in the second part of this section. To model the interaction between the two heterogeneous nodes, I employ a probabilistic random access policy, which is particularly well-suited for the uncoordinated nature of our two-node network. The access behavior is defined as follows:

1. Node $S_1$, which maintains a data queue, attempts to transmit a packet to the destination with probability $q_1$, provided its queue is non-empty.

2. Node $S_2$, powered via energy harvesting, initiates a status update with probability $q_2$ when its energy buffer contains at least $N$ energy units. Upon activation, it consumes all $N$ units to perform the transmission.

The decision-making processes of the two nodes are statistically independent and do not require mutual coordination, thus reflecting a decentralized and scalable design suitable for heterogeneous and resource-constrained environments.

To begin our analysis, I evaluated the stability condition at node $S_1$ and then the performance metric for node $S_2$. The stability condition for the data queue at node $S_1$ is that the average service rate $\mu$ must be greater than the arrival rate $\lambda$. The service rate $\mu$ is defined as the expected probability of successful transmission, which includes the following three cases:

(1) Node $S_2$ does not have enough energy to transmit.

(2) Node $S_2$ has enough energy but does not access the channel.

(3) Both nodes transmit simultaneously, generating interference.

Accordingly, the average service rate $\mu$ is given by:

$$\begin{aligned}\mu = &(1 - \mathbb{P}[B(t) \geq N])q_1 p_{1,1} \\ &+ \mathbb{P}[B(t) \geq N]q_1(1 - q_2)p_{1,1} \\ &+ \mathbb{P}[B(t) \geq N]q_1 q_2 p_{1,2},\end{aligned} \tag{6.10}$$

where $\mathbb{P}[B(t) \geq N]$ represents the probability that node $S_2$ has sufficient energy to attempt a transmission.

Queue stability implies a finite average queuing delay. When the queue at $S_1$ is stable, $Q(t)$ admits a unique stationary distribution. The probability that the queue is non-empty is given by:

$$\mathbb{P}[Q(t) \neq 0] = \frac{\lambda}{\mu}. \tag{6.11}$$

Having defined the conditions for queue stability at node $S_1$, which strictly depends on $\mathbb{P}[B(t) \geq N]$), I can get insights about this quantity by looking at the two different situations. Following

the same line of derivation presented in [167] for defining the probability of having enough energy for the transmission as:

$$\mathbb{P}[B(t) \geq N] = \frac{\delta}{Nq_2}. \tag{6.12}$$

Conversely, in ESR, the node harvests energy faster than it consumes, ensuring sufficient energy for transmission whenever needed, so that the probability will be equal to 1 when the system is in a steady state.

#### 6.1.2.5 *Stability Analysis of Data Queue of $S_1$*

The stability analysis of the data queue at node $S_1$ can be performed under two operational regimes described in the previous section. For each case, we derive the corresponding queue stability condition as a function of the transmission probability $q_1$. This formulation enables us to explicitly characterize the conditions under which the queue at node $S_1$ remains stable, providing insight into the interplay between access probabilities and the influence of heterogeneous network dynamics.

*Energy Constrained Regime* (*ECR*). In the energy-constrained regime (ECR), where $q_2 N > \delta$, the energy harvesting process is sufficiently active to ensure that the underlying Markov chain governing the energy queue of node $S_2$ is positive recurrent. Under this condition, the probability of having sufficient energy for transmission at node $S_2$ can be modeled using Equation (6.12).

In this scenario, the stability condition for the data queue at node $S_1$ is expressed as:

$$q_1 > \frac{N\lambda}{Np_{1,1} - \delta p_{1,1} + \delta p_{1,2}}, \tag{6.13}$$

where $\lambda$ is the arrival rate of packets at $S_1$, and $p_{1,1}$ and $p_{1,2}$ denote the successful transmission probabilities of $S_1$ when $S_2$ is inactive and active, respectively.

**Remark 6.1.** In the energy-constrained regime, the stability condition of node $S_1$'s data queue is independent of the access probability $q_2$ of node $S_2$. Specifically, it depends solely on the energy consumption level $N$ and the transmission power (via $p_{1,1}$ and $p_{1,2}$) of node $S_2$.

*Energy Sufficient Regime* (*ESR*). In ESR $\mathbb{P}[B(t) \geq N] = 1$, since the node $S_2$ always has enough energy for the transmission of data updates. For this reason, the probability of transmission success presented in (6.10) is simplified as

$$\mu = q_1((1 - q_2)p_{1,1} + q_2 p_{1,2}), \tag{6.14}$$

and consequentially the stability condition for node $S_1$ in ESR is

$$q_1 > \frac{\lambda}{(1 - q_2)p_{1,1} + q_2 p_{1,2}}, \tag{6.15}$$

#### 6.1.2.6 *Long-time Average Age of Information of $S_2$*

The AoI at time $t$ is defined as the time elapsed since the most recently received status update was generated by the source, that is,

$$\Delta(t) = t - u(t), \tag{6.16}$$

where $u(t)$ denotes the time at which the most recently received packet was generated.

The average AoI over a long time horizon $[0, T]$ is then given by

$$\bar{\Delta} = \lim_{T \to \infty} \frac{1}{T} \int_0^T \Delta(t)\, dt. \tag{6.17}$$

In our model, the evolution of AoI is determined by the inter-update time $T$ (i.e., the time between two successful update deliveries from node $S_2$ to the destination), which is a random variable due to the stochastic nature of both energy arrivals and access attempts. Under renewal-based models, where inter-update times are independent and identically distributed, the average AoI admits a closed-form expression as

$$\bar{\Delta} = \lim_{N \to \infty} \Delta_N = \frac{\mathbb{E}[T^2]}{2\mathbb{E}[T]} + \frac{\mathbb{E}[T](1 - \bar{p}_2)}{\bar{p}_2} + \frac{1}{2}, \tag{6.18}$$

where:

- $\mathbb{E}[T]$ is the average time between two consecutive update transmissions from $S_2$,

- $\mathbb{E}[T^2]$ is its second moment,
- $\bar{p}_2$ is the average success probability of a transmission attempt by node $S_2$, accounting for interference from $S_1$.

Similarly to what I defined for the node $S_1$, and by using the definition of non-empty queue of node $S_1$, it is possible to define the successful transmission probability of node $S_2$ as:

$$\begin{aligned}\bar{p}_2 &= p_{2,2}(1 - q_1\mathbb{P}[Q(t) \neq 0]) + p_{2,1}q_1\mathbb{P}[Q(t) \neq 0] \\ &= p_{2,2}(1 - q_1\frac{\lambda}{\mu}) + p_{2,1}q_1\frac{\lambda}{\mu},\end{aligned} \tag{6.19}$$

which corresponds to the sum of the probability of not having the node $S_1$ transmitting, plus the probability of having the node $S_2$ transmitting with the interference from node $S_1$.

The total inter-update time $T$ can be decomposed into two independent components:

- $\mathbb{E}[T_E]$: the waiting time to accumulate enough energy for a transmission,
- $\mathbb{E}[T_A]$: the waiting time until the access attempt is made.

#### 6.1.2.7 *Energy accumulation waiting time*

Since the energy arrivals constitute a Bernoulli process, the energy accumulation time follows a Negative Binomial distribution, i.e., $T_E \sim NB(W, \delta)$, where W is the number of energy units needed to be harvested for transmitting an update. The first and second moment of $T_E$ will be:

$$\mathbb{E}[T_E] = \sum_{l=1}^{N} \mathbb{P}(W = l)\mathbb{E}[T_E|W = l] \tag{6.20}$$

$$\mathbb{E}[T_E^2] = \sum_{l=1}^{N} \mathbb{P}(W = l)\mathbb{E}[T_E^2|W = l] \tag{6.21}$$

The conditional first and second moment of the recharging time can be computed as

$$\mathbb{E}[T_E|W = l] = \frac{l}{\delta}, \tag{6.22}$$

$$\mathbb{E}[T_E^2|W = l] = \frac{l(l-\delta+1)}{\delta^2}. \tag{6.23}$$

The probability $\mathbb{P}(W = l)$ of having $W$ energy units is given by the energy store after the last transmission and the energy arrival process:

$$\mathbb{P}(W = l) = \begin{cases} \dfrac{S_{2N-l}(1-\delta) + S_{2N-l-1}\delta}{\sum_{i=N}^{B} S_i}, & l \in \{1, \dots, N-1\} \\ \dfrac{S_N(1-\delta)}{\sum_{i=N}^{B} S_i}, & l = N. \end{cases} \tag{6.24}$$

*Access waiting time*. The expectation of access time $E[T_A]$, referred to as the time needed to try to access the channel, only depends on the independent access slot probability $q_2$. To that end, the access waiting time $T_A$ follows a geometric distribution with parameter $q_2$. Hence, $\mathbb{E}[T_A] = \frac{1}{q_2}$ and $\mathbb{E}[T_A^2] = \frac{2-q_2}{q_2^2}$.

The expectation of the total time $\mathbb{E}[T]$ and its second moment $\mathbb{E}[T^2]$ can be written as:

$$\mathbb{E}[T] = \frac{1}{q_2} + \frac{\sum_{i=0}^{N-1}(N-i-\delta)S_{N+i}}{\delta \sum_{i=N}^{B} S_i}, \tag{6.25}$$

$$\begin{aligned} \mathbb{E}[T^2] = \frac{2-q_2}{q_2^2} &+ \frac{\sum_{i=0}^{N-1}(N-i)(N-i+1-3\delta)S_{N+i}}{\delta^2 \sum_{i=N}^{B} S_i} \\ &+ \frac{2\sum_{i=0}^{N-1}(N-i-\delta)S_{N+i}}{\delta q_2 \sum_{i=N}^{B} S_i} + \frac{\sum_{i=0}^{N-1} S_{N+i}}{\sum_{i=N}^{B} S_i}. \end{aligned} \tag{6.26}$$

By substituting Equations (6.19), (6.25), and (6.26) into the general AoI Expression (6.18), and by leveraging the identity $\sum_{i=N}^{B} S_i = \frac{\delta}{Nq_2}$, along with the implicit load balance condition encoded in the root $z$ of the system, we derive the closed-form expression for the average AoI in the ECR, as shown in Equation (6.27). The derivation of the closed-form expression for the ESR regime can be obtained by following the same procedure as in the ECR case,

with the key differences being the fact that the expectation of the energy arrival time and its second moment, i.e., $\mathbb{E}[T_E]$ and $\mathbb{E}[T_E^2]$, are both equal to zero, since there is no need to wait for the energy arrival when the system reach the steady state.

The following section formalizes this AoI minimization as a constrained optimization problem, distinguishing between two operational regimes and deriving conditions under which optimal transmission strategies can be identified, with the final aim of obtaining the best parameter configuration and useful insights.

$$\bar{\Delta}_{ECR} = \frac{N}{\delta(1-\epsilon)}\left[p_{2,2} + \frac{\lambda(-p_{2,2}+p_{2,1})}{\exp\left(-\frac{\theta_1}{\beta_1 P_1}\right)\left(1-\frac{\delta}{N}+\frac{\delta}{N}\frac{1}{1+\theta_1\frac{\beta_2 P_2}{\beta_1 P_1}}\right)}\right]^{-1} - \frac{z}{\delta(1-z)} + \frac{z}{Nq_2(1-z)} - \frac{N-1}{2\delta} + \frac{1}{q_2} - 1, \quad (6.27)$$

$$\bar{\Delta}_{ESR} = \frac{1}{q_2(1-\epsilon)}\left[p_{2,2} + \frac{\lambda(-p_{2,2}+p_{2,1})}{\exp\left(-\frac{\theta_1}{\beta_1 P_1}\right)\left((1-q_2)+\frac{q_2}{1+\theta_1\frac{\beta_2 P_2}{\beta_1 P_1}}\right)}\right]^{-1}. \quad (6.28)$$

### 6.1.3 *Optimization Problem*

The interaction between the two energy regimes and the interference patterns from node $S_1$ creates a non-trivial optimization problem. When node $S_1$ transmits (with probability $q_1$ when its queue is non-empty), it affects both the success probability of node $S_2$'s transmissions and, indirectly, the optimal energy allocation strategy. This requires us to jointly optimize the transmission parameters of both nodes, considering not only the AoI objective but also the energy dynamics and queue stability constraints. Having clarified the step needed to obtain the expectation values, the formal definition of the optimization problem under study can now be defined. The objective is to investigate the effect of

energy harvesting on the AoI at node $S_2$, while ensuring queue stability at node $S_1$ (i.e., maintaining $\mu > \lambda$). The problem can be formulated as follows:

**Problem 6.1** (AoI Optimization).

$$\min_{P_1, N, q_1, q_2} \quad \bar{\Delta} \tag{6.29a}$$

$$\text{s.t.} \quad \mu > \lambda, \tag{6.29b}$$

$$P_1 \in [P_{\min}, P_{\max}], \tag{6.29c}$$

$$N \in [1, N_{\max}], \tag{6.29d}$$

$$q_1 \in (0, 1], \quad q_2 \in (0, 1], \tag{6.29e}$$

where $\mu$ is defined in Equation (6.10). The parameters $P_{\min}$ and $P_{\max}$ represent the minimum and maximum allowable transmit powers at node $S_1$, respectively, and $N_{\max}$ denotes the maximum energy storage capacity at node $S_2$. Constraint (6.29b) ensures queue stability at node $S_1$, while constraints (6.29c)–(6.29e) impose physical feasibility conditions on the transmit power, energy capacity, and transmission probabilities.

In what follows I try to get more insights about the problem providing a closed-form for ECR and ESR, by deriving insights for the optimal values of $q_1$ and $q_2$. These two regimes lead to fundamentally different expressions for the AoI, making it infeasible to evaluate the system behavior in a unified framework, therefore the closed-form derviation will proceed separately.

#### 6.1.3.1 *Optimization Problem under the ECR Configuration*

Depending on the energy and data arrival rates, the optimal transmission probabilities $q_1$ and $q_2$ can be characterized as follows.

**Lemma 6.1.** Under the ECR configuration, the optimal transmission probabilities $q_1^*$ and $q_2^*$ can be determined as follows:

- If $0 < \lambda < \zeta$, then there exists a feasible $q_1 \in (0, 1]$ satisfying the queue stability condition, while the $q_2$ is equal to its maximum value. The optimal values are

$$q_1^* \geq \frac{\lambda}{p_{1,1}} - \frac{\lambda N}{\delta(p_{1,1} - p_{1,2})}, \quad q_2^* = 1 \tag{6.30}$$

- If $\lambda \geq \zeta$, then the best value for node $S_1$ stability is 1, and exists a feasible $N \leq \frac{q_1\delta(p_{1,1}+p_{1,2})}{\lambda - q_1 p_{1,1}}$. The optimal values are:

$$q_1^* = 1, \quad q_2^* = 1 \tag{6.31}$$

where $\zeta = p_{1,1} - \frac{\delta p_{1,1}}{N} + \frac{\delta p_{1,2}}{N}$.

A reduced version of Problem 6.1 for ECR is presented below.

**Problem 6.2** (AoI Optimization under ECR).

$$\min_{P_1, N} \quad \bar{\Delta}_{ECR} \tag{6.32a}$$

$$\text{subject to} \quad p_{1,1} > \lambda, \tag{6.32b}$$

$$P_{\min} \leq P_1 \leq P_{\max}, \tag{6.32c}$$

$$1 \leq N \leq \frac{q_1\delta(p_{1,1}+p_{1,2})}{\lambda - q_1 p_{1,1}}, \tag{6.32d}$$

$$q_1^* = \min\{1, \frac{\lambda}{p_{1,1}} - \frac{\lambda N}{\delta(p_{1,1}-p_{1,2})}\}, \tag{6.32e}$$

$$q_2^* = 1. \tag{6.32f}$$

*Proof of derivation of Probelm 6.2.* Let us consider the case where node $S_2$ operates in the ECR, i.e., $\delta < Nq_2$. In this regime, the long-time average AoI at node $S_2$ is given by Equation (6.27). This function is strictly decreasing with $\delta$, while an evaluation on $q_2$ over different values of $N$ can prove the optimal value. The first part of the equation ($\frac{\mathbb{E}[T]}{\bar{p}_2}$) does not depend on $q_2$, while the remaining part depends on $q_2$ both explicitly and included in the computation of $z$. By evaluating the function for $N = 1$, it is possible to notice that the second part will be voided due to the implicit expression of $z$ and thus is non-variant for the value of $q_2$. This means that if $\delta > q_2$ (so that node $S_2$ is constrained by the arrival of energy, rather than the access probability) and $N = 1$, then the entire AoI is non-sensitive to $q_2$. For $N \geq 2$, let me follow the same demonstration of [167] to prove that the best value of $q_2 = 1$ since the right side is a positive component, and since the limit of $z$ for $q_2 \to 1$ is equal to 0, then the right side will goes to 0 when increasing $q_2$. At this point it is possible to confirm that $q_2^* = 1$. When $q_2 = 1$, the stability condition of $S_1$ becomes:

$$\lambda < q_1 \left( (1 - \frac{\delta}{N}) p_{1,1} + \frac{\delta p_{1,2}}{N} \right) \tag{6.33}$$

which depends on $q_1$. Evaluating this inequality for $q_1 \to 1$, we can prove that this is the most favorable condition which permits the node $S_1$ to maintain the stability independently from the other parameters. If activating node $S_1$ continuously is undesirable, e.g., due to energy or access costs, the minimum access probability that preserves stability under $q_2 = 1$ is:

$$q_1^* = \frac{\lambda}{p_{1,1}} - \frac{\lambda N}{\delta(p_{1,1} - p_{1,2})}. \tag{6.34}$$

Since $q_1$ does not affect the AoI perceived at node $S_2$, any value in the interval $[q_1^*, 1]$ is AoI-optimal and can be chosen based on design trade-offs. When the condition described in (6.33) is violated, then it is needed to take into account the value of $q_2$ in the definition of the constraint

$$\begin{aligned}
\lambda &< q_1 \left( (1 - \frac{\delta}{q_2 N}) p_{1,1} + \frac{\delta}{q_2 N} ((1 - q_2) p_{1,1} + q_2 p_{1,2}) \right) \\
\lambda &< q_1 \left( p_{1,1} - \frac{\delta p_{1,1}}{q_2 N} + \frac{\delta p_{1,1}}{q_2 N} - \frac{\delta q_2 p_{1,1}}{q_2 N} + \frac{\delta q_2 p_{1,2}}{q_2 N} \right) \\
\lambda &< q_1 \left( p_{1,1} - \frac{\delta p_{1,1}}{N} + \frac{\delta p_{1,2}}{N} \right)
\end{aligned} \tag{6.35}$$

Anyway, as it is possible to notice the value of $q_2$ does not impact the stability of node $S_1$, hence the only parameter that can be adjusted is the value of $N$, which is constrained to an higher-bound value, causing it to be

$$N < \frac{q_1 \delta (p_{1,2} - p_{1,1})}{\lambda - q_1 p_{1,1}} \tag{6.36}$$

Having derivate the stability condition, it is now possible to reformulate the optimization problem by incorporating the structural insights derived in the ECR regime. The objective remains the minimization of the long-term average AoI at node $S_2$, under the stability constraint of node $S_1$ and system feasibility constraints. □

#### 6.1.3.2 *Optimization Problem under the ESR Configuration*

In the ESR scenario, the stability condition at node $S_1$ again dictates two cases, leading to different optimal transmission strategies:

**Lemma 6.2.** Under the ESR configuration, the optimal transmission probabilities are:

- If $0 < \lambda < p_{1,2}$, then:

$$q_1^* > \frac{\lambda}{p_{1,2}}, \quad q_2^* = \frac{\delta}{N}. \tag{6.37}$$

- If $\lambda \geq p_{1,2}$, then:

$$q_1^* = 1, \quad q_2^* < \frac{p_{1,1} - \lambda}{p_{1,1} - p_{1,2}}. \tag{6.38}$$

These hold under the same condition $\lambda < p_{1,1}$ as in the ECR case.

**Problem 6.3** (AoI Optimization under ESR)**.**

$$\min_{P_1, N} \quad \bar{\Delta}_{ESR} \tag{6.39a}$$

$$\text{s.t.} \quad p_{1,1} > \lambda, \tag{6.39b}$$

$$P_{\min} \leq P_1 \leq P_{\max}, \tag{6.39c}$$

$$1 \leq N \leq N_{\max}, \tag{6.39d}$$

$$q_1^* = \min\left\{1, \frac{\lambda}{p_{1,2}}\right\}, \tag{6.39e}$$

$$q_2^* = \min\left\{\frac{\delta}{N}, \frac{p_{1,1} - \lambda}{p_{1,1} - p_{1,2}}\right\}. \tag{6.39f}$$

*Proof of derivation of Probelm 6.3.* Let me consider the case where node $S_2$ operates in the ESR, characterized by the condition $\delta \geq Nq_2$. In this regime, the long-time average AoI at node $S_2$ is given by Equation (6.27). Starting the analysis from the optimal $q_2$, it is worth to notice that differently from the derivation of ECR, this time it cannot be simplified, and it still exist in the first AoI term $(\frac{\mathbb{E}[T]}{\bar{p_2}})$. To obtain the direction of the function w.r.t. $q_2$, one can consider the derivate of the function,

$$\frac{d}{dq_2}\left[\frac{1}{q_2\bar{p}_2}\right] = -\frac{1}{\bar{p_2}q_2^2} + \frac{\lambda q_1(p_{2,2} - p_{2,1})(p_{1,1} - p_{1,2})}{\bar{p_2}^2 q_2 \mu^2}, \tag{6.40}$$

which is negative if the following inequality hold:

$$\mu^2\bar{p_2} > \lambda q_1 q_2(p_{2,2} - p_{2,1})(p_{1,1} - p_{1,2}). \tag{6.41}$$

By evaluating this inequality using the system parameters, this always hold for all the $(\lambda, \delta \in (0,1))$. By recalling that the system under consideration is in ESR, then $q_2 \leq \frac{\delta}{N}$, hence, the optimal value of $q_2^* = \frac{\delta}{N}$, under the stability of queue $S_1$:

$$\lambda < q_1 p_{1,2} \implies q_1^* > \frac{\lambda}{p_{1,2}}. \tag{6.42}$$

However, under ESR, the transmission attempts by node $S_2$ is more frequent (no need to wait for energy), which causes an easier instability in the queue of node $S_1$. In particular, in ESR, where $S_2$ is fully powered, it is necessary to reduce $q_2$ to alleviate the interference experienced by $S_1$, to mantain stability of its queue. In such a case, as in ECR, the minimal value of $q_1$ will be 1 and the maximum admissible value of $q_2$ that ensures stability is given by:

$$q_2^* = \frac{p_{1,1} - \lambda}{p_{1,1} - p_{1,2}}. \tag{6.43}$$

These closed-form expressions can be used to bound the feasible region in the optimization problem. □

Given the coupled nature of the optimization problem, it is not possible to derive closed-form expressions for the optimal values of $N$ and $P_1$. Therefore, an heuristic approach to solve the problem numerically is needed. In the following, I describe a methodology based on a GA, which effectively explores the solution space and identifies near-optimal configurations for the system parameters.

#### 6.1.3.3 *Genetic Algorithm*

The GA is a heuristic optimization technique inspired by the process of natural selection. GA is particularly well-suited for problems with discrete decision variables and, as is the case with our AoI minimization problem involving coupled parameters $N$and $P_1$.

For the genetic operations, I adopted Gaussian Mutation to introduce controlled stochastic variations in the offspring, thereby

**Algorithm 2** Genetic Algorithm for Minimizing $\Delta_k$

**Input:** $\lambda$, $\delta$, B, $k \in \{\text{ECR}, \text{ESR}\}$
**Initialize:** $|C| = 100, i_{max} = 200$
Define bound for $c_1$: $P_1, \in [P_{min}, P_{max}]$
Define bound for $c_2$: $N \in [1, N_{max}]$
Initialize population $C_0$ between constraints
**while** $i < i_{max}$ **do**
    Select parents $(c_1^i, c_2^i) \in C_i$
    Recombine $(c_1^i, c_2^i)$ to create new offspring
    Apply mutation to maintain genetic diversity
    Compute $q_1^*$ according to (6.32e) or (6.39e)
    Compute $q_2^*$ according to (6.32f) or (6.39f)
    Evaluate $\Delta_k$ for all the $c_j \in C_i$
    Update the population with new offspring
**end while**
Return the best individual $c_j \in C_{i_{max}}$
**Output:** Optimal $(P_1^*, N^*)$ and $\Delta_k$ for $\lambda, \delta$, B

enhancing the exploration of the search space and avoiding premature convergence. Selection is performed using a tournament strategy, which balances exploitation of high-quality solutions and maintenance of population diversity. The population size is set to 100, which corresponds to twice the number of decision variables involved in the optimization. The algorithm is allowed to run for a maximum of 200 generations, equivalent to twice the population size, ensuring sufficient iterations to reach convergence while keeping the computational overhead manageable.

## 6.2 THE OPTIMAL LOAD SHIFTING POLICY

The second contribution applies framework outlined Chapter 4 to investigate the potential of dynamic provisioning strategies based on load shifting in SWIPT networks. Specifically, IoT device can harvest energy from the environment, and the way they act with can be exploited to design a transmission policy which optimize the energy harvesting process.

### 6.2.1 *Problem Statement and Motivation*

The rise of massive machine-type communications (mMTC) and increasing device density are placing significant challenges on future wireless networks [19, 88]. In this context, EH becomes essential, particularly in 6G heterogeneous networks where diverse users and devices coexist and share limited resources [70]. When combined with wireless power delivery [58], EH supports large-scale deployments, reduces reliance on finite batteries, and extends device lifetimes in remote or inaccessible environments. Unlike conventional cellular systems with predictable energy scaling, SWIPT networks exhibit non-monotonic energy dynamics due to the dual role of user devices. Indeed, all transmitting devices in a SWIPT RAN act not only as service consumers but also as distributed contributors to wireless power delivery.

This shift, explored in the previous chapters, undermines traditional energy management strategies, such as sleep modes or energy proportionality, which assume a quasi-linear relation between traffic load and energy consumption [124]. In particular, an increase in user density may lead to lower overall energy requirements and fewer active BSs needed to maintain QoS, within certain operating regimes [124, 150]. This phenomenon is due to emerging cooperative energy transfer among UEs, where active devices help power neighboring IoT nodes via passive EH. Among the techniques with the largest potential for energy savings in traditional RANs, load shifting has proven to enable significant improvements of both energy efficiency and network performance [77, 133, 151].

However, all these findings assume a quasi-linear and monotonic relationship between load and energy consumption, an assumption that does not apply to SWIPT networks, due to their inherently nonlinear and non-monotonic energy dynamics. Thus, it is unclear how can load-shifting strategies for delay-tolerant applications be redesigned or optimized in SWIPT-enabled RANs to maximize overall energy efficiency, while satisfying both connectivity and energy harvesting quality-of-service (QoS) constraints for heterogeneous IoT devices. The results can be summarized as follows:

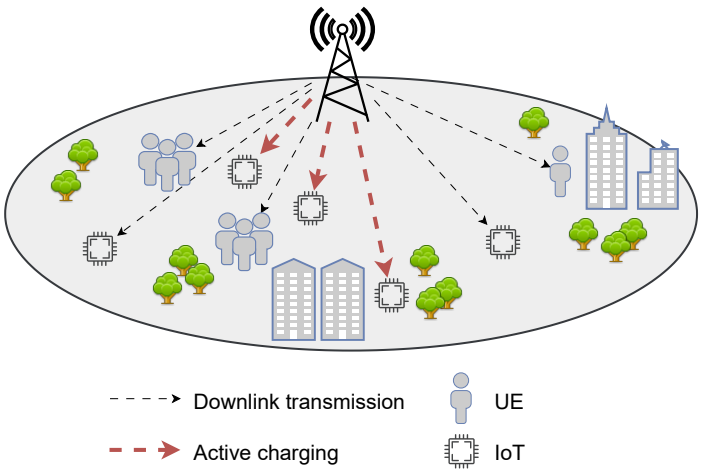


Figure 6.2: Illustration of a SWIPT network where the base station provides connectivity for both BB and IoT UEs while actively charging IoT UEs.

- Proposal of an analytical model of SWIPT networks performance under delay tolerant IoT traffic, based on stochastic geometry and on an IoT energy model that accounts for the effects of duty cycling on user perceived performance.
- Formulation of an optimization problem from the perspective of the Mobile Network Operator (MNO), to determine QoS-aware energy optimal load shifting strategies for IoT traffic.
- Numerical charactherization of the energy-optimal network provisioning strategies emerging from the framework. On a realistic daily traffic profile, it is shown that the framework is effectively able to shift the load towards those operating conditions in which the power consumed is the least sensitive to load.

### 6.2.2 *Methodological Approach*

Let me consider a cellular network where BSs are distributed in space according to a homogeneous planar Poisson Point Process (PPP) $\Phi_b$ with intensity $\lambda_b$ BSs per $m^2$. Similarly, UEs are distributed in space according to a homogeneous PPP $\Phi_u(t)$ with intensity of $\lambda_u$ UEs per $m^2$. UEs can be broadband (BB) or IoT,

though our analysis can easily be extended to account for other categories of users.

I considered the case in which IoT devices harvest the energy necessary for their operation from RF signals. Thus, every IoT device is capable of exploiting downlink signals from its serving BS to decode its intended information and charge its battery (*active charging*), as well as any signal transmitted from BSs and UEs for energy harvesting (*passive charging*).

Thus, each IoT device can use downlink signals from its serving base station to decode its intended information and to actively recharge its battery (*active charging*), and it can also harvest energy from any signals transmitted by base stations and user equipments in its vicinity (*passive charging*). Specifically, each IoT device is equipped with two separate receivers, one for information transfer and the other for energy harvesting. IoT devices commute between energy harvesting and information decoding via Time Splitting (TS) [99]. In such an operating mode, a fraction $\eta$ (the *time split ratio, with* $0 \leq \eta \leq 1$) of the BS time dedicated to serving that device is devoted to active power transfer, while the remaining fraction $1 - \eta$ of BS time dedicated to that user is devoted to receiving information. When an IoT device is not actively served by the BS to which it is associated, it is performing passive harvesting. I assume $\eta$ to take the same value for all devices.

#### 6.2.2.1 *Service model*

BSs use a generalized processor-sharing (GPS) mechanism to divide BS time among all the connected devices. In the downlink, the GPS weights are 1 for IoT devices, and $\omega_d$ for BB UEs. To take into account the difference in QoS between IoT and BB, I defined $\omega_d = \delta_d(1 - \eta)$, where $\delta_d$ defines the ratio of QoS between the downlink process of the two categories of UEs. The time spent by the BS without transmitting is modeled as a user with a GPS weight $\beta_d$. As for uplink, in all configurations, the GPS weights are 1 for IoT UEs, $\delta_u$ for BB UEs, and $\beta_u$ for the uplink BS time not assigned to any UE. BB UEs always have data to transmit and receive, and $\tau_u^0$ denotes the target per-bit uplink delay, while $\tau_d^0$ denotes the downlink target. IoT device generate with a constant

rate equal to $T_u^0$ bits per second. Similarly, each BS, need to transmit data to IoT devices with a constant rate of $T_d^0$ bits per second.

To optimize energy consumption (and thus autonomy), IoT UEs follow periodic cycles of activity and idle time, independently in downlink and uplink. Specifically, they transmit for a fraction $\phi_u$ of their time and receive data for a fraction $\phi_d$ of their time. This models IoT UEs whose activity is triggered by human presence, such as event detection systems.

To ensure fairness in the system, the values of $\omega_d$ and $\delta_u$ are set as the ratio between the traffic requirements of BB users and that of IoT UEs in active state in downlink and in uplink, respectively [123]. Thus, in general, the BS time dedicated to serving an IoT device is a fraction $\phi_d$ of the time that the BS might dedicate to serving it according to the GPS weight.

The BS utilization is the fraction of time during which it is busy serving all associated users. Specifically, if $S(x)$ denotes the BS serving a user located in $x$, the utilization in downlink is

$$U_d(S(x)) = \frac{\phi_d N_{iot}(S(x)) + \omega_d N_{bb}(S(x))}{\phi_d N_{iot}(S(x)) + \omega_d N_{bb}(S(x)) + \beta_d} \tag{6.44}$$

while in uplink,

$$U_u(S(x)) = \frac{\phi_u N_{iot}(S(x)) + \delta_u N_{bb}(S(x))}{\phi_u N_{iot}(S(x)) + \delta_u N_{bb}(S(x)) + \beta_u} \tag{6.45}$$

$N_{iot}(S(x))$ and $N_{bb}(S(x))$ are the number of IoT and BB UEs associated with $S(x)$, while $\phi_d N_{iot}(S(x))$ (respectively, $\phi_u N_{iot}(S(x))$) denote the mean number of IoT UEs in active state in downlink (resp. in uplink). Thus, given $\omega_d$ and $\delta_u$, by tuning $\beta_j$, $j \in \{u, d\}$, the network controls the mean amount of service received by UEs for both communications and energy transfer, and the overall BS utilization, both in downlink and uplink.

Let me define the *ideal-per bit delay* $\tau_j$ with $j \in \{d, u\}$ as the per bit delay which a UE would perceive if the BS with which the UE is associated had utilization equal to one. Leveraging tools from stochastic geometry and following the proof in [123], let me consider the per-bit delay perceived by a BB UE at distance $x$ from its nearest BS as:

$$\tau_d^{id}(x) = \frac{\phi_d N_{iot}(S(x)) + \omega_d N_{bb}(S(x))}{\omega_d C(x, P, G, I)}, \tag{6.46}$$

$$\tau_u^{id}(x) = \frac{\phi_u N_{iot}(S(x)) + \delta_u N_{bb}(S(x))}{\delta_u C(x, P_I, 1, 0)}. \tag{6.47}$$

I denoted the capacity of a user located at a distance $r$ from the BS by $C(r, P, G, I)$ bit/s per Hertz, where $P$ is the BS transmit power, and $I$ the total received interfering power. Using Shannon's capacity law, the Capactiy $C(r, P, G, I)$ can be defined as $C(r, P, G, I) = \frac{B}{\rho} \log_2 \left(1 + \frac{PGr^{-\alpha}}{N_0 + I(r,\rho)}\right)$, where $\alpha$ is the attenuation coefficient, $N_0$ the power spectral density of the additive white Gaussian noise, $\rho$ the reuse factor. BS antennas use beamforming, and we denote with $G$ the beamforming gain and with $L$ the side lobes attenuation.

### 6.2.3 *Analytical Model*

This subsection presents the main analytical results used in our optimization framework, based on recent stochastic geometry results. They are derived from [20, 124].

#### 6.2.3.1 *IoT Power Consumption and Energy Harvesting Model*

The energy model of an IoT device relates its communication activity and its states (active, standby, off) to the power consumed. Specifically, in this work, I refer to a class of IoT UEs with an overall power consumption between 1 and 10 mW, such as those whose operations can be sustained by active and passive RF EH [5]. Examples are medical and sensing devices for body area networks, such as [95] and [74]. The adopted model is derived from [171] through a measurement-based characterization, and it can be parametrized to account for a wide range of device architectures and types. The expression of the consumed power for an IoT device at $x$, denoted as $h_{req}(x)$, is

$$h_{req}(x) = e_c\big(w_1 + w_2 P_{IoT} U_{tx}(x)\big) \tag{6.48}$$

with $w_1 + w_2 P_{IoT} U_{tx} \leq 1$. $P_{IoT}$ is the transmit power of the device, which I assumed to be lower or equal than a maximum value $P_{max}$, and $e_c$ is the maximum power consumed by the device. $w_1$ is the part of the consumed power that does not depend on the load

or device configuration, and which models the power consumption due to other tasks (sensing, computing). $w_2$ modulates the contribution due to communication activity and transmit power. $U_{tx}(x)$ is the mean fraction of time the device at $x$ is busy transmitting. Note that downlink processing and sensing are modeled as proportional to the transmitted data, thus via $w_2$.

**Lemma 6.3.** $U_{tx}(x) = \frac{\bar{\tau}_u}{\tau_u^0} \frac{\phi_u}{f(r,\delta_u)}$ where $f(\cdot,\cdot) \leq 1$ is given by Theorem 4.1.

*Proof of Lemma 6.3.* To derive the uplink utilization $U_{tx}(x)$ of IoT located at distance $x$ from the associated BS, I considered the time the device is busy transmitting, which corresponds to the ratio $\phi_u$ over the entire uplink time. Similar to base stations, the energy consumption of an IoT device is a rescaling of the maximum energy consumed when the IoT device is transmitting at its peak capacity. The rescaling factor is determined by a fixed quantity that represents the energy consumed when the IoT is not transmitting data and a variable component that relies on both the transmission power and the IoT's utilization. The latter can be derived from the mean uplink utilization of BS $\frac{\bar{\tau}_u}{\tau_u^0}$. Given that BS resources are distributed among $f(r,\delta_u)$ users and the uplink weight of IoTs is 1, it is possible to calculate the amount of resources (time) allocated by the BS to IoTs, which corresponds to the duration in which the device is actively transmitting information. The actual transmitting time is then multiplied by the fraction of time the IoT scheduled to use for transmitting, i.e., $\phi_u$ □

IoT device can perform both active and passive harvesting. The power harvested via active charging is

$$h_{in}^{active}(x) = \frac{U_d(x) P r^{-\alpha} G \eta \phi_d}{f(r, w_d)} \tag{6.49}$$

The power harvested via passive charging is given by several contributions:

1. Power harvested from transmissions of the serving BS to the other associated users, which depends on the time where the user is not served by the associated BS corresponding to $1 - \frac{1}{f(r,w_d)}$:

$$h_{ass_{BS}}^{passive}(x) = U_d(S(x)) P r^{-\alpha} L \left(1 - \frac{\phi_d}{f(r, w_d)}\right) \tag{6.50}$$

2. Power harvested from the transmission of other BS to the cell of the user

$$h^{passive}_{other_{BS}}(x) = I(r(x),\rho)\left(1 - \frac{U_d(S(x))(\phi_d - \eta)}{f(r,w_d)}\right) \quad (6.51)$$

3. Power harvested from the transmission of other user in uplink in the same cell as the typical user

$$h^{passive}_{other_{UE}}(x) = \left(1 - \frac{U_d(S(x))(\phi_d - \eta)}{f(r,w_d)}\right)\bar{O} \quad (6.52)$$

where

$$\bar{O} = \frac{(1-\gamma)\delta_u P_{bb} + \phi_u \gamma P_I}{(1-\gamma)\delta_u + \phi_u \gamma} \frac{\lambda_b \pi \alpha}{\alpha - 2} \frac{\bar{\tau}_u}{\tau_u^0}$$

By denoting with $h_{in}(x)$ the sum of all of the four quantities for a device located at a distance $x$ from the nearest BS:

$$h_{in}(x) = h^{active}_{in}(x) + h^{passive}_{ass_{BS}}(x) + h^{passive}_{other_{BS}}(x) + h^{passive}_{other_{UE}}(x), \quad (6.53)$$

then let us consider the *energy neutrality* of an IoT device at distance $x$ from the closest BS, denoted as $h_0(x)$, as the difference between the power required to operate and the power harvested. Thus,

$$h_0(x) = h_{req}(x) - h_{in}(x). \quad (6.54)$$

**Lemma 6.4.** Let $R$ be the random variable describing the distance of a user from its serving BS with CDF $F_R(\cdot)$, then the fraction of devices that achieve energy neutrality is:

$$\mathbb{P}(h_0(R) \geq 0) = \mathbb{E}[\mathbb{1}_{h_0(R)\geq 0}] = 1 - F_R(h_0^{-1}(0)) \quad (6.55)$$

*Proof of Lemma 6.4.* Let $R$ denote the user distance from the serving BS with CDF $F_R$. Consider the indicator $\mathbb{1}_{\{h_0(R)\geq 0\}}$. By the definition of probability as an expectation of an indicator,

$$\mathbb{P}(h_0(R) \geq 0) \;=\; \mathbb{E}[\mathbb{1}_{\{h_0(R)\geq 0\}}].$$

Since $h_0$ is non-decreasing function of the distance, let denote $r_0 = h_0^{-1}(0)$ and

$$\{h_0(R) \geq 0\} = \{R \geq r_0\},$$

then, since $R$ has a continuous distribution at $r_0$:

$$\mathbb{P}(h_0(R) \geq 0) = \mathbb{P}(R \geq r_0) = 1 - \mathbb{P}(R < r_0) = 1 - F_R(r_0).$$

□

This metric is used to evaluate which is the percentage of users with a nonnegative power budget, corresponding to a regime where IoT UEs can harvest all of the consumed power from active and passive RF sources.

#### 6.2.3.2 *BS Energy Consumption Model*

To model the BS power consumption, I adopted a flexible and widely-used BS power model from [98], where the total power consumption is expressed as:

$$q_1 + U_d[q_2 + q_3(P - P_{\min})] \tag{6.56}$$

where $q_1$ is the static power consumed when the BS is idle, $q_2 U_d$ captures load-dependent power unrelated to transmit power, and $q_3 U_d(P - P_{min})$ models the transmit-power-dependent component, where $P$ is the actual transmit power within $[P_{\min}, P_{\max}]$, and $U_d$ is the downlink utilization. This model accounts for both fixed and traffic-dependent energy consumption and is suitable for analyzing dynamic energy-efficient network strategies.

#### 6.2.3.3 *Energy-Optimal Load Shifting*

In the following sections, I refer to time as an observation window that is divided into $K$ time slots, where $k \in \{1, ..., K\}$ denotes the label of the $k$-th slot. Each slot is characterized by the density $\lambda_u^k$ of installed devices, including both BB and IoT devices. In the no-shifting scenario, I assumed that in each time slot, IoT devices transmit the traffic they generate by utilizing the entire available channel capacity. In this case, the per-bit delay corresponds to the value defined in Theorem 4.1 with $\phi_d^k = \phi_u^k = 1$ for each $k$. When the active state $\phi_j^k, j \in \{d, u\}$ of IoTs is not equal to 1, the downlink throughput $T_d^k$ and the uplink throughput $T_u^k$ available to the IoT devices at time slot $k$, are given by:

$$T_d^k(\phi_d^k) = \frac{\phi_d^k(1-\eta^k)}{\omega_d \tau_d^{0,k}} = \frac{\phi_d^k(1-\eta^k)}{(1-\eta^k)\delta_d \tau_d^{0,k}} = \frac{\phi_d^k}{\delta_d \tau_d^{0,k}}, \tag{6.57}$$

$$T_u^k(\phi_u^k) = \frac{\phi_u^k}{\delta_u \tau_u^{0,k}}, \tag{6.58}$$

where $\tau_j^{0,k}$ represents the BB UEs target for the related process and time slot $k$. Assuming over-provision the system when convenient, it is also reasonable to assume target different per-bit delays for each time slot. These expressions are based on the fact that, in our system, the per-bit delay is the inverse of the throughput. Additionally, the weights for downlink and uplink scheduling for BB UEs, which are utilized to calculate the per-bit delay, depend on both $\delta_j$ and $\eta^k$. The traffic sent (resp. received) by IoT devices during time slot $k$ can be expressed as:

$$B_j^k = \gamma^k \lambda_u^k T_j^k(\phi_j^k) \tag{6.59}$$

To optimize network resource usage and create a more energy-efficient system, our proposed load-shifting mechanism models the ability to redistribute transmission loads across adjacent time slots. In traditional systems, the load generated at time $k$ must be delivered within a certain delay constraint. To capture this behavior, a window of size $D$ has been defined, which represents the maximum delay allowed for shifting traffic to neighboring time slots. Considering the periodic nature of a 24-hour day, our model also permits shifting some load from the last time slot to the first. As a result, each time slot can receive load from up to $D$ preceding time slots and forward traffic to up to $D$ subsequent time slots. Let $\phi_{j,0}^k$ be the target and $\phi_j^k$, which depends on $\tau_j^{0,k}$, describing the target activation during time slot $k$, indicating how many bits are generated or received. Denoting by $\chi_j^k$ the amount of requested traffic at time slot $k$:

$$\chi_j^k = \lambda_u^k \gamma^k T_j^k(\phi_{j,0}^k), \tag{6.60}$$

the total amount of traffic sent (resp. received) in time slot $k$ under the load shifting assumption can be now expressed as:

$$B_j^k = \sum_{i=k-D}^{k-1} B_j^{i,k} + \chi_j^k - \sum_{i=k+1}^{k+D} B_j^{k,i} \tag{6.61}$$

where $B_j^{i,z}$ with $j \in \{u, d\}$ defines the uplink (resp. downlink) load moved from timeslot $i$ to $z$. At the end of the observation period consisting of $K$ equal time slots, the total traffic sent (resp. received) will be given by the sum $\sum_{k=1}^{K} B_j^k$.

The proposed modelization implies that some devices may transmit at a throughput lower than their assigned target during specific time slots, while in others they may fully utilize the channel capacity for transmission or reception.

### 6.2.4 *Optimization Problem*

Under the load-shifting assumption, it is now possible to formulate the energy-optimal problem, which aims to identify for each time slot $k$, the best system configuration in terms of density of active base stations $\lambda_b^k$, splitting factor $\eta^k$, BS transmission power $P^k$, and fraction $\phi_d^k$, $\phi_u^k$ of active IoT devices in downlink and uplink, respectively. Specifically:

**Problem 6.4** (Energy-Optimal Dynamic Network Management).

$$\underset{\substack{\{\lambda_b\},\{P\},\\ \{\phi_u\},\{\phi_d\},\{\eta\}}}{\text{minimize}} \sum_{k=1}^{K} e_k \lambda_b^k \left[ q_1 + \frac{\bar{\tau}_d^k}{\tau_d^0} \left( q_2 + q_3 (P^k - P_{\min}) \right) \right] \quad (6.62)$$

Subject to, $\forall t$:

$$\begin{aligned}
&(\text{C1}) \ \frac{\bar{\tau}_d^k}{\tau_d^0} \leq 1, \quad \frac{\bar{\tau}_u^k}{\tau_u^0} \leq 1 \\
&(\text{C2}) \ \mathbb{P}(h_0(R) \geq 0) \geq \iota \\
&(\text{C3}) \ 0 \leq B_d^k \leq (D+1) B_d^k \\
&(\text{C4}) \ \textstyle\sum_{k=1}^{K} \chi_d^k \leq \sum_{k=1}^{K} B_d^k \\
&(\text{C5}) \ 0 \leq B_u^k \leq (D+1) B_u^k \\
&(\text{C6}) \ \textstyle\sum_{k=1}^{K} \chi_u^k \leq \sum_{k=1}^{K} B_u^k \\
&(\text{C7}) \ 0 \leq \phi_u^k, \phi_d^k \leq 1 \\
&(\text{C8}) \ 0 \leq \eta^k \leq 1 \\
&(\text{C9}) \ P_{\min} \leq P^k \leq P_{\max} \\
&(\text{C10}) \ 0 \leq \lambda_b^k \leq \lambda_{b,\max}
\end{aligned}$$

where $e_k$ is the energy cost at time slot $k$. Constraints (C1) ensure that the QoS in downlink and uplink is satisfied for all users, with $\bar{\tau}_d^k$ and $\bar{\tau}_u^k$ as in Equation 4.13 and Equation 4.14. Constraint (C2) ensure that the percentage of satisfactory harvesting is higher than $\iota$, where probability is given according to Equation 6.4. $D$ represents the maximum allowable delay for the load shift, and the delay constraints are detailed in (C3) and (C5). Constraints (C4), (C6) ensure that the total shiftable traffic in DL and UL is preserved over the observation window, with $\chi_j^k$ and $B_j^k$ as in Equation 6.60 and Equation 6.61, respectively. Constraints (C7)-(C10) reflect realistic bounds on the values of the active ratios in DL and UL, splitting factor, transmission power, and density of active base stations, respectively. The problem is non-convex and highly non-linear, which makes deterministic approaches impractical. A Genetic Algorithm (GA), was adopted given its effectiveness in related optimization tasks [20]. The computational complexity mainly scales with the number of time slots, since each gene encodes the decision for one slot. To keep the search space manageable, I constrained gene values to the range [0,1] with a discretization step of 0.02, which substantially reduces the number of candidate solutions while preserving solution accuracy.

## 6.3 CONCLUSION

This chapter introduced two different approaches for optimizing user transmission policies. The first is related to the AoI, typical in time-sensitive scenario, while the second one is related to load shifting, typical in non-sensitive scenario, where the primary objective is reduced the power consumption. To study the first scenario, a two-node network has been put in place, and by leveraging Markov chain and queue theory, it has been possible to model both the energy accumulation at EH-node, and data packets accumulation at non-EH node. Two AoI optimization problems have been defined depending on the energy availability. Regarding the second scenario, a network composed by broadband and IoT devices, has been considered. From the methodological perspective, this approach is close to the one presented in the Chapter 4, where BS density, transmit power and splitting factor have been jointly considered in a non-convex optimization problem, anyway this

problem introduce the definition over 24-hours, charachterizing the load over multiple time-slot. Numerical evaluations of the problem is discussed in Chapter **??**, together with experimental set-up and major findings.

# Part III

# RESULTS AND DISCUSSION

This part reports and analyses the results obtained from the methodologies described in Part **??**. The discussion is structured according to the research questions, enabling a direct mapping between the proposed approaches and the corresponding findings. The analysis highlights the key insights on how heterogeneous SWIPT network parameters influence performance and energy efficiency, and discusses their practical implications for enhancing real IoT applications.

# 7

# PERFORMANCE OUTCOMES FOR SYSTEM PARAMETER OPTIMIZATION

This chapter presents the validation of the framework introduced in Chapter 4 and discusses the insights obtained from its numerical evaluation. The first section focuses on the PPP-based approach, where BSs are randomly distributed in space, while the second section analyzes the PLCP-based approach, where BSs are arranged along lines. Since the simulation setup is shared by both PPP and PLCP cases, it is described only once in the first section; any additional variations or specific settings are introduced when necessary. This chapter ends with the main findings, giving a concrete response to RQ1, reported here as reminder:

**RQ1.** *How do system parameters and deployment configurations influence the trade-offs between energy harvesting and information transfer in SWIPT-enabled HetNet?*

## 7.1 PLANAR DEPLOYMENT ANALYSIS

### 7.1.1 *Parameter Setup*

Base stations work in the 1.5 GHz band and use a bandwidth of 50 MHz, compatible with 4G+ standards. Unless otherwise indicated, the percentage of IoT devices equal to 80% of the total number of UEs (representative of many present-day scenarios), a transmit power equal to 0.2 W for both IoT and BB UEs, and a frequency reuse factor of 3. Moreover, by default, beamforming gain equal is set to 10, constant over the whole main lobe aperture (equal to 45 degrees), and a path loss exponent equal to 3, typical of urban areas. For linear energy harvesting, conversion efficiency of 0.9 is considered, with no lower/upper threshold (as discussed below, this condition is not relevant for the purpose of

this study, which uses the percentage of satisfied users as a metric). Deployed base stations belong to macro type, with a transmit power that varies between 1 and 11 W. Unless otherwise stated, the target mean per-bit delay in downlink for BB (resp. IoT) UEs equal to $10^{-5}$ s (resp. $10^{-3}$ s), and in uplink equal to $10^{-4}$ s for all UEs, (e.g., typical of IoT systems for environmental monitoring [89]). User density vary from $10^{-4}$ users per $m^2$ (modeling settings with a high share of BB users) to $10^{-1}$ users per $m^2$ (modeling scenarios with crowds of BB UEs and high-density IoT deployments). Unless otherwise specified, IoT UEs are active all the time ($\phi = 1$). The maximum acceptable share of IoT users who are not able to harvest the target minimum energy is set to 5%.

The parameters of the BS energy model are chosen to fit two different types of BSs. The first type (labeled LLP — low load proportionality) reflects the behavior of the majority of current stand-alone BSs, and is characterized by a 27% load proportionality (with $q_1 = 1100$, $q_2 = 100$, and $q_3 = 30$). Conversely, the high load proportionality (HLP) BS type (with $q_1 = 482.3$, $q_2 = 48.23$, and $q_3 = 144.69$) corresponds to a 75% load proportionality, achievable, e.g., through time-domain duty-cycling at the sub-system level, i.e., through micro-sleep techniques involving modules of the BS or of the BBU in cloud-RAN designs [84]. For the sake of comparison, these parameters were chosen to fit a per-BS maximum consumed power of 1500 W, typical of stand-alone macro BSs [47]. The value of BS density has been varied with a granularity of $10^{-4}$ $m^{-2}$, to guarantee good accuracy of the GA search process. To avoid unrealistic environment, the mean number of users per base station is lower bounded by 5. This models the simple energy-saving strategy common among MNOs, which switch off those BSs that serve very few users to no user at all, as they represent a very high energy cost per user and a small benefit for performance. The size $n$ of the initial population in the GA algorithm was set to 100 chromosomes. This choice proved to be a good compromise between computational load and convergence speed. In the fitness function, parameters $k_1$, $k_2$ and $k_3$ were set to $1,000$, $5,000$, and $1,000$, respectively, as these values proved appropriate to enable GA approach to explore effectively the borders of the feasibility region. The termination condition of the GA was set based on the convergence of the fitness value.

Specifically, convergence is reached when the geometric average of the relative change in the value of the spread over ($i = 10$) generations is less than $10^{-6}$, and the final spread is less than the mean spread over the past $i$ generations. Generation limit $m$ is set to 150 to prevent potential infinite iterations. This value was chosen based on an empirical evaluation of the typical number of iterations required across different starting points. Regarding the Crossover Heuristic, a $ratio = 1.9$ has been chosen, in order to have a good distance from parents, and prevent the algorithm from easily getting stuck at a local minimum.

The setup consists of an Intel Core i5 6-core - used in parallel - processor and 16 GB 2667 MHz DDR4 RAM, $T_{sim}$ has been always less than 2s. However, empirically observation confirms that in $x$ tries of the GA, out of the number of points evaluated for all the six configurations analyzed, the termination condition always brought the GA to converge before the maximum number of iterations. This confirmed the validity of the heuristic choice of the three constants $k_1$, $k_2$, and $k_3$, as it is hard to model analytically the mutual relationships between these constants and their impact on the resulting value assumed by the overall function.

### 7.1.2 *Receiver Architectures and Splitting Strategies*

To assess the accuracy and validity of the proposed framework, the simulatation evaluated the system for several values of user and BS densities, in the linear EH case. For each of the three power harvesting configurations, and over different values of user density, Fig. 7.1 shows the values of power per $km^2$ consumed by the network at the optima derived by GA, as well as those derived by simulating the system in those optima.

As the figure shows, the power consumed by EH IoT users has a strong impact on the total power consumed by the network, irrespective of the degree of energy proportionality of BSs. Indeed, at low user densities, consumed power more than doubles when the target minimum harvested power passes from 1 to 6 mW. At high user densities instead, the difference is smaller because the power consumed to provide information transfer dominates the overall energy footprint of the network. This is also due to the growing inefficiency of information transfer at high user densities, due to

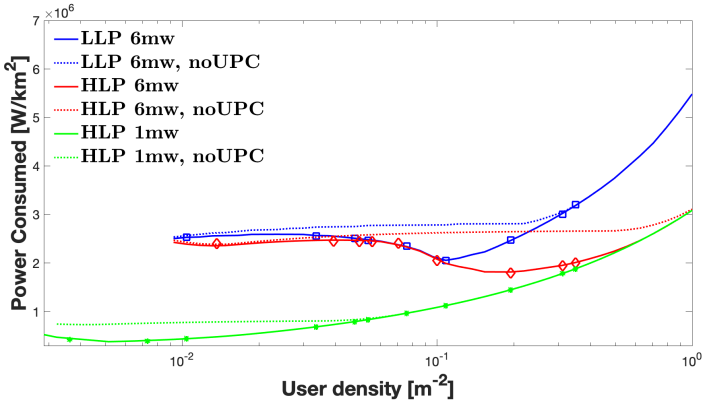


(a) Time Switching

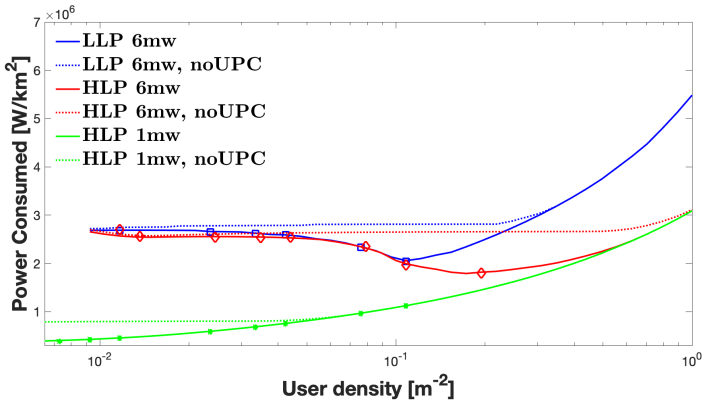


(b) Dynamic Power Splitting

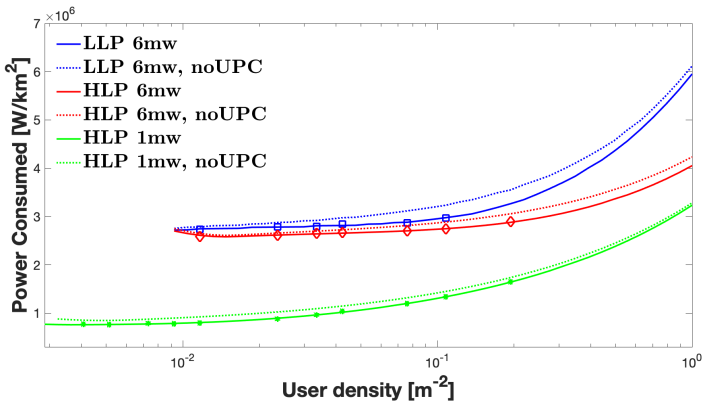


(c) Static Power Splitting

Figure 7.1: Power per $km^2$ consumed by the network at the optimum vs user density, for different target minimum harvested power and IoT UE receiver configurations. Markers denote values from simulations, derived with a 95% confidence interval of at most 8%.

rising interference levels.
Fig. 7.1 suggests also that modeling approach is extremely accurate across very diverse system configurations. Indeed, the markers reporting simulation results overlap the curves obtained with analytical model. In particular, very good accuracy is achieved even for low values of user density, for which the dense IoT regime assumption of Theorem 2 does not hold.

These results suggest that, in sharp contrast to RANs delivering only connectivity, as the density of IoT users increases, their contribution to the service capacity of the whole SWIPT network (in the form of power delivered to other IoT users) increases too. The effect is visible in all configurations when comparing the setting in which the energy harvested originates only from BS transmissions (the *no UPC* curves in Fig. 7.1), with those in which users can harvest energy also from transmissions of other users. In all configurations, as user density increases, its effects manifest as a decrease in the power consumed by the network. Such a decrease continues until a minimum is reached, after which the power consumed increases again with increasing user density. Such behavior is quite surprising, but is the result of the interplay between, on the one side, the detrimental effect of rising interference on communications (which decreases the efficiency with which network resources are used), and on the other, the beneficial effect of the increase in user transmissions on the amount of power harvested by IoT users. When increasing user density from very low values, these two contrasting effects cause the overall power consumed by the network to decrease, before increasing again due to the effects of high levels of interference on user-perceived QoS for data. The impact of user contribution to network service capacity is less marked when the target minimum service capacity is low (e.g., in the 1 mW plots), due to the low impact of power delivery on the overall consumed power of the network, and it increases for higher target minimum harvested power. Such impact is limited also in the SPS mode, due to the lower efficiency of passive EH in that configuration.

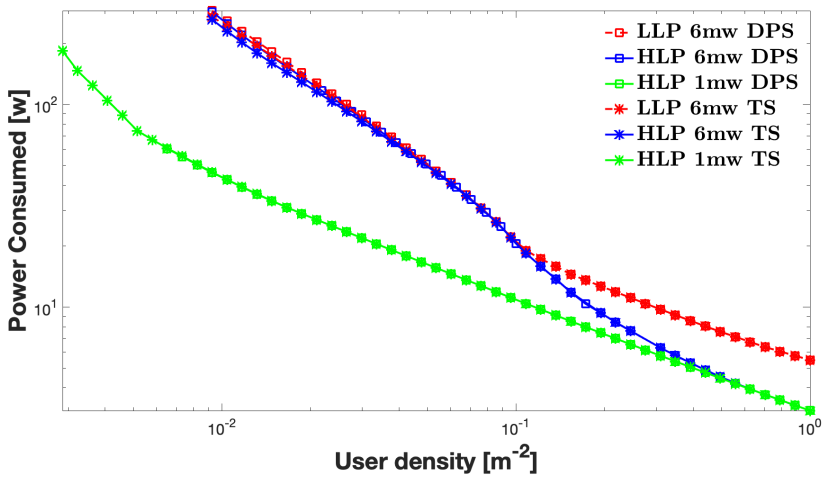


Figure 7.2: Power consumed by the network for each user (broadband or IoT) vs. user density, for different target minimum harvested power and IoT UE receiver configurations.

### 7.1.3 *Traffic Patterns and Base Station Density*

These features of optimal power consumption suggest that (possibly dynamic) configuration tuning holds the potential to play a key role in minimizing the energy footprint of a SWIPT network. Indeed, these features suggest that by taking advantage of user-provided service capacity, it is possible to make the network increasingly more energy efficient when the demand (of both energy and communication) it must satisfy grows. This is suggested also by Fig. 7.2, which shows that for all configurations and target minimum harvested power, the network energy efficiency increases when user density increases. Here too, when the user-provided service capacity dominates the overall energy footprint of the network, the decrease of per-user energy consumed is faster, while it tends to slow down for those user densities for which the effects of interference dominate. Quite surprisingly, for the same target minimum harvested power, when user-provided service capacity dominates, the power per user consumed by the network does not depend on the amount of load proportionality of the BS energy model (red and blue curves are very close). It is only when interference dominates that the higher BS densities

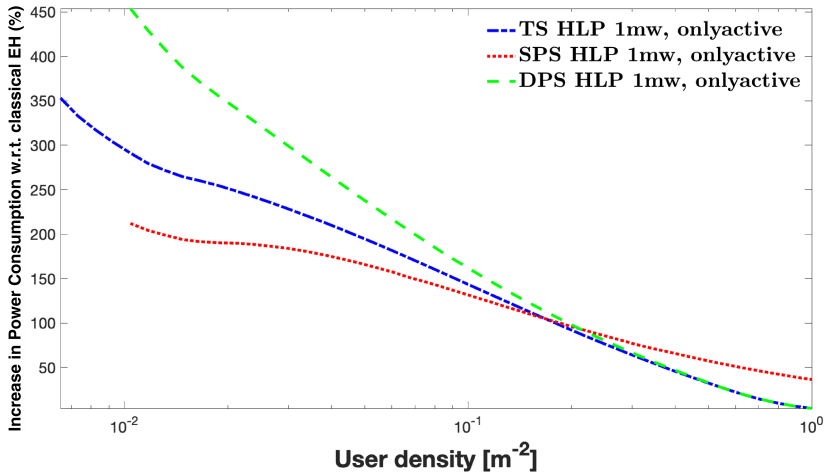


Figure 7.3: Increase in the power per $km^2$ consumed by the network with respect to linear EH, as a function of user density, for HLP 1 mW target minimum harvested power, and for different IoT UE receiver configurations.

required to satisfy the target QoS for information transfer bring an increase in the impact of the fixed energy costs of BSs on the overall energy footprint of the network.
The importance of passive energy harvesting in SWIPT networks is also visible from Fig. 7.3, which shows the increase in the network consumption when only active charging from the serving BS is available. Indeed, when passive EH is not available (e.g., due to limitations in the HW architecture of devices) the energy consumed by the network can be several times larger than in the case in which passive EH is available.

Another noteworthy feature of a SWIPT network emerging from Fig. 7.1 is that for each configuration of EH receiver architecture and target minimum harvested power, there is a value of user density below which no feasible solution to Problem 1 exists. This is due to the lower bound on the mean number of users per base stations (equal to 5 in evaluations). Indeed, as with increasing distance from the serving base station the power received by users decays much faster than channel capacity, guaranteeing a target QoS for harvested power at low user densities requires ever in-

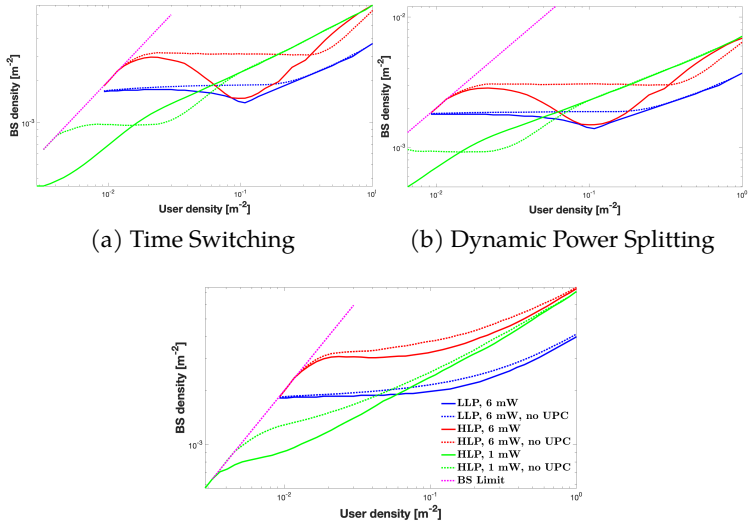


(a) Time Switching (b) Dynamic Power Splitting

(c) Static Power Splitting

Figure 7.4: Optimal BS density for different target minimum harvested power and IoT UE receiver configurations.

creasing BS densities and thus very low mean number of users per BS, up to the point of economic unfeasibility.

Note however that this is relative to a scenario in which users are distributed uniformly at random in space. In realistic settings, this implies that deployments of small amounts of EH IoT devices are of course feasible, but they should be, at least locally, dense enough to be able to deliver power with the target QoS while satisfying the system constraints.

Figures 7.4, 7.5, and 7.6 plot the optimal values of BS density, of transmit power, and of time split ratio (respectively, power split ratio), for the three EH receiver configurations. As Fig. 7.4 shows, in the TS and DPS cases the evolution of the optimal BS density as a function of user density is characterized by three regimes. First, for very low user densities, the optimal BS density increases with user density, as expected. For higher user densities, the optimal BS density reaches a plateau in the case without user-supplied service capacity, and it decreases in the case in which the full potential of passive EH is available. This feature suggests new and quite surprising patterns of BS sleep modes which, in con-

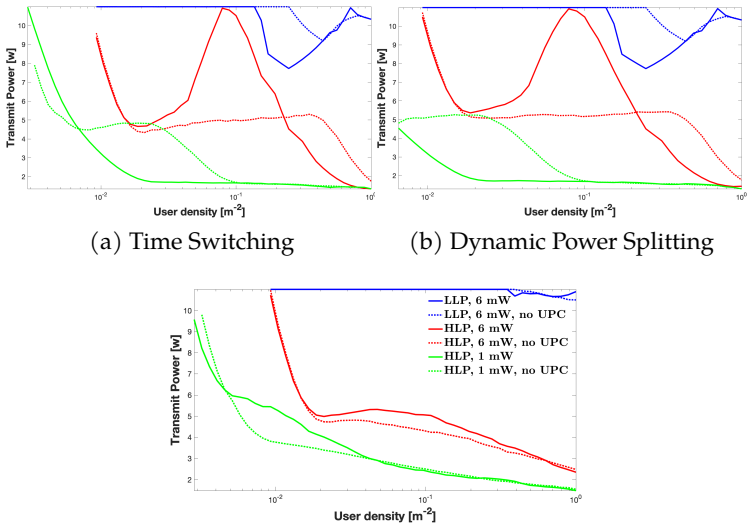


(a) Time Switching (b) Dynamic Power Splitting

(c) Static Power Splitting

Figure 7.5: Optimal transmit power for different target minimum harvested power and IoT UE receiver configurations.

trast to those for non-SWIPT RANs, turn off BSs when demand increases. Finally, for even larger user densities, in the interference-dominated regime, the optimal BS density increases again. These three regimes are not present however for all values of target minimum harvested power, due to the minimum user-per-BS limit adopted. These three regimes are not present in the SPS case, in which the lower efficiency of passive EH brings optimal BS densities which increase monotonically with user density.

Fig. 7.5 shows that optimal transmit power varies with user density in a specular manner to optimal BS density, decreasing when it increases, and vice versa. That is, the energy optimal strategies emerging from GA algorithm tend to compensate for the thinning (resp. densification) of BS density with cell zooming (resp. shrinking), via transmit power tuning. This is likely due to the fact that, when IoT node density increases, the impact on the system of the inefficiency due to high distance between BS and EH IoT users is stronger, pushing the optimal solution towards larger BS densities.

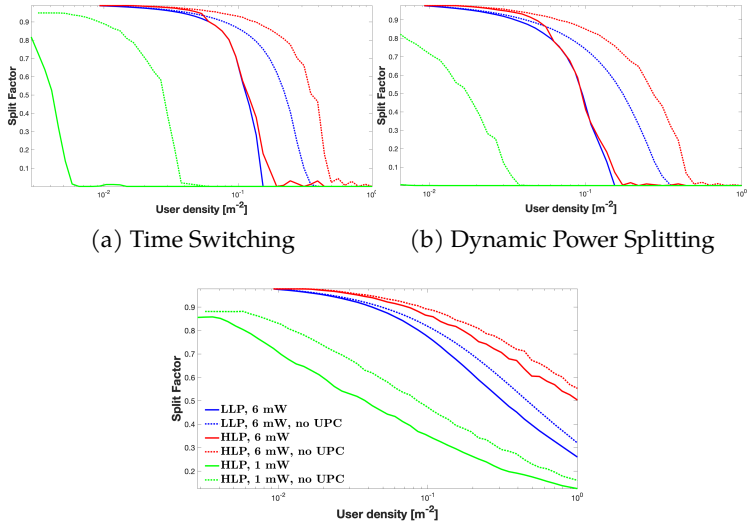


(a) Time Switching (b) Dynamic Power Splitting

(c) Static Power Splitting

Figure 7.6: Optimal time splitting factor (for TS) and power splitting factor (for DPS and SPS) for different target minimum harvested power and IoT UE receiver configurations.

### 7.1.4 *Impact of Splitting Factor*

Fig. 7.6 offers some key insights on how tuning split factor contributes to achieving energy-optimal operation of a SWIPT network. For low-load proportional BSs, as well as for configurations with high target minimum harvested power, the bulk of the energy consumed must be supplied by the serving BS, which thus has to allocate the majority of its time to transferring energy to IoT users. As expected, such a share of BS time is larger in scenarios with a larger target minimum harvested power. However, in all configurations, for increasing user densities, the share of BS time dedicated to active charging decreases, thanks to the combined effect of user-supplied service capacity, and higher BS density. Beyond a given user density (which depends on the BS energy model and receiver EH architecture) the SWIPT network effectively stops actively delivering power to IoT users (the split factor gets values close to zero), as passive power supply from ambient sources is sufficient to achieve the target QoS for energy harvesting. Again, note that for the SPS configurations, as har-

vesting from user transmissions is less efficient, the decrease in the splitting factor with increasing user density is substantially slower than in TS or DPS.
Finally, to characterize the effectiveness of GA algorithm, a comparison of the results derived from it with those achieved with a simple grid search heuristic has been done. This latter is based on the discretization of the optimization parameters, and on an exhaustive search over these discrete values. In all tests, overall considered settings and for different values of the discretization step, the difference in results was only due to the chosen discretization step, and could be made arbitrarily small with a finer discretization step. This suggests that, for all the considered settings, GA algorithm proved effective in avoiding the search process to get stuck into local minima, while being substantially more efficient.

### 7.1.5 *Nonlinear Energy Harvesting Effects*

A crucial aspect of the energy harvesting process is the presence of nonlinearities in the relation between the output power of the energy harvester circuit at the IoT devices and its input power. Indeed, such aspect may heavily affect the amount of harvested power as a function of the network settings, and thus the energy-optimal configuration of the whole SWIPT network. To investigate its impact on the energy-optimal strategies derived by GA, Equation 5.4 has been levaraged for another set of experiments. Following indications from the literature [145], the maximum output power $h_{max}$ has been set to 10 mW, $\chi$ to 274, and the sensitivity threshold $h_s$ to 0.064 mW. Figure 7.7 shows the nonlinear EH curve for the chosen parameters and for two values of $\iota$, which tunes the maximum efficiency of the nonlinear harvesting process. Its values have been chosen not to have a maximum efficiency larger than one, and to approximate the linear harvesting curve considered in the previous experiments. The figure also shows the linear harvesting functions whose slope approximates well that of the two sigmoids. As the plot shows, both sigmoids are characterized by a range of input power within which they are well approximated by a linear function (denoted henceforth as a *quasilinear regime*). Note that, with the given settings, choosing $\iota = 0.9$ (respectively, 1.30) produces a sigmoid which in the

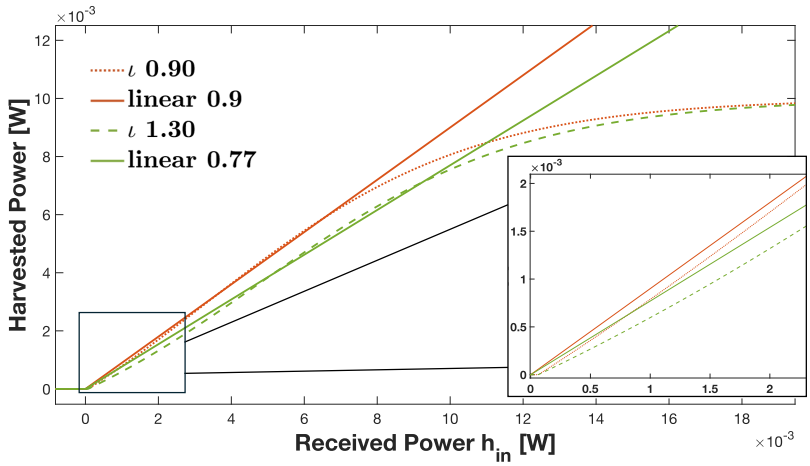


Figure 7.7: Harvested power as a function of power received by IoT EH user, for a linear (with conversion efficiency of 0.9 and 0.77 respectively) as well as for the nonlinear model (Equation 5.4) with $h_s = 0.064$ mW, and $\chi = 274$.

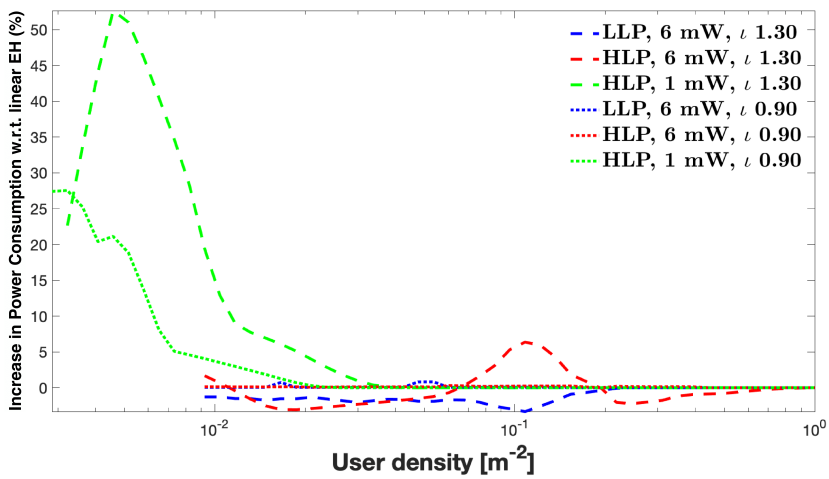


Figure 7.8: Increase in consumed power with respect to linear EH, as a function of user density, for different values of the parameter $\iota$ of the nonlinear EH curve, and for different network setups, in the time splitting configuration.

quasilinear regime approximates well a linear model with slope 0.9 (respectively, 0.77).

Figure 7.8 illustrates the increase in power consumed at the optimum induced by the nonlinear EH function versus that of its linear approximation, for the given values of $\iota$, and for time splitting EH mode. As the plot suggests, nonlinearity brings to an increase of the consumed power for target minimum harvested power values which are much lower than $h_{max}$, and for low values of user density. For a target harvested power of 1 mW the sigmoid is in a regime in which the conversion efficiency is 20% to 30% less than its maximum value, pushing the system to compensate with a more conservative transmit power allocation, thus bringing to a higher overall consumed power. This is more evident for lower user densities, as in those regimes the lower mean amount of users per base station brings (by the law of small numbers) to larger variance and thus to greatly amplify the effect of the 20% to 30% decrease in conversion efficiency on those users whose harvested power falls on the tail of the distribution.

## 7.2 VEHICULAR DEPLOYMENT ANALYSIS

In this section, we evaluate the impact of adopting the PLCP distribution in a SWIPT-enabled vehicular network, and compare it against the classical PPP baseline. Altough the main objective of the optimization problem is to evaluate the quality of the solution, some interesting insights will be carried out by loooking at the system parameters. Network power consumption, optimal BSs density, transmit power, splitting factor, and harvested energy will be evaluated.

### 7.2.1 *Network Power Consumption and Deployment Strategies*

Fig. 7.9 reports the total power consumption per square kilometer at the optimum. At low user densities, both PPP and PLCP exhibit a nearly linear increase in consumption, since interference remains limited and the BSs operate under low load. As the density grows, both the PPP and PLCP configuration shows a faster-than-linear increase, due to the higher probability of spatial overlap among BSs randomly scattered in the plane, which generates too much interference, and consequential causes the deployment

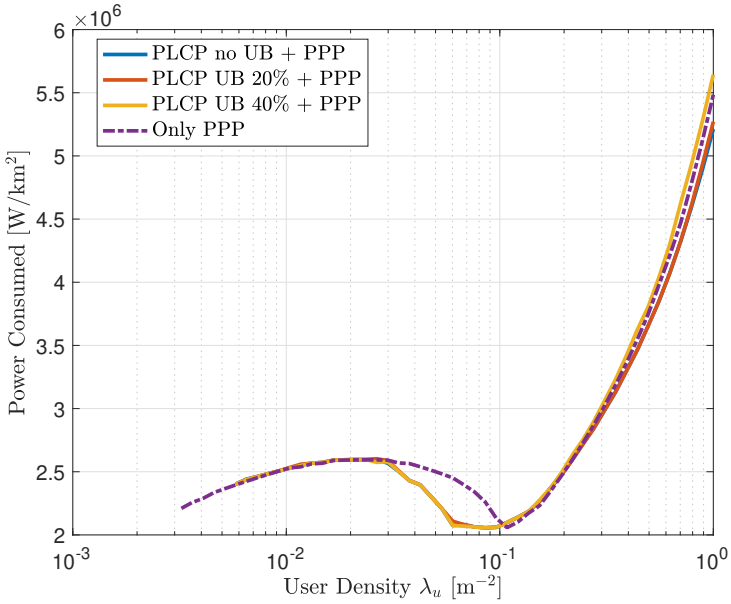


Figure 7.9: Power per $km^2$ consumed by the network at the optimum vs user density, for different BS distributions.

of additional BS. Interestingly, the curves behave similarly for the entire range of UEs considered, except for a short range in the middle, where the new approach reduces the overall power consumed; suggesting PLCP can give advantages over PPP. This is somehow counterintuitive since placing BSs randomly in the space should put typical user closer to the associated BS, as confirmed also by the CDF of the UEs distribution. Therefore, a deeper analysis on main system parameters will give an explanation for this behavior.

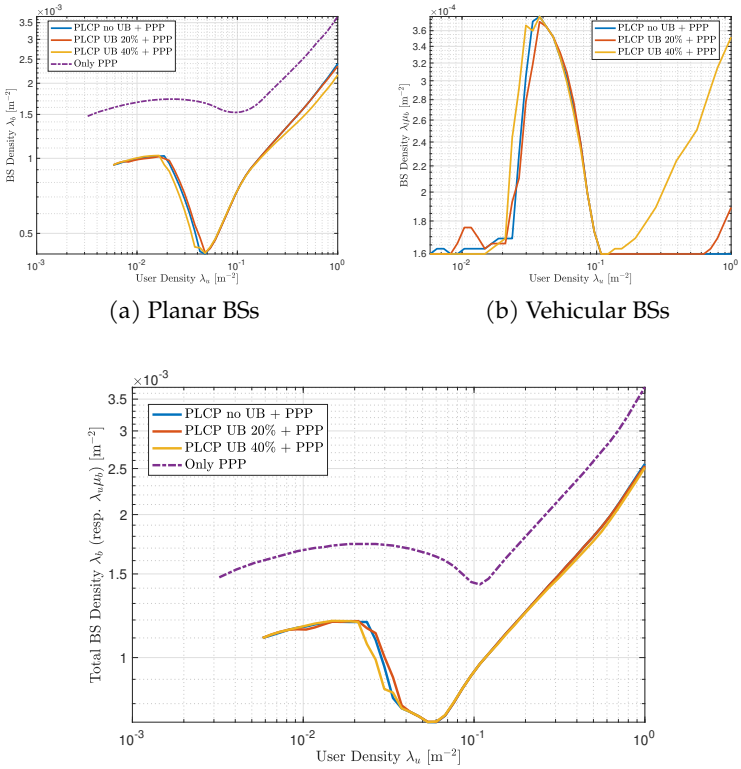


(a) Planar BSs (b) Vehicular BSs

(c) Total BSs

Figure 7.10: Optimal BSs densities for different minimum number of vehicular BS and system design.

Figures 7.10a, 7.10b, and 7.10c illustrate the optimal density of PBSs, VBSs, and their total, respectively. Here it is possible to notice a strong change in the total amount of deployed BS, in particular for the range where PLCP introduces some advantages into the system. In fact, at intermediate user densities, the optimization favors a reduction in PBS deployment, compensated by an increase in VBSs (plateau in Fig. 7.10b). This behavior suggests that this trade-off is particularly effective where the road-constrained distribution allows for better spatial alignment between users and BSs. It seems that system benefit from the distance between the users and the BSs, suggesting that interference generated by the users transmission might be relevant. At very low or very high densities, the difference between PPP and PLCP diminishes, since

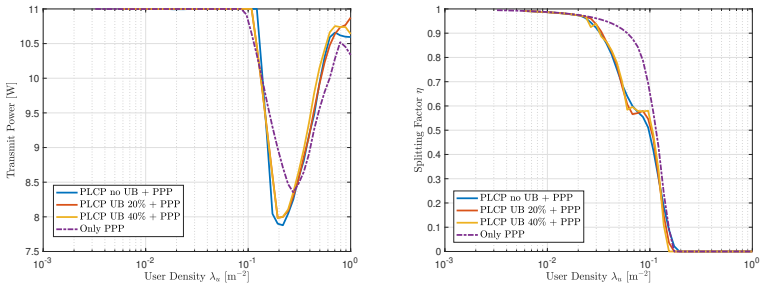


(a) Transmit Power (b) Splitting Factor

Figure 7.11: Optimal system parameters for different minimum number of vehicular BS and system design.

either the system is underutilized or it becomes saturated, forcing the system to deploy additional BSs in both cases. The only relevant remark is that PLCP tries to push on the PBSs when the densities are high or lower, and this seems to be caused by the fact that placing BSs on the street results in a lower probability of finding a close BSs. Anyway the behaviour in the center is still an open point, and the only confirmation till this point is that placing BSs on the streets is beneficial, suggesting a benefit in having UEs far away from the closest BS.

### 7.2.2 *Transmit Power and Splitting Optimization*

Figures 7.11a and 7.11b present the optimal transmit power and splitting factor. Both PPP and PLCP lead to similar power levels, confirming that the primary advantage of PLCP is not in raw transmission but in spatial distribution. The splitting factor, however, exhibits a slightly different trend under PLCP, which is the key factor which lead to the conclusion introduced at the beginning and suggested by the vehicular BSs increase, which is motivated by the interference generated by the other UEs in the system.

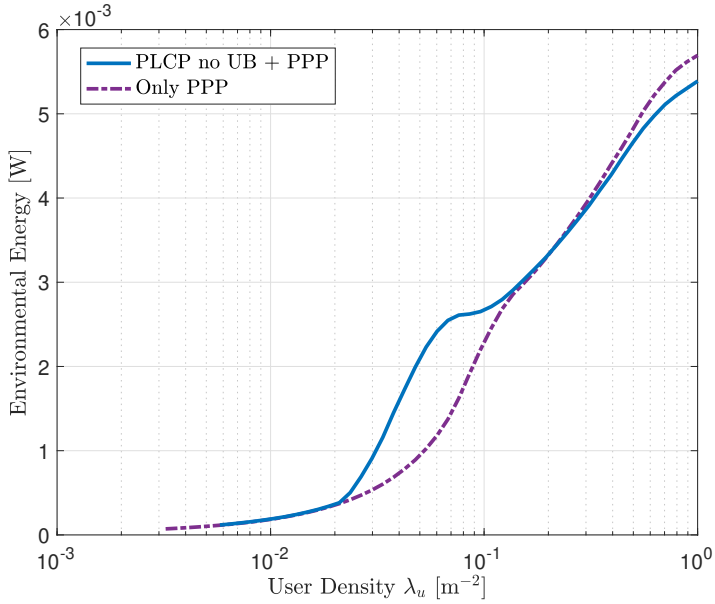


Figure 7.12: Energy Harvested from other UEs vs. user density for different BS distributions.

### 7.2.3 *Harvested Energy Performance*

The most striking evidence of PLCP's benefit is given in Fig. 7.12. Here, the harvested energy from interfering BSs and UEs is plotted against user density. In the PLCP case, users are on average located further away from their serving BS compared to the PPP case. While this may appear disadvantageous from a connectivity perspective, it actually increases the contribution of surrounding transmitters as energy sources. The interference, which is typically harmful in a pure communication system, becomes a valuable source of wireless power for IoT devices. This explains why the harvested energy under PLCP consistently exceeds that of PPP in the intermediate density range. Importantly, this effect highlights the dual role of interference in SWIPT networks: detrimental to rate, but beneficial to energy harvesting.

## 7.3 SUMMARY OF FINDINGS

This section summarizes the main results obtained from the numerical validation of the proposed optimization framework, highlighting how system-level tuning, receiver architecture, and deployment geometry influence the energy efficiency of SWIPT-enabled heterogeneous networks.

**F1.1** *Stochastic geometry provides a good approximation for massive SWIPT Networks for all the harvester architectures.*

The stochastic-geometry framework, consistently converges to result produced by simulations, confirming the accuracy of such an approach. Moreover, I demonstrated the usage of such a framework in combination with an optimization problem that reduce the total consumed power per km$^2$ while satisfying delay and EH targets across a broad range of user densities and EH receiver configurations (TS/DPS/SPS). The results between analysis and simulation in Fig. 7.1 confirms the analytical curves and confidence intervals within 8%. The inclusion of a realistic BS energy model (LLP vs. HLP) further shows that proportionality affects the absolute impact and the behavior, indicating the framework's robustness to architectural differences.

**F1.2** *Interference, traditionally negatively affecting the throughput, can be transformed into a useful energy source when properly managed and accounted for by the optimizer.*

The curves in Fig. 7.1 and the per-user impact in Fig. 7.2 reveal a non-monotonic behavior with user density: beyond a sparse regime, the network-wide power decreases as density rises, before increasing again at very high densities. This *valley* is explained by the user-provided service capacity: uplink and downlink transmissions from surrounding UEs and BSs become an ambient RF resource for EH devices. When UPC contributions are significant, the optimizer reduces active charging (split factor $\rightarrow 0$) and relies more on passive harvesting, thereby lowering $P_{\mathrm{BS}}$ or the effective BS "on-time." Conversely, when interference is too low, the optimizer increases the BS transmission power, since devices cannot harvest energy from the environment. This duality implies that interference management in SWIPT should be two-sided: reduce

it for reliable information decoding; while shaping and exploiting it as an energy reserve for EH under dense context.

**F1.3** *Receiver architecture and splitting strategy decisively influence efficiency: TS and DPS outperform SPS and enable a progressive shift toward passive harvesting as density grows.*

The optimal splitting patterns in Fig. 7.6 show that TS/DPS architectures allow the network to transition from active to predominantly passive EH as density increases. The curves in SPS context show that in this case it is hard to take advantage from the environment. In SPS, the devices cannot harvest the part of the signal dedicated to data transfer, because the harvester is designed to harvest only at a given set of frequencies, reserved to power transfer. This is reinforced by Fig. 7.1, where removing passive EH leads to marginal consumption increase only in the case of SPS, evidence that architecture-level choices directly set a limit to achievable efficiency.

**F1.4** *Three density-dependent regimes emerge: (i) a feasibility-limited sparse regime, (ii) an intermediate regime where passive harvesting support the EH-nodes, and (iii) a high-density, interference-dominated regime that re-inflates power demand.*

The sparse regime is bounded by feasibility (mean users per BS $\geq 5$), reflecting the rapid decrease of power harvested by other devices. The intermediate regime is where the system is most efficient: passive harvesting compensates active EH, the split factor decrease, and per-user power drops. At very high densities, interference dominates, forcing densification of BS or power increases to preserve QoS, causing the exponential increase in power consumption. This characterization provides a clear policy: target the intermediate density UEs is beneficial with respect to having few users, suggesting that it is beneficial to have UEs active, despite it is not needed.

**F1.5** *Nonlinear EH characteristics can be well-approximated by linear harvesting in dense context where additional harvested energy does not contribute to the reduction of energy spent by the network operator.*

The sigmoid mapping (Fig. 7.7) shows a quasi-linear regime whose slope is below the linear model efficiency; at a 1 mW tar-

get the operating point sits 20–30% below the peak conversion efficiency. As Fig. 7.8 indicates, the optimal consumed power rises relative to the linear case, differently by the low densities where the variance of received power is high.

**F1.6** *Vehicular deployments modeled via PLCP offer advantages over planar PPP for medium-dense context: line-constrained BSs increase interference and enhance ambient harvesting.*

The total consumed power in Fig. 7.9 shows a consumption gap in favor of PLCP within a medium-density window. Fig. 7.10 reveals the behavior: the optimizer reduces planar BSs and increases vehicular BSs, exploiting road-aligned geometry to reshape interference and spatial proximity. Although the average UE–-BS distance can increase under PLCP, the spatial correlation of transmitters along lines broadens the useful ambient RF field, boosting harvestable energy (see Fig. 7.12) without raising nominal transmit powers (cf. transmit-power parity in Fig. 7.11a). The splitting factor responds accordingly (Fig. 7.11b), shifting load away from active EH.

SG is a powerful tool for analyzing network, and results demonstrate that is possible to extend its usage to SWIPT networks as well. Findings give a concrete answer to RQ1, related to the optimal tradeoff. The role of interference is the most important parameters, followed by the harvesting architecture, and BS displacement. If by one side the interference disrupt the broadband communication, under certain limits it can be beneficial to reduce the active harvesting of EH-devices. For medium density context the interference is beneficial, and can EH-devices can benefit from it.

# 8 NEXTGEN ENABLERS RESULTS

This chapter presents the numerical evaluation of the impact of beamforming on SWIPT network, using a two-level framework introduced in Chapter 5. The goal is to validate the analytical model and investigate the role of beamforming on the harvesting process. The numerical analysis focuses on two aspects: (i) the optimal beam allocation derived for a given user distribution, and (ii) the expected performance in scenarios where UE positions follow a random spatial distribution, approximating the results of the fine-grined algorithm of individual deployment.

The simulation setup, parameters, and performance metrics are first detailed. Then, the obtained results are discussed in relation to the analytical expectations, highlighting the quality of the approximation provided by the analytical framework as well as the impact of the beamforming configuration on energy harvesting efficiency. This chapter ends with a summary of findings, giving a concrete response to RQ2, reported here as reminder:

**RQ2.** *How can enabling technologies from NextGen networks* (e.g. beamforming) *be exploited to enhance the efficiency of EH in SWIPT-enabled HetNet?*

## 8.1 BEAMFORMING DESIGN AND OPTIMIZATION

### 8.1.1 *Parameter Setup*

To conduct the experiment I considered a scenario composed by a single BS capable of performing beamforming using IRS. The BS covers a varying area with $R_{\min} = 2$ meters and $R_{\max}$ varying from 25 meters up to 100 meters, with a UEs spatial density $\lambda_u$ varying from $6 \times 10^{-2}$ to $6 \times 10^{-3}$, unless otherwise indicated. The BS delivers energy using the NB-IoT channel, therefore working with a bandwidth of 180 $MhZ$. For the path-loss I adopted an $\alpha = 2.2$ typical of suburban and macrocell with Line of Sight

(LOS). The time frame $\tau$ is normalized, and its value is 1. The transmission power $P_{tx}$ is 4 $W$, with the power adjusted depending on the directionality of the beam according to the formula defined in Chapter 5.

### 8.1.2 *Optimal antenna design*

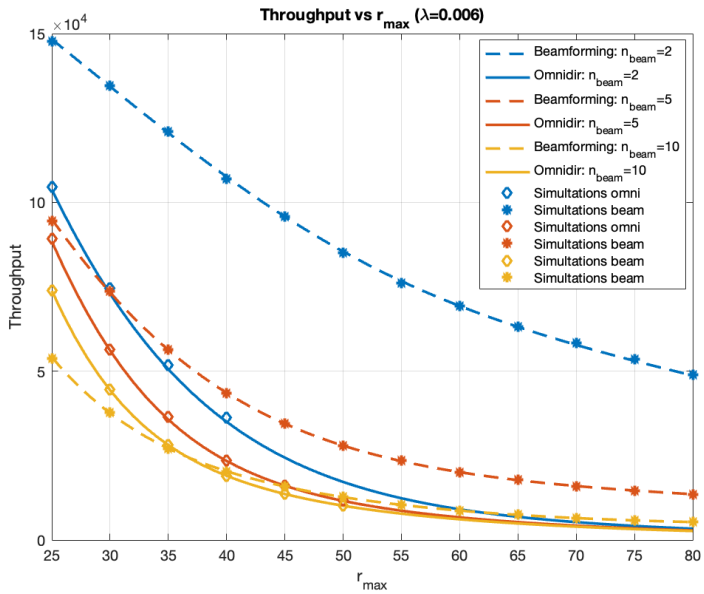


Figure 8.1: Throughput vs $r_{\max}$ for $\lambda = 0.006$ and $\sigma_b = \frac{10\pi}{180}$ for different number of sectors in the disk.

Evaluating the considered analytical frameworks lead us to some preliminary results represented in Figures 8.2 and 8.1, respective for $\lambda_u = 0.06$ and $\lambda_u = 0.006$. In both cases I considered a $\sigma_b = \frac{10\pi}{180}$. I represented the system under different number of active beams, and with corresponding omnidirectional scenario. As illustrated in Figures 8.1 and 8.2, the optimal strategy strongly depends on the user distribution. For shorter distances from the BS and higher user densities, the omnidirectional transmission is preferable. In fact, in such cases the omnidirectional approach is able to provide sufficient received power while covering a large number of users simultaneously, which translates into longer periods of pas-

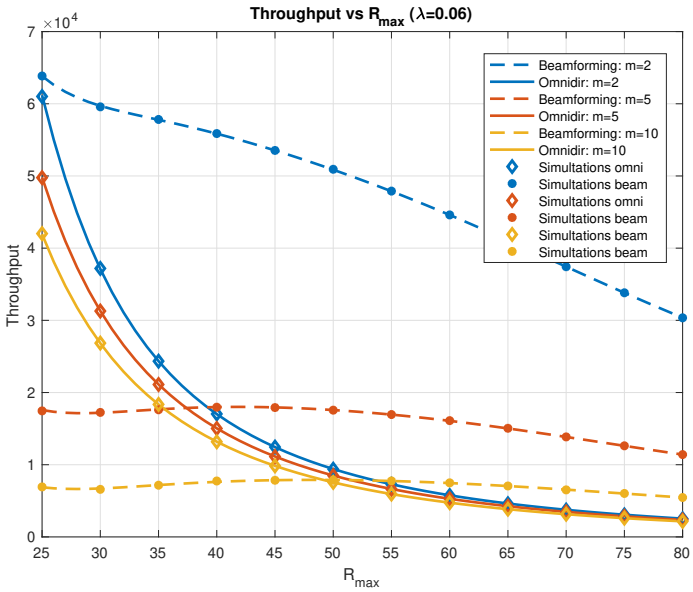


Figure 8.2: Throughput vs $r_{\max}$ for $\lambda = 0.06$ and $\sigma_b = \frac{10\pi}{180}$ for different number of sectors in the disk.

sive harvesting. Conversely, narrow beams restrict the number of users and limit the harvesting time. Interestingly, when the number of active beams is reduced, beamforming becomes advantageous since the lower user density within each beam does not provide enough energy, making it more effective to concentrate the transmitted power toward that sector.

Fig. 8.3 provides further insights on this beahvior. In the single-user case, the omnidirectional strategy clearly leads to lower harvested power. However, due to the sigmoidal nature of the harvesting function, increasing the transmit power beyond a certain point no longer increases the harvested energy. This saturation effect reduces the benefits of beamforming. On the other hand, in the omnidirectional scenario the higher number of users compensates for the individual harvesting loss, resulting in a higher aggregate harvested energy. From the combined effect of (1) and (2), it emerges that beamforming may lead to worse user performance under specific conditions. Although beamforming increases the instantaneous received power, the harvesting circuit cannot fully exploit it due to saturation. In such cases, harvest-

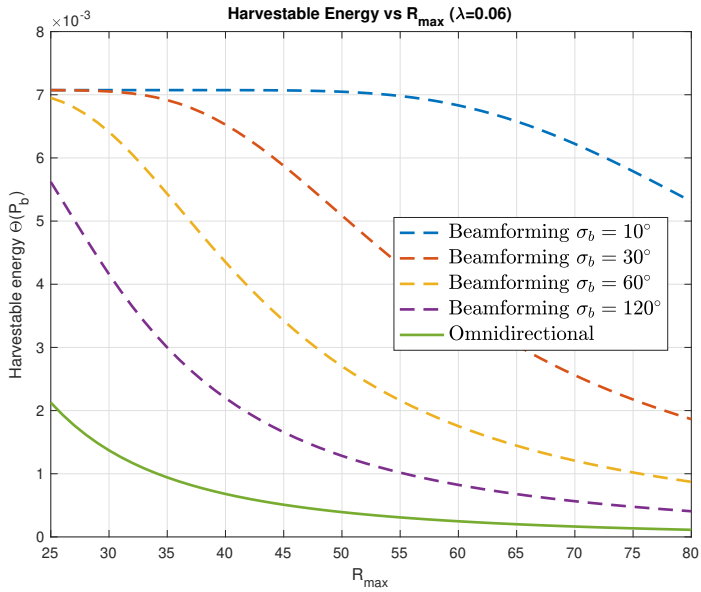


Figure 8.3: Instantaneous harvestable energy at distance $R_{\max}$ vs $R_{\max}$ for $\lambda = 0.06$ and $\sigma_b = \frac{10\pi}{180}$ for different number of sectors in the disk.

ing over longer periods (as in the omnidirectional scenario) is more beneficial than receiving higher but short energy bursts. As shown in Figure 8.3, the harvested energy under beamforming does not scale with the number of beams, since each user can only harvest when its beam is active. In contrast, for omnidirectional transmission the harvested energy decreases with $r_{\max}$, highlighting the stronger dependence on received power. This shows that even with additional users, the progressive reduction in received energy cannot be fully compensated.

Finally, Figure 8.4 reveals a key system behavior. In omnidirectional transmission, the optimal fraction $\delta^*$ increases with user density (or equivalently with $R_{\max}$), meaning that the system gradually shifts from being transmission-constrained to energy-constrained. Conversely, in beamforming scenarios $\delta^*$ decreases, indicating the opposite behavior: the BS transmits more power to a large set of UEs, which increase the total time of the beam. This observation highlights the trade-off: beamforming is particularly beneficial for distant users, while omnidirectional transmission is more

effective at short distances, where user density and interference dominate system performance.

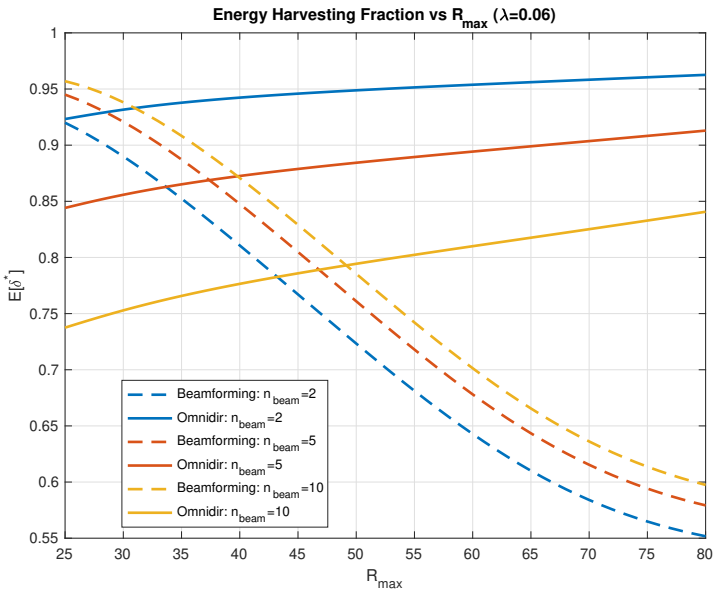


Figure 8.4: Energy Harvesting Fraction vs $r_{\max}$ at distance $r_{\max}$ for $\lambda = 0.06$ and $\sigma_b = \frac{10\pi}{180}$ for different number of sectors in the disk.

### 8.1.3 *Optimal non-overlapping beam scheduling*

Having defined which is the best antenna design depending on the UEs distribution, and density, I will introduce the performance of the optimal non-overlapping beam scheduling. The usage of dynamic programming can provide an optimal solution by definition, anyway such heuristic is not always applicable due to the missing knowledge on the scenario. In fact, in some cases beamforming cannot be established on the fly, such as the case of fixed-size beam. To this end I evaluated the system using the analytical formulation, and compared with the results given by the optimal scheduling policy.

Results reported in Fig. 8.5 show the comparison between the analytical framework and the dynamic programming approach for two different UEs distribution. In the first case UEs are dis-

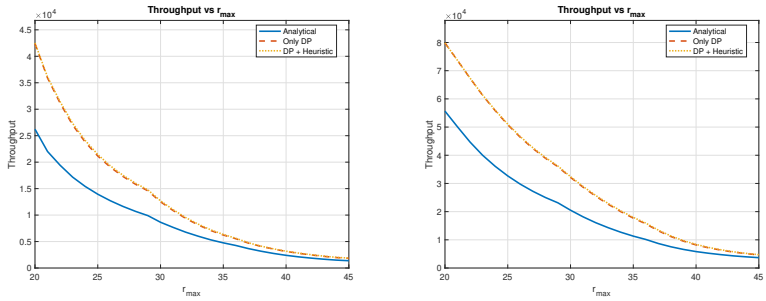


(a) UEs distributed in 2 sectors of 90° (b) UEs distributed in 3 sectors of 30°

Figure 8.5: Throughput vs $R_{\max}$ for different optimization methodology for $\lambda = 0.006$

tributed in two sectors of 90° degrees, while in the second case UEs are distributed in three sectors of 30°. In both cases, the main different is for low $R_{\max}$ distances, where the dynamic programming yield an interesting increase with respect to the analytical framework. This is mostly due to the characterization of UEs distribution. In the case of analytical framework UEs are distributed randomly in the sector, hence the only possible strategy is to create a beam of the size of the sector itself. This approach is not the best choice for context where UEs are close to the BS. In fact, as shown in discusses in the previous section, when UEs are close to the BS, it is preferred to use an omnidirectional antenna yielding the best result.

### 8.1.4 *Heuristic for beam overlapping*

The scheduling discussed in the previous section can be extended with the heuristic in Section 5.1.3.2. However, as shown in Fig. 8.5, allowing beam overlaps does not provide additional insight or measurable gains over the dynamic programming solution without overlap. The main reason is the saturation of the harvesting module: once devices receive enough power to reach the harvester capacity, increasing instantaneous received power does not translate into more harvested energy.

Consequently, the DP schedule for the non-overlapping case remains a very good approximation even when overlaps are al-

lowed. Adding an extra beam typically requires taking time away from an existing beam that already lead the UE near saturation. This redistribution neither improves the worst-case UE—since the DP schedule already covers as many UEs as possible—nor extends their effective harvesting time. In particular, inserting a narrow beam for a single UE brings no benefit to the worst-case metric if that UE is already energy-saturated. While overlap can increase the instantaneous sum of received power, with a saturating harvester it does not yield additional harvested energy nor longer active time.

## 8.2 SUMMARY OF FINDINGS

**F2.1** *In SWIPT networks, the throughput is not proportional to the beam narrowness.*

This finding, despite counterintuitive when compared to traditional wireless networks, holds in the case of SWIPT systems. The underlying reason lies in the energy harvesting process: UEs can only harvest energy when they are covered by an active beam, which requires each beam to remain active for as long as possible. In a fair resource allocation scheme (e.g., TDMA with equal time per user), the activation time of each beam is inversely proportional to the number of UEs it serves. As a result, the narrower the beam, the less time each UE has to harvest energy, leading to reduced performance. SWIPT networks start to behave like conventional ones only in very sparse user regimes, where distant users require narrow beams to receive enough energy to support uplink transmission.

**F2.2** *Omnidirectional transmission is the optimal antenna design in SWIPT network under a given maximum user distance from the BS and user density.*

Under small $R_{\max}$ ($\approx 30m$), all the UEs are close to the BS and the received RF power often lead the rectifier into (or near) saturation, so the harvestable power is capped by the harvester limit (see Fig. 8.3), around $\approx 0.007$ W in the considered setup. In this regime, increasing the instantaneous received power above the saturation point yields no extra DC output: the energy peaks cre-

ated by narrow beams are wasted. Moreover, a narrow beam covers any given UE only for a smaller time, as evident from the fact that at low UEs densities, the system increase the splitting factor (see Fig. 8.4); thus the UE experiences short recharging-periods. Omnidirectional transmission, instead, keeps each UE persistently near the efficient operating region for the entire frame, maximizing time at effective power and therefore the net harvested energy. As $R_{\max}$ increases (or effective user density per sector increase), the edge UEs move out of the saturation region: the omnidirectional instantaneous power is below the rectifier limit, and the system becomes energy-limited. In this regime, directional antenna can overcome the rectifier threshold during its on-periods and produce more DC energy despite the smaller number of devices, leading to a gradual benefit.

**F2.3** *Beamforming degrades the performance of SWIPT network under a given maximum user distance from the BS and user density due to sectorization and harvester limitations.*

The usage of beamforming introduces a drawback for the UEs, since it reduces the overall activation time of the beam, directly impacting the ability of harvester to harvest energy for long time. As highlighted in Fig. 8.2, it exist a region, where throughput is no longer a decreasing function of UEs distance, with the behavior being reversed. Such a region exists because in low UEs densities region, beamforming leads to performance deterioration due to the reduced number of UEs covered. This means that for the same region where omnidirectional is preferred, the narrow beam must be avoided, and this is proportional to the beam aperture; the more the narrowness, the worse the performance achieved.

**F2.4** *An optimal policy for SWIPT network must take into account the distribution of UEs and design beam accordingly, taking the positions of UEs as extreme points of beam.*

The spatial distribution of users is a key factor in determining the performance of SWIPT systems. Since both power transfer and information delivery depend on beam coverage, an optimal configuration requires covering the highest number of UEs while not making the worst-case UE loose energy. This ensures that every user within a beam can simultaneously benefit from sufficient

energy harvesting and communication opportunities. The DP approach is able to design such a scenario by creating custom beams, whose extreme points are in the location of two UEs of the scenario. Analytical framework, on the contrary, is only able to give an approximate result which get closer to the DP only for high user density, and for high $R_{\max}$, due to the increase of the probability to find a UE on the border of the sector.

**F2.5** *The heuristic enabling overlapping by creating additional beam directed towards the worst-case users produces marginal effects.*

It should be clear now that increasing the number of beam toward a direction should be beneficial, this because if a UE is covered by two beams, then can benefit from both. Anyway, results (see Fig. 8.5) show that proposed heuristic does not add any contribution to the result proposed by DP algorithm. The motivation for this behavior is related to the fact that DP already choose for the best beam able to increase the throughput of the worst UE, therefore if a better beam involving such a user exist, then the UE would move there, causing the DP to yield a different solution involving such a beam. Therefore, unless carefully designed, is hard to define a strategy able to increase the performance of DP, therefore creating additional beam towards the worst-case users produces marginal effects.

# 9 DEVICE-SIDE POLICY RESULTS

This chapter discusses the results related to the device-side policy introduced in Chapter 6 with the aim of highlighting the best policy for energy harvesting devices in HetNet. The first part of this chapter discusses a two node scenario, seeking to optimize the AoI at EH-node under the stability of queue at non-EH node. This characterization allows for the analysis of a time-sensitive application. The second part, instead, focuses on the analysis of load shifting policies in a cellular network, outlining the optimal policy for non-critical HetNet, allowing devices to shift the load across time slots. This chapter ends with the main findings, giving a concrete response to RQ3, reported here as reminder:

**RQ3.** *Which UEs policies can be employed to enhance performance and harvesting process in SWIPT-enabled HetNet?*

## 9.1 ANALYSIS OF TIME-SENSITIVE POLICY

### 9.1.1 *Parameter Setup*

Let us consider a fixed energy buffer size, denoted as $B = 1000$ for the EH-node. For the physical layer, the threshold for successful decoding was set to $-1$ dB. The path loss coefficients for nodes $S_1$ and $S_2$ were both set to 1, represented by $\beta_{S_1} = 1$dB and $\beta_{S_2} = 1$dB, respectively. The probability of successful decoding was defined as $\epsilon = 10^{-6}$. The transmit power of node $S_1$ was allowed to vary between a minimum of $P_{\text{min}} = -2$ dBm, and a maximum of $P_{\text{max}} = 20$ dBm, which is typical for ZigBee antennas. Similarly, the transmit power for node $S_2$ was set to vary between 0 and 20 dBm, depending on the energy units used for the transmission. The maximum number of energy units that it is possible to use for the transmission by $S_2$, $N_{\text{max}}$, was set at 100, suitable for the infinity condition of B ($N \ll B$), and corresponding to batteries of 100mW. To better understand the behaviour

of system parameters, we relaxed the transmission probability of both nodes, considering $q_i = 1$ for $i \in \{1, 2\}$.

### 9.1.2 *Effect of Energy Availability and Thresholds*

The first objective of our analysis is to evaluate which operational configuration-ECR, where $q_2 N > \delta$, or ESR, where $q_2 N \leq \delta$, offers optimal performance under different packet and energy arrival rates. Figure 9.1 shows that ECR consistently outperforms ESR in terms of minimizing AoI across all considered scenarios, thus confirming that energy availability does not imply any reduction in the overall AoI. Despite this behaviour seems to be counter-intuitive, the main motivation is that in ESR, the EH-enabled device pick up an access probability $q_2$, which is lower with respect to ECR-case to prevent the exceeding of the energy arrival rate. This has a direct consequence on the accessing time, which is much more higher. This advantage is particularly evident at higher values of $\lambda$, where interference becomes more significant, while at lower values of $\lambda$, and higher values of $\delta$, the gap between ECR and ESR is marginal.

This behavior is further illustrated in Fig. 9.2, where AoI is shown as a function of the access probability $q_2$ for a fixed arrival rate $\lambda = 0.001$. The AoI exhibits a monotonic decrease as $q_2$ increases, confirming that higher access probabilities are beneficial in both operational regimes. For low energy harvesting rates $\delta$ and higher energy requirements $N$, ECR clearly outperforms ESR, as the AoI transition point shifts to lower values of $q_2$. Conversely, when the interference from node $S_1$ is negligible and the energy consumption of node $S_2$ does not significantly affect AoI, the performance of ECR and ESR becomes asymptotically equivalent. This convergence is primarily attributed to two factors: (1) the absence of interference from node $S_1$, which means node $S_2$ has no incentive to increase its transmission power; and (2) the reduced impact of $N$ on the transmission success probability of node $S_2$, a condition that becomes more evident as the blocklength-induced decoding error probability $\epsilon$ increases.

These findings are crucial for heterogeneous network design: although ESR may seem ideal in low-interference settings, prac-

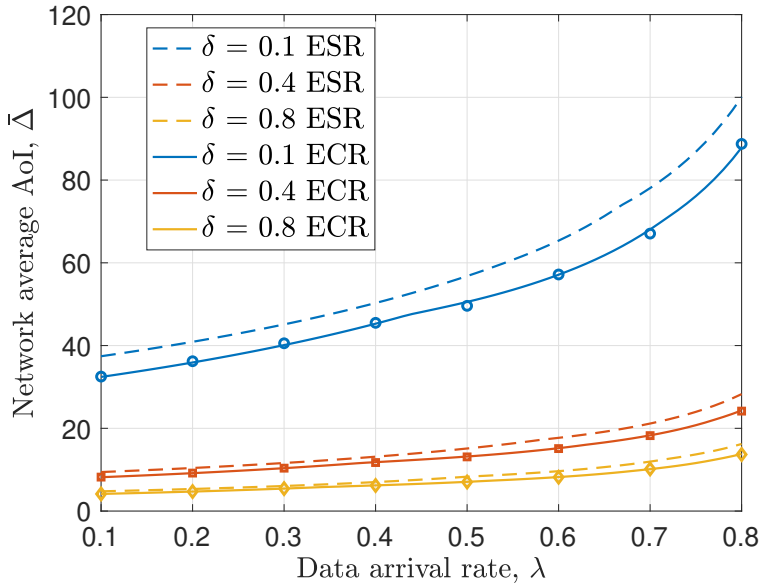


Figure 9.1: Optimal AoI at EH-node ($S_2$) vs. data arrival rate $\lambda$ at node $S_1$, for different energy harvesting rates $\delta \in \{0.1, 0.4, 0.8\}$ and different regimes. Markers represent simulations.

tical scenarios with moderate to high interference clearly favor ECR-driven strategies.

To further investigate the best configuration, we focus the analysis on the ECR regime; where Figure 9.1 illustrates that optimal AoI increases monotonically with $\lambda$, with steeper growth observed at lower $\delta$. For example, when $\delta = 0.1$, AoI exhibits superlinear growth beyond $\lambda > 0.5$, indicating a threshold beyond which interference critically impairs update timeliness. A clear motivation of this increase can be found in Figure 9.3, which reveals a threshold-driven allocation of the energy units $N$, which can be divided into two regimes: (1) Low-Traffic Regime, where the optimal strategy is to maintain $N = 2$, regardless of $\delta$, due to minimal interference from $S_1$; (2) High-Traffic Regime, where the system increases $N$ to enhance transmission robustness in the presence of stronger interference.

As shown in Fig. 9.3, increasing $\delta$ shifts the transition to higher $N$ values earlier. This reflects faster energy replenishment at node $S_2$, enabling it to adopt more aggressive transmission policies un-

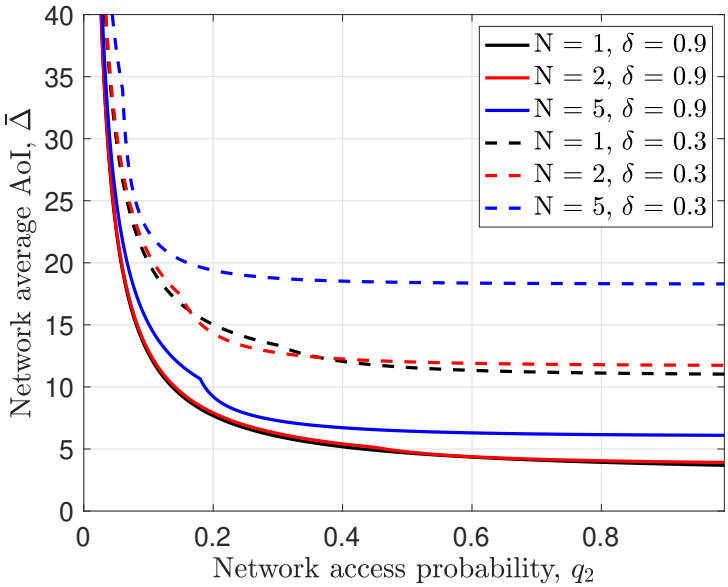


Figure 9.2: AoI at the EH-node $S_2$ vs. access probability $q_2$, under both ECR and ESR for a fixed data arrival rate $\lambda = 0.001$ at node $S_1$. Transition between regimes happens at $q_2 = \delta/N$.

der high interference. The influence of $N$ on AoI is further examined in Fig. 9.4, which compares AoI performance for fixed $N$ values. Higher $N$ values reduce AoI at larger $\lambda$, confirming that robust transmissions help counteract increasing interference from $S_1$.

### 9.1.3 *Effect of Interference on Freshness*

To complete the discussion of the effect of interference on the non-EH node, it is possible to take a look to Figures 9.5 and 9.6, representing the optimal access probability $q_1$ and transmit power $P_1$ for node $S_1$, respectively. Also in this case, similarly to the EH-node, two operational regimes emerge: (1) Non-Saturation Regime $q_1 < 1$, where $S_1$ can adapt its activity to improve AoI of $S_2$ while maintaining queue stability; (2) Saturation Regime $q_1 = 1$, where system adjust $P_1$ to sustain stability as no further control via $q_1$ is possible.

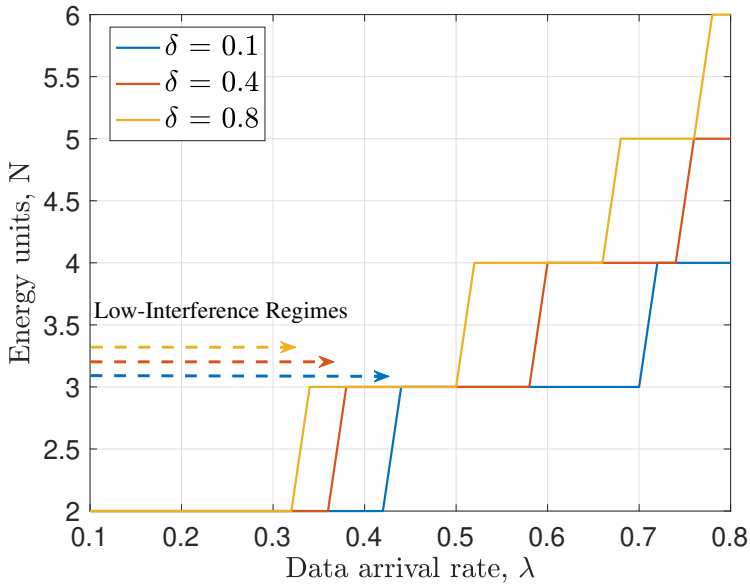


Figure 9.3: Number of energy units $N$ used per transmission by the EH node $S_2$ at optimal AoI vs. data arrival rate $\lambda$ at node $S_1$, for different energy harvesting rates $\delta \in \{0.1, 0.4, 0.8\}$ in ECR.

As a demonstration of this theory, we can notice that $q_1$ exhibits discrete jumps at critical values of $\lambda$, coinciding with transitions in $N$ (cf. Fig. 9.3). In these intervals, flat regions emerge in the $P_1$ plots—an equilibrium arises where a fixed power level minimizes AoI without compromising $S_1$'s queue stability. As $\delta$ increases, higher values of $P_1$ are needed due to increased interference from a more active $S_2$. This also anticipates the jump in $q_1$, showing the system's preference to modulate power before increasing channel access probability.

To further clarify this mechanism, Fig. 9.7 decomposes the average success probability $\bar{p}_2$ of $S_2$ into two components: $p_{2,2}$ (interference-free) and $p_{2,1}$ (under interference). At low $\lambda$, $S_2$ benefits from high $p_{2,2}$. As $\lambda$ increases, the system compensates with higher$N$, which requires increased $q_1$ and ultimately, adjustment of $P_1$ when $q_1$ saturates.

As a result of our analysis, we highlight three main insights. The AoI in ECR is lower with respect to ESR, due to the presence of external interference which does not guarantee a succes-

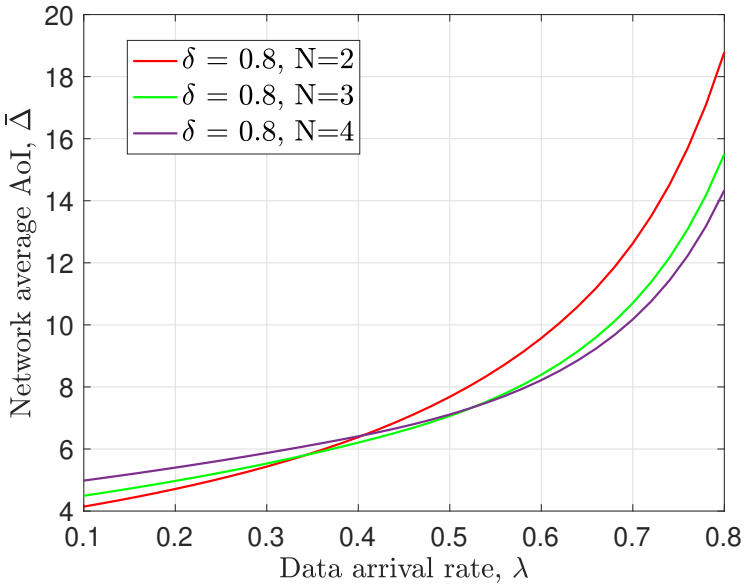


Figure 9.4: Optimal AoI for fixed values of energy units $N \in \{2, 3, 4\}$ vs. data arrival rate $\lambda$ at node $S_1$, under different energy harvesting rates in ECR.

ful transmission, despite EH-node holding enough energy frame, therefore ECR is preferred. The AoI in general is an increasing function of data arrival rate $\lambda$ and a decreasing function of the energy harvesting rate $\delta$, with the impact of $\delta$ being more evident than that of $\lambda$. The impact of $\lambda$ is manifested through the optimal number of energy units $N$, which increases with higher traffic loads (larger $\lambda$) and decreases with reduced energy availability (lower $\delta$). This behavior is primarily influenced by the interference generated by node $S_1$ and the waiting time required for energy accumulation at node $S_2$. Finally, the system suggests a transition between flat-power and saturation regimes. In the non-saturated regime, the optimal transmit power $P_1$ remains constant and is determined by the interplay of other system parameters. Once the system enters the saturated regime, $P_1$ becomes a strictly increasing function of $\lambda$, reflecting the loss of flexibility in adjusting the access probability $q_1$.

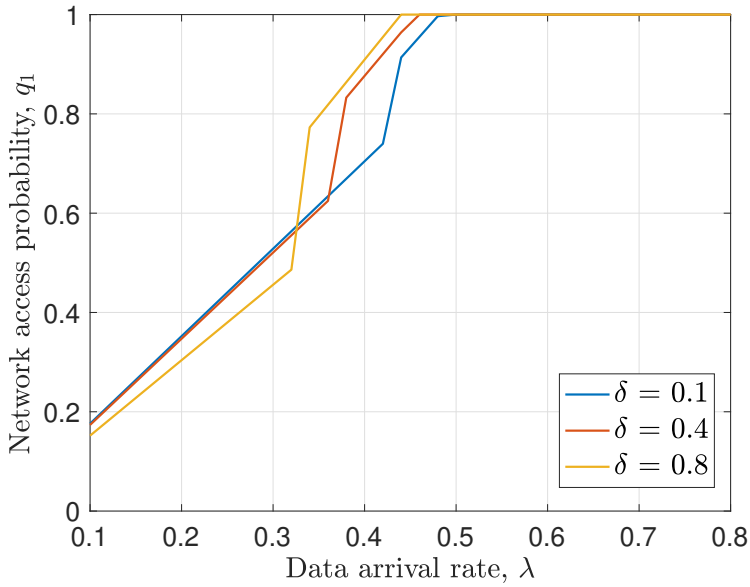


Figure 9.5: Access probability $q_1$ for the grid-powered node $S_1$ at optimal AoI vs. data arrival rate $\lambda$, for various energy harvesting rates $\delta$ at node $S_2$ in ECR.

## 9.2 LOAD-SHIFTING POLICY

### 9.2.1 *Parameter Setup*

In this section we present the optimization results and the optimal load-shifting strategies deducible. We assume that base stations operate in the 1.5 GHz band and utilize a bandwidth of 50 MHz, in accordance with 5G standards. Unless otherwise specified, the proportion of IoT devices is set to 80% of the total number of UEs, reflecting many current deployment scenarios. Both IoT and BB UEs are assumed to transmit at a power of 0.2 W, and a frequency reuse factor of 3 is adopted. By default, we consider a beamforming gain of 10, constant across the main lobe aperture, which is assumed to be 45°. The path loss exponent is set to 3, representative of urban environments. The base stations are of the macro type, with transmit power ranging from 1 W to 11 W. Unless otherwise stated, the target mean per-bit delay in the downlink is set to $10^{-5}$ s for BB UEs and $10^{-3}$ s for IoT UEs. In the uplink, the

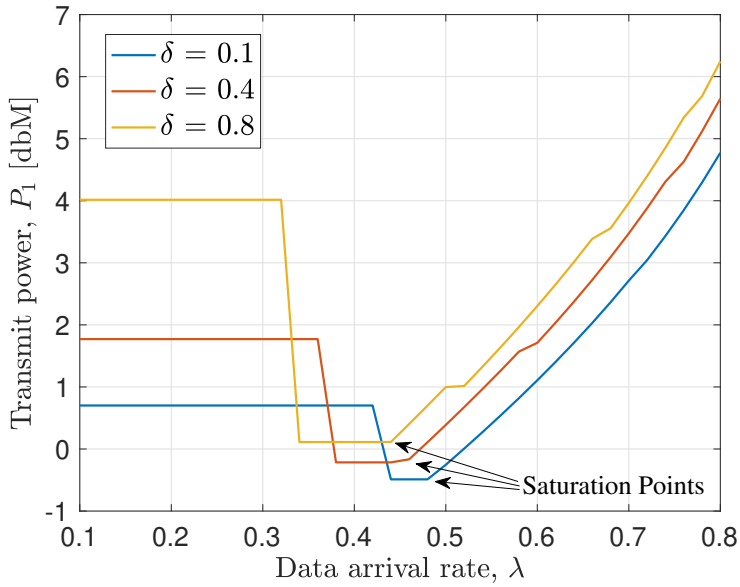


Figure 9.6: Transmit power $P_1$ of node $S_1$ at optimal AoI vs. data arrival rate $\lambda$, for different values of $\delta$ at node $S_2$ in ECR.

target delay is $10^{-4}$ s for all UEs, consistent with typical IoT applications such as environmental monitoring [89]. User density is considered to vary between $10^{-2}$ and $10^{0}$ users per $m^2$, modeling scenarios ranging from sparse BB deployments to dense IoT environments. The maximum acceptable proportion of IoT users unable to harvest this minimum energy is limited to 5%. The parameters of the BS energy model are selected to represent the behavior of the high load proportionality (HLP) BS type, with values of $q_1 = 482.3$, $q_2 = 48.23$, and $q_3 = 144.69$. This corresponds to a 75% load proportionality, which can be achieved, for example, through time-domain duty cycling at the subsystem level [84]. These parameters were specifically chosen to reflect a maximum power consumption of 1500W per BS, which is typical for standalone macro BSs [47]. While, the maximum energy consumed by IoT devices is assumed to be $e_c = 6$mW. The cost of energy per time slot $e_k = 131.47$€/MWh, corresponding to an average daily

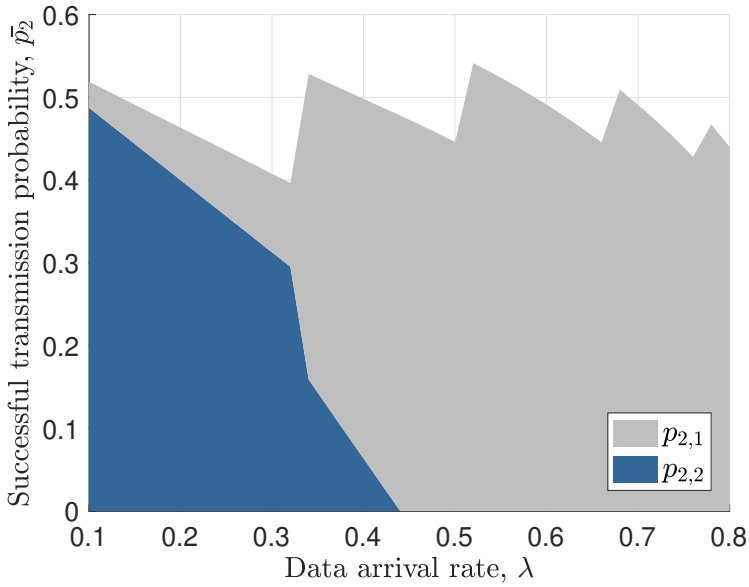


Figure 9.7: Decomposition of the successful transmission probability $\bar{p}_2$ of the EH-node $S_2$ into interference-free ($p_{2,2}$) and interference-affected ($p_{2,1}$) components, for $\delta = 0.8$ as a function of $\lambda$ in ECR.

value for the north of Italy, is assumed to be constant[1]. For $j = d, u$ the target $\phi_{j,0}^{k}$ is set to 0.08 if $\tau_j^{0,k} = 10^{-6}$, to 0.8 elsewhere. The maximum acceptable delay $D$ for shifting is set to 6. The value of BS density has been varied with a granularity of $10^{-4}\ m^{-2}$, to guarantee good accuracy of the GA search process. We assume the mean number of users per base station to be lower bounded by 5. This models the simple energy-saving strategy common among MNOs, which switch off those BSs that serve very few users to no users at all, as they represent a very high energy cost per user and a small benefit for performance. The initial population size $n$ in the genetic algorithm (GA) was set to 100 chromosomes. This choice struck a good balance between computational load and convergence speed.

1 Energy costs can be extracted from the API in https://www.electricitymaps.com/

### 9.2.2 *Delay Constraints and BS Utilization*

We begin our analysis by examining the system behavior with respect to different target per-bit delays in downlink over a single time slot. Figure 9.8 shows the optimal energy cost with respect to the overall density of connected UEs. The continuous lines correspond to the novel findings. The green and blue lines correspond to a IoT throughput $T_d^0 = \frac{1}{10^{-4}}$. In the green line configuration, the per-bit delay for broadband users is $\tau_d^0 = 10^{-6}$, with a delay ratio $\delta_d = 100$. In the blue line configuration, the per-bit delay for BB users increases, while $\delta_d$ decreases, resulting in the same effective throughput for IoT devices as in the green configuration.

The red line, on the other hand, maintains the same per-bit delay for BB users as the red configuration but achieves higher throughput for IoT devices, with $\delta_d = 10$. This scenario is particularly relevant to give UEs a greater throughput, which serves as the foundation for load-shifting. In our system, we aim to identify optimal timeslots that can accommodate data originally scheduled for other timeslots. Without adequate available throughput, these timeslots would be unable to handle the additional data. As the required throughput for BB users increases, the system shows a corresponding rise in overall energy consumption compared to the previous scenario. This is due to the need to deploy additional BSs to meet performance requirements.

Interestingly, at low user densities, the price increase for improved throughput for BB and IoT UEs is minimal. This indicates that enhancing throughput for users does not significantly impact the network's energy consumption. This is advantageous for MNOs because they can provide users with better service without incurring higher energy costs, thereby preserving energy efficiency.

The slight difference in the optimal energy configuration for the two considered values of target per-bit delays is possible thanks to the key role of BS utilization in SWIPT networks. Specifically, at the optimum, in the higher-throughput configuration, the system deploys an additional active BS that enhances the performance of active harvesting because the average distance from the serving BS is decreased. The improved harvesting performances allow for a reduction of $\eta$ as it is visible in Figure 9.9. This means that BS

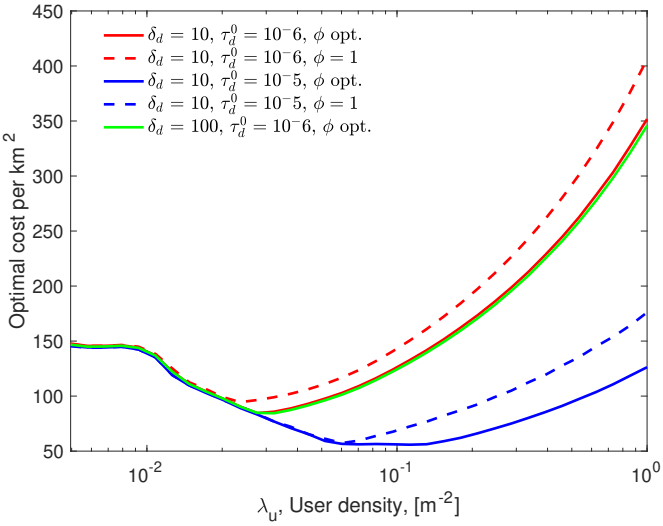


Figure 9.8: Energy consumed at the optimum vs. densities of users for different BB and IoT target per-bit delays. $\phi = 1$ refers to the baseline configuration where the IoTs cannot manage their duty cycle tuning $\phi_u$ and $\phi_d$.

can allocate more resources to BB users to satisfy their required QoS. Since the QoS requested is high, they manage to push the downlink utilization to 1. This feature is fundamental to maximizing the passive and active harvesting performances. In fact, from its value depend both the active and the passive harvesting: a higher utilization allows for a more efficient harvesting, as it is evident from Equations 6.49, 6.50, 6.51, and 6.52. In the lower-throughput configuration, it is not convenient to activate more BS since it will translate into an average lower BS downlink utilization, with negative consequences on the harvesting performances. This explains why the DL utilization in both configurations is always at the maximum (even if the energetic model is high-load proportional). Since the amount of bits received by IoTs is constant across all configurations, the red and green lines coincide because IoTs do not require an additional channel for their transmissions.

The dashed lines correspond to the baseline scenario where IoT devices are always active both in downlink and uplink (i.e.,

$\phi_u = \phi_d = 1$). When IoT devices cannot tune their duty cycle, the energy consumed by the networks increases for higher densities because the BSs are underused even if the passive harvesting is more effective due to the longer duration of transmissions (as it is evident from the earlier decrease in $\eta$ visible in Figure 9.9). On the contrary, the dynamic increase of the active users achieves a balance point where the power harvested from surrounding users equals the power required to operate the device, without requiring additional energy. This allows the system to maintain the splitting factor near zero for a wider range of densities, as devices can adapt their consumption and reduce overall energy consumption. Such a behavior is only possible through flexible control over device activation.

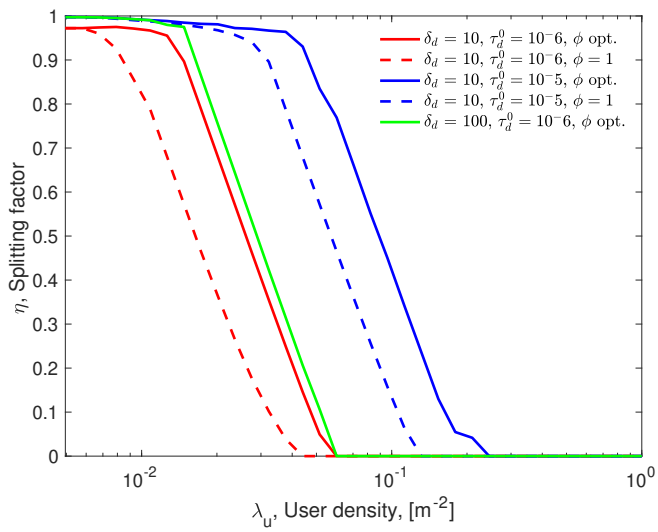


Figure 9.9: Splitting factor at the optimum vs. densities of users.

### 9.2.3 *IoT Duty Cycling Impact*

Furthermore, the divergent behavior of the curves for $\lambda_u > 3 \times 10^{-2}$, is clarified by Figure 9.10, which shows the energy cost with respect to the downlink activation of IoTs, for different densities of installed users. For high densities, the activation time impacts the network energy consumption. Indeed, reducing the load in

that specific density (i.e., time slots) could allow for saving up to 15% of the energy cost. The load can then be shifted during a less crowded time slot in which the impact of the load is lower. To explore this possibility, we focused on an average daily traffic profile derived from [94]. The system's behavior is illustrated in Figure 9.11. In this figure, the red color indicates the time slots where over-provisioning the network is advantageous, as shown in the previous analysis. Consistent with the trend observed in Figure 9.10, the most congested time slots correspond to the highest gains in energy costs (i.e., the amount of load shifted). Reducing the duty cycle during those time slots allows for higher relative savings. Consequently, the load is redirected to lighter slots, which are now more heavily utilized. This is possible thanks to network over-provisioning.

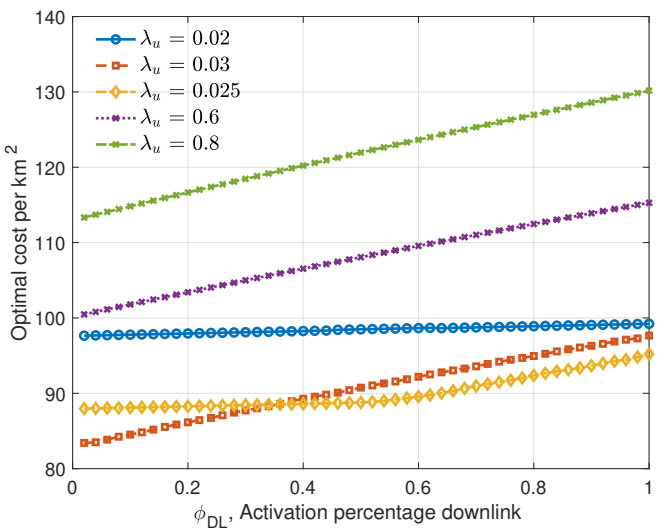


Figure 9.10: Energy consumed at the optimum vs. $\phi_d$ for different users' configurations.

## 9.3 SUMMARY OF FINDINGS

This section summarizes the main results obtained from the numerical validation of the two policies presented in Chapter 6. In particular those policies give insights about two complementary

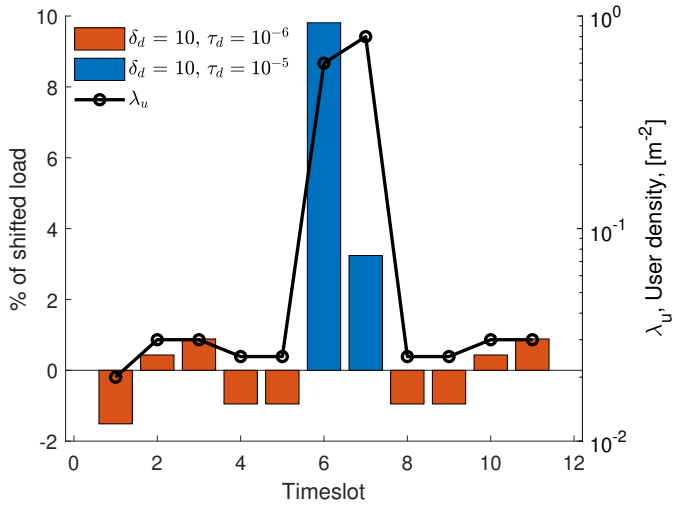


Figure 9.11: Optimal shifting strategy for a 24-hour observation window with a time slot duration of 2 hours. The black line represents the considered traffic profile.

context: the time-sensitive one with AoI, and the non-sensitive one with load shifting.

**F3.1** *The availability of energy not always lead to a better AoI performance. It is better to increase devices access to the channel, even if with lower energy, as compromise to transmission quality.*

This aspect is a direct consequence of the fact that waiting for longer time, and hence increasing the transmission energy, does not give any guarantee on the medium access. In fact, in a HetNet, the non-EH node might produce high interference, causing the device to not accomplishing a complete transmission despite holding high energy for performing a reliable transmission. Low-energy transmission, and eventual retransmission increase the chance to deliver a packet using short inter-transmission time.

**F3.2** *For low-intereference HetNet, it exists a fixed transmit power level for the non-EH devices, which guarantee both stability at non-EH device, and optimal AoI at EH device.*

When the interference generated by non-EH node, and its packet arrival rate is marginal, it is possible to define a fixed power which hold for an entire range, till the moment when the EH-node need

to increase the transmission power, due to the interfernce and so interfering with the non-EH policy. This is a consequence of the complex balance between the transmission of those two nodes.

**F3.3** *Overprovisioning is beneficial for SWIPT networks, so policies which guarantee higher rates for non-EH devices, must be preferred in order to increase the energy harvested. This, despite not reducing the overall power consumed, decrease the per-bit delay without increasing the network consumption.*

It has been shown that decrease the uplink and downlink per-bit delay causes an increase in the transmission and receiving time, therefore progressively making the system creating more interference. This interference can be harvested by EH-enabled devices making this configuration the best one. Therefore, overprovisioning a network can lead to power consumption reduction under a given set of parameters.

**F3.4** *Shifting the transmission in less dense context is not the best choice for SWIPT, since interference is too low and this negatively impact the harvesting.*

Shifting load in low-density context might be seen as the best choice, anyway it is important to recall that interference plays an important role in SWIPT networks, therefore shifting load in very low densities means increasing the energy request, which is not possible to harvest from the surrounding environment; leading to increase of request. For the opposite argument, it is not suggested to move the load in very high time slots, because of the high interference characterizing these contexts which lead to the worst performance.

Those findings define complementary choices depending on the scenario under consideration. In time-sensitive context, to achieve lower AoI, it is necessary to reduce the transmission of the non-EH node; while in non-sensitive context, it is beneficial to have such an interference, and it is particularly beneficial to transmit in some users densities regions.

# Part IV

# CONCLUSIONS AND FUTURE WORK

The final part of the thesis consolidates the key contribution of the research and reflects on their impact in the broader context of heterogeneous SWIPT networks for IoT applications. It summarizes the main findings, highlighting the novel contributions and the limitations of the proposed approaches. The discussion then continues with potential future research directions.

# 10 CONCLUSION

The thesis provided a three-level approach to the study of SWIPT networks: first evaluating the network operator parameters, such as transmit power and BS density, then evaluating the impact of new-generation features on the energy harvesting process, and third by investigating the role of end-device in increasing the efficacy of SWIPT networks. The results confirmed the role of SG in modeling the network parameter and association rules, extending the usage of such approach to energy harvesting networks. The harvesting process is strongly influenced by the spatial design of the network by preferring those configurations able to balance the interference. In fact, increasing interference is counter-productive even in SWIPT networks, if not properly designed. Time switching architecture are better for the increase of the energy collection from the environment, while power splitting is more effective for the active harvesting. In general, there is no architecture who is beneficial independently of the context, and this choice must be adequately balanced depending on the kind of surrounding infrastructure. Additionally, placing BSs away from the UEs generates additionally interface, that might be exploited by EH-devices.

Apart from the traditional network, the thesis also provided guidelines for the integration of SWIPT in NextGen networks. Those highlights the need to require the knowledge of the spatial distribution of UEs, to have an optimal beamforming schedule. SG in this case can provide a good approximation, but lack of precision in case of low-density scenarios because of the reduced probability of finding UEs on the border of a sector. Dynamic programming can be used to optimize beam design, using polynomial time; while a realistic implementation requires the usage of intelligent reconfigurable interfaces. Beam overlapping, instead, does not produce any valuable contribution, and this is mostly due to capacity of the harvester module.

Coming to the devices decision of implementing a transmission policy; it strongly depends on the context. When critical updates are needed, a balance of interference with other non-EH nodes must be properly designed. Similarly, when load can be shifted, is preferable to do that when the network offers good harvesting opportunities. This is an interesting behavior, because in traditional network it is preferred to shift the load when the network is less crowded, but in this case it might become beneficial. Lastly, overprovision the networks, offering higher performance to non-EH node, can be beneficial for EH-node since can benefit from the additional intereferece generated; similarly to the case of prolonged transmission.

The proposed thesis shows that optimal SWIPT design requires a cross-layer perspective, where both network-level and device-level decisions contribute to overall system performance. This includes adapting beam configurations to user distribution, optimizing time allocation policies, and leveraging device-side decision to make SWIPT network more efficient.

## 10.1 PRACTICAL IMPLICATIONS

From a practical point of view, the findings of this thesis provide insights that can guide the design of future SWIPT architecture in traditional cellular network. For instance, the understanding of interference as both a source of degradation and potential energy support can inform the configuration of network parameters such as power control and beam management. It has been shown that placing BB devices far from the BS can be beneficial for EH devices, due to the added interference generated; so, it is more likely that a network operator will put EH devices in highly dense context, or in scenario where the surrounding devices can transmit for more time. Additionally, the study on beamforming gives concrete guideline on their usage, making it possible to directly implement the proposed algorithm in 5G context. Usage of Software Defined Networks can introduce algorithmic choice in the beam management, therefore making this study much more valuable. Thesis insights suggest that SWIPT integration should not be considered as a plugin, but rather as a native component of future communication infrastructures. Regarding the econom-

ical perspective, companies are currently investigating SWIPT for post-disaster scenario, where networks need to run despite not being fully connected to the power source. In fact, in this scenario, drones and other kind of mobile BSs can be used to power-up devices.

Apart from the network-related implications, the analytical frameworks developed in this thesis can be extended to other wireless paradigms, such as vehicular communications. In particular, the vehicular environment can be effectively modeled through PLCP, which capture both the spatial correlation of vehicles along roads and the dynamic topology of moving nodes. The modeling approach adopted in this work provides a clear example of how to characterize key network metrics, such as association probability or interference patterns, independently of the energy harvesting process itself. This separation between structural properties and energy dynamics makes this thesis a valuable contribution also from the methodological perspective, allowing its application to various scenarios, beyond SWIPT.

## 10.2 LIMITATIONS

This thesis explored SWIPT networks from three perspectives, giving insights for their development in concrete context; however, some limitations need to be acknowledged. Analytical framework proposed in response to RQ1, despite being very accurate for highly dense context, cannot be used in the case of sparse scenario. In fact, the assumption where the system hold, requires to have at least 5 UEs per each BS. A more valid definition of such a framework requires the analysis of interference as function of the activation of the surrounding devices, both UEs and BSs; rather than being a function of the coverage area of the BS, as in the proposed analysis.

Regarding RQ2, the framework relied on a simplified antenna model, which made the analytical formulation tractable and allowed for closed-form expressions. However, this simplification may lead to a pessimistic estimation of performance in scenarios where propagation losses differ significantly from those assumed in the model; such as the current beamforming networks. Although this represents a limitation, the emergence of reconfig-

urable antenna surfaces can mitigate such effects by dynamically adapting their surface properties and beam patterns. This adaptability aligns well with the analytical principles adopted in this framework, suggesting that future implementations could bridge the gap between theoretical modeling and real-world performance.

Lastly, the policy adopted for evaluating information freshness assumed devices equipped with infinite battery capacity. This assumption was introduced to simplify the analysis and is reasonable for systems where the storage capacity largely exceeds the amount of energy harvested: a condition that holds for most current implementations. However, as energy harvesting efficiency and storage technologies evolve, this assumption may no longer be valid. In future networks with more capable harvesters and adaptive power management, the interaction between battery dynamics and information freshness will need to be reconsidered to maintain analytical accuracy.

# 11 FUTURE WORK

This thesis provided the reader with a comprehensive understanding of the relevance of SWIPT and of how this technology can be leveraged to enhance IoT networks and extend their operational lifetime. This chapter outlines possible extensions of the present work and discusses potential research directions that may further advance the efficacy of SWIPT networks.

## 11.1 RELYING ARCHITECTURES

Broadband devices in SWIPT network can be used to increase the amount of energy harvested, but this can be further exploited in some specific architectures. Devices closer to the BS can be used as relaying devices for more distant users. As an example, the usage of Unmanned Aerial Vehicles (UAVs) as a means for transmitting data and harvesting energy can be a revolutionary technology. The UAVs can be deployed to provide temporary wireless coverage to replace network infrastructure failure. The network architecture presented in the thesis can be extended to include a Device to Device (D2D) communication, where UAVs are connected to static BSs and are used for serving the devices[126]. In such a system only one BS is considered, which is associated with $k$ UAVs that are interested in offering services and power to two devices. Modelization of noise and fading follows the same approach of [157]. [71] extendeds the investigation in a multicasting scenario, where UAVs are dispatched to perform SWIPT to multiple users on the ground. The proposed optimization problem aims to maximize the minimum average achievable rate among all the users, differently from the other works interested in reducing the outage probability. Considering the limited batteries of UAVs and the importance of offering services in a post-disaster context, the flying path is another important challenge in order to cover the maximum number of devices while reducing power consumption [30]. Optimization problems can be formulated tak-

ing into consideration the location of devices and the minimal power requirements; while an approach based on stochastic geometry could be helpful for modeling the system [122].

## 11.2 OPPORTUNISTIC ENERGY SCHEDULING

IoT devices are mostly used to transmit sensors data, and therefore integrating information from such data in the transmission policy might be beneficial to reduce the power consumption. AoI policies transmit only the last updates, discarding the previous one, as considered no longer relevant [167]. This demonstrates the reduction of the energy request demand while delivering the last update [68]. A new path for SWIPT might be the opportunistic choice of device to choose for the harvesting. Usage of wireless channel information [48] can be used to create an opportunistic scheduler, delivering energy only to devices who need, saving BS time for the transmission. The same apporach can be applied to beamforming to serve only the UEs who are currenly most distant [62], and create on-purpose beam for deliver the energy needed for the future transmission.

# BIBLIOGRAPHY


[1] Rami Ahmad. "Smart remote sensing network for disaster management: An overview." In: *Telecommunication Systems* 87.1 (2024), pp. 213–237.

[2] Ayse Ipek Akin, Nafiseh Janatian, Ivan Stupia, and Luc Vandendorpe. "SWIPT-based real-time mobile computing systems: A stochastic geometry perspective." In: *2019 IEEE Wireless Communications and Networking Conference (WCNC)*. IEEE. 2019, pp. 1–7.

[3] Ayse Ipek Akin, Ivan Stupia, and Luc Vandendorpe. "On the Effect of Blockage Objects in Dense MIMO SWIPT Networks." In: *IEEE Transactions on Communications* 67.2 (2019), pp. 1059–1069. DOI: 10.1109/TCOMM.2018.2876308.

[4] Ahmad AlAmmouri, Jeffrey G. Andrews, and François Baccelli. "A Unified Asymptotic Analysis of Area Spectral Efficiency in Ultradense Cellular Networks." In: *IEEE Transactions on Information Theory* 65.2 (2019), pp. 1236–1248. DOI: 10.1109/TIT.2018.2845380.

[5] Panos N Alevizos and Aggelos Bletsas. "Sensitive and nonlinear far-field RF energy harvesting in wireless communications." In: *IEEE Transactions on Wireless Communications* 17.6 (2018), pp. 3670–3685.

[6] Kamran Ali, Huan X Nguyen, Quoc-Tuan Vien, Purav Shah, and Zheng Chu. "Disaster management using D2D communication with power transfer and clustering techniques." In: *IEEE Access* 6 (2018), pp. 14643–14654.

[7] M.-S. Alouini and A.J. Goldsmith. "Area spectral efficiency of cellular mobile radio systems." In: *IEEE Transactions on Vehicular Technology* 48.4 (1999), pp. 1047–1066. DOI: 10.1109/25.775355.

[8] Mohammed H Alsharif, Anabi Hilary Kelechi, Abu Jahid, Raju Kannadasan, Manish Kumar Singla, Jyoti Gupta, and Zong Woo Geem. "A comprehensive survey of energy-efficient computing to enable sustainable massive IoT networks." In: *Alexandria engineering journal* 91 (2024), pp. 12–29.

[9] Maliha Amjad, Omer Chughtai, Muhammad Naeem, and Waleed Ejaz. "SWIPT-assisted energy efficiency optimization in 5G/B5G cooperative IoT network." In: *Energies* 14.9 (2021), p. 2515.

[10] Jeffrey G. Andrews, Francois Baccelli, and Radha Krishna Ganti. "A Tractable Approach to Coverage and Rate in Cellular Networks." In: *IEEE Transactions on Communications* 59.11 (2011), pp. 3122–3134. DOI: 10.1109/TCOMM.2011.100411.100541.

[11] Jeffrey G Andrews, Abhishek K Gupta, Ahmad Alammouri, and Harpreet S Dhillon. *An introduction to cellular network analysis using stochastic geometry*. Springer, 2023.

[12] Jeffrey G. Andrews, Abhishek K. Gupta, and Harpreet S. Dhillon. "A Primer on Cellular Network Analysis Using Stochastic Geometry." In: *CoRR* abs/1604.03183 (2016). arXiv: 1604.03183. URL: http://arxiv.org/abs/1604.03183.

[13] François Baccelli, Bartłomiej Błaszczyszyn, et al. "Stochastic geometry and wireless networks: Volume II Applications." In: *Foundations and Trends in Networking* 4.1–2 (2010), pp. 1–312.

[14] François Baccelli. "Stochastic Geometry and Wireless Networks: Volume I Theory." en. In: *Foundations and Trends® in Networking* 3.3–43–4 (2009), pp. 249–449. ISSN: 1554-057X, 1554-0588. DOI: 10.1561/1300000006.

[15] Baran Tan Bacinoglu and Elif Uysal-Biyikoglu. "Scheduling status updates to minimize age of information with an energy harvesting sensor." In: *2017 IEEE International Symposium on Information Theory (ISIT)*. June 2017, pp. 1122–1126. DOI: 10.1109/ISIT.2017.8006703. URL: https://ieeexplore.ieee.org/document/8006703/.

[16] Mohammed Banafaa, Ibraheem Shayea, Jafri Din, Marwan Hadri Azmi, Abdulaziz Alashbi, Yousef Ibrahim Daradkeh, and Abdulraqeb Alhammadi. "6G Mobile Communication Technology: Requirements, Targets, Applications, Challenges, Advantages, and Opportunities." In: *Alexandria Engineering Journal* 64 (2023), pp. 245–274. ISSN: 1110-0168. DOI: https://doi.org/10.1016/j.aej.2022.08.017. URL: https://www.sciencedirect.com/science/article/pii/S111001682200549X.

[17] Chathuranga M Wijerathna Basnayaka, Dushantha Nalin K Jayakody, Tharindu D Ponnimbaduge Perera, and Marko Beko. "DataAge: Age of information in SWIPT-driven short packet IoT wireless communications." In: *IEEE Internet of Things Journal* (2024).

[18] David Blackwell. "Discounted dynamic programming." In: *The Annals of Mathematical Statistics* 36.1 (1965), pp. 226–235.

[19] Carsten Bockelmann, Nuno Pratas, Hosein Nikopour, Kelvin Au, Tommy Svensson, Cedomir Stefanovic, Petar Popovski, and Armin Dekorsy. "Massive machine-type communications in 5g: physical and MAC-layer solutions." In: *IEEE Communications Magazine* 54.9 (2016), pp. 59–65. DOI: 10.1109/MCOM.2016.7565189.

[20] Biagio Boi et al. "Green Operations of SWIPT Networks: The Role of End-User Devices." In: *arXiv preprint arXiv:2312.08232* (2024). Available at: https://arxiv.org/abs/2312.08232.

[21] Elena Boshkovska, Derrick Wing Kwan Ng, Nikola Zlatanov, and Robert Schober. "Practical non-linear energy harvesting model and resource allocation for SWIPT systems." In: *IEEE Communications Letters* 19.12 (2015), pp. 2082–2085.

[22] Ismail Butun, M Almgren, V Gulisano, and M Papatriantafilou. *Industrial IoT*. Springer, 2020.

[23] He Chen, Yonghui Li, Yunxiang Jiang, Yuanye Ma, and Branka Vucetic. "Distributed power splitting for SWIPT in relay interference channels using game theory." In: *IEEE*

*Transactions on Wireless Communications* 14.1 (2015), pp. 410–420. DOI: 10.1109/TWC.2014.2349892.

[24] Weiwei Chen, Chin-Tau Lea, Shiming He, and Zhe XuanYuan. "Opportunistic Routing and Scheduling for Wireless Networks." In: *IEEE Transactions on Wireless Communications* 16.1 (2017), pp. 320–331. DOI: 10.1109/TWC.2016.2623308.

[25] Xiaoming Chen, Xiumin Wang, and Xianfu Chen. "Energy-Efficient Optimization for Wireless Information and Power Transfer in Large-Scale MIMO Systems Employing Energy Beamforming." In: *IEEE Wireless Communications Letters* 2.6 (Dec. 2013), pp. 667—670. ISSN: 2162-2345. DOI: 10.1109/WCL.2013.092813.130514.

[26] Zheng Chen, Nikolaos Pappas, Emil Björnson, and Erik G. Larsson. "Age of Information in a Multiple Access Channel with Heterogeneous Traffic and an Energy Harvesting Node." In: *IEEE INFOCOM 2019 - IEEE Conference on Computer Communications Workshops (INFOCOM WKSHPS)*. 2019, pp. 662–667. DOI: 10.1109/INFCOMW.2019.8845083.

[27] Zheng Chen, Nikolaos Pappas, Emil Björnson, and Erik G. Larsson. "Optimizing Information Freshness in a Multiple Access Channel With Heterogeneous Devices." In: *IEEE Open Journal of the Communications Society* 2 (2021), pp. 456–470. DOI: 10.1109/OJCOMS.2021.3062678.

[28] Chang-Sik Choi and François Baccelli. "Modeling and Optimization of Direct Communications from IoT Devices to Vehicles." In: *2018 IEEE Globecom Workshops (GC Wkshps)* (2018), pp. 1–7. URL: https://api.semanticscholar.org/CorpusID:67864212.

[29] Chang-Sik Choi and François Baccelli. "Poisson Cox Point Processes for Vehicular Networks." In: *IEEE Transactions on Vehicular Technology* 67.10 (Oct. 2018), pp. 10160–10165. ISSN: 1939-9359. DOI: 10.1109/TVT.2018.2859909.

[30] Evander Christy, Rina Pudji Astuti, Budi Syihabuddin, Bhaskara Narottama, Obed Rhesa, and Furry Rachmawati. "Optimum UAV flying path for Device-to-Device communications in disaster area." In: *2017 International Conference on*

*Signals and Systems* (*ICSigSys*). 2017, pp. 318–322. DOI: 10.1109/ICSIGSYS.2017.7967064.

[31] Man Chu, An Liu, Junting Chen, Vincent K. N. Lau, and Shuguang Cui. "A Stochastic Geometry Analysis for Energy-Harvesting-Based Device-to-Device Communication." In: *IEEE Internet of Things Journal* 9.2 (2022), pp. 1591–1607. DOI: 10.1109/JIOT.2021.3091723.

[32] Bruno Clerckx, Rui Zhang, Robert Schober, Derrick Wing Kwan Ng, Dong In Kim, and H. Vincent Poor. "Fundamentals of Wireless Information and Power Transfer: From RF Energy Harvester Models to Signal and System Designs." In: *IEEE Journal on Selected Areas in Communications* 37.1 (2019), pp. 4–33. DOI: 10.1109/JSAC.2018.2872615.

[33] Bruno Clerckx, Rui Zhang, Robert Schober, Derrick Wing Kwan Ng, Dong In Kim, and H. Vincent Poor. "Fundamentals of Wireless Information and Power Transfer: From RF Energy Harvester Models to Signal and System Designs." In: *IEEE Journal on Selected Areas in Communications* 37.1 (2019), pp. 4–33. DOI: 10.1109/JSAC.2018.2872615.

[34] Alessandra Costanzo, Diego Masotti, Giacomo Paolini, and Dominique Schreurs. "Evolution of SWIPT for the IoT world: Near-and far-field solutions for simultaneous wireless information and power transfer." In: *IEEE Microwave Magazine* 22.12 (2021), pp. 48–59.

[35] Milad Dabiri and Mohammad Javad Emadi. "Average Age of Information Minimization in an Energy Harvesting Wireless Sensor Node." In: *2018 9th International Symposium on Telecommunications* (*IST*). Dec. 2018, pp. 123–126. DOI: 10.1109/IS□.2018.8661099. URL: https://ieeexplore.ieee.org/abstract/document/8661099.

[36] Haipeng Dai, Yunhuai Liu, Guihai Chen, Xiaobing Wu, Tian He, Alex X. Liu, and Huizhen Ma. "Safe Charging for Wireless Power Transfer." In: *IEEE/ACM Transactions on Networking* 25.6 (2017), pp. 3531–3544. DOI: 10.1109/TNET.2017.2750323.

[37] Songita Das and Gourab Ghatak. "A Stochastic Geometry Analysis of Energy-Age Tradeoff in Wireless IoT Network." In: *2024 22nd International Symposium on Modeling and Optimization in Mobile, Ad Hoc, and Wireless Networks (WiOpt)*. IEEE. 2024, pp. 46–53.

[38] Songita Das and Gourab Ghatak. "Analysis of Age-Energy Trade-off in IoT Networks Using Stochastic Geometry." In: *IEEE Transactions on Green Communications and Networking* (2025), pp. 1–1. DOI: 10.1109/TGCN.2025.3574810.

[39] Sujit Das and Elizabeth Mao. "The global energy footprint of information and communication technology electronics in connected Internet-of-Things devices." In: *Sustainable Energy, Grids and Networks* 24 (2020), p. 100408.

[40] Bjorn Debaillie, Claude Desset, and Filip Louagie. "A flexible and future-proof power model for cellular base stations." In: *Vehicular Technology Conference (VTC Spring), 81st*. IEEE. 2015, pp. 1–7.

[41] Remi Dekimpe, Pengcheng Xu, Maxime Schramme, Denis Flandre, and David Bol. "A Battery-Less BLE IoT Motion Detector Supplied by 2.45-GHz Wireless Power Transfer." en. In: *2018 28th International Symposium on Power and Timing Modeling, Optimization and Simulation (PATMOS)*. Platja d'Aro: IEEE, July 2018, pp. 68–75. ISBN: 978-1-5386-6365-3. DOI: 10.1109/PATMOS.2018.8464144. URL: https://ieeexplore.ieee.org/document/8464144/.

[42] Erfan Delfani and Nikolaos Pappas. "Semantics-aware status updates with energy harvesting devices: Query version age of information." In: *2024 22nd International Symposium on Modeling and Optimization in Mobile, Ad Hoc, and Wireless Networks (WiOpt)*. IEEE. 2024, pp. 177–184.

[43] Marco Di Renzo. "System-Level Analysis and Optimization of Cellular Networks With Simultaneous Wireless Information and Power Transfer: Stochastic Geometry Modeling." en. In: *IEEE Trans. Veh. Technol.* 66.3 (Mar. 2017), pp. 2251–2275. ISSN: 0018-9545, 1939-9359. DOI: 10.1109/TVT.2016.2574811. (Visited on 04/07/2022).

[44] Christian Esposito and Gianluca Rizzo. "Help From Above: UAV-Empowered Network Resiliency in Post-Disaster Scenarios." In: *2022 IEEE 19th Annual Consumer Communications & Networking Conference (CCNC)*. 2022, pp. 477–480. DOI: 10.1109/CCNC49033.2022.9700675.

[45] Effatsadat Faregh and Mohammad Javad Dehghani. "Performance analysis of MIMO and MISO time division duplexing wireless links with SWIPT and antenna selection." In: *Wireless Networks* 26 (2020), pp. 4517–4528.

[46] Safiu Abiodun Gbadamosi, Gerhard P Hancke, and Adnan M Abu-Mahfouz. "Building upon NB-IoT networks: A roadmap towards 5G new radio networks." In: *IEEE Access* 8 (2020), pp. 188641–188672.

[47] Xiaohu Ge, Jing Yang, Hamid Gharavi, and Yang Sun. "Energy efficiency challenges of 5G small cell networks." In: *IEEE communications Magazine* 55.5 (2017), pp. 184–191.

[48] Zhouyou Gu, Wibowo Hardjawana, and Branka Vucetic. "Opportunistic scheduling using statistical information of wireless channels." In: *IEEE Transactions on Wireless Communications* 23.8 (2024), pp. 9810–9825.

[49] Kamal Gulati, Raja Sarath Kumar Boddu, Dhiraj Kapila, Sunil L Bangare, Neeraj Chandnani, and G Saravanan. "A review paper on wireless sensor network techniques in Internet of Things (IoT)." In: *Materials Today: Proceedings* 51 (2022), pp. 161–165.

[50] Fengxian Guo, F. Richard Yu, Heli Zhang, Xi Li, Hong Ji, and Victor C. M. Leung. "Enabling Massive IoT Toward 6G: A Comprehensive Survey." In: *IEEE Internet of Things Journal* 8.15 (2021), pp. 11891–11915. DOI: 10.1109/JIOT.2021.3063686.

[51] Fengxian Guo, F Richard Yu, Heli Zhang, Xi Li, Hong Ji, and Victor CM Leung. "Enabling massive IoT toward 6G: A comprehensive survey." In: *IEEE Internet of Things Journal* 8.15 (2021), pp. 11891–11915.

[52] Amardeep Gupta and Ranjeet Kumar Rout. "Energy harvesting-enabled energy-efficient routing using spotted hyena optimization in wireless sensor network." In: *International Journal of Communication Systems* 37.8 (2024), e5747.

[53] Shu Han, Xiao-ming Liu, Hong-yu Huang, Fei Wang, and Yuan-hong Zhong. "Research on energy-efficient routing algorithm based on SWIPT in multi-hop clustered WSN for 5G system." In: *EURASIP Journal on Wireless Communications and Networking* 2021.1 (2021), p. 49.

[54] Sanae El Hassani, Hind El Hassani, and Noureddine Boutammachte. "RF Energy Harvesting for 5G: An Overview." In: *2017 International Renewable and Sustainable Energy Conference (IRSEC)*. Dec. 2017, pp. 1—6. DOI: 10.1109/IRSEC.2017.8477242. URL: https://ieeexplore.ieee.org/document/8477242/.

[55] Tao He, Yingsheng Peng, Yong Liu, and Hui Song. "AoI-oriented resource allocation for NOMA-based wireless powered cognitive radio networks based on multi-agent deep reinforcement learning." In: *IEEE Access* (2024).

[56] Naoya Hirosawa, Hiroki Iimori, Koji Ishibashi, and Giuseppe Thadeu Freitas De Abreu. "Minimizing Age of Information in Energy Harvesting Wireless Sensor Networks." In: *IEEE Access* 8 (2020), pp. 219934–219945. ISSN: 2169-3536. DOI: 10.1109/ACCESS.2020.3038954.

[57] Jun Huang, Cong-Cong Xing, and Chonggang Wang. "Simultaneous wireless information and power transfer: Technologies, applications, and research challenges." In: *IEEE Communications Magazine* 55.11 (2017), pp. 26–32.

[58] Kaibin Huang and Vincent KN Lau. "Enabling wireless power transfer in cellular networks: Architecture, modeling and deployment." In: *IEEE Transactions on Wireless Communications* 13.2 (2014), pp. 902–912.

[59] Yuwen Huang, Mengyu Liu, and Yuan Liu. "Energy-Efficient SWIPT in IoT Distributed Antenna Systems." en. In: *IEEE Internet of Things Journal* 5.4 (Aug. 2018), pp. 2646–2656. ISSN: 2327-4662, 2372-2541. DOI: 10.1109/JIOT.2018.2796124.

[60] Yuwen Huang, Mengyu Liu, and Yuan Liu. "Energy-Efficient SWIPT in IoT Distributed Antenna Systems." en. In: *IEEE Internet Things J.* 5.4 (Aug. 2018), pp. 2646–2656. ISSN: 2327-4662, 2372-2541. DOI: 10.1109/JIOT.2018.2796124. (Visited on 04/07/2022).

[61] Zihao Huang, Hai Chen, Bo Gu, Shimin Gong, Zhou Su, and Mohsen Guizani. "A Learning-Based Iterative Algorithm for AoI-Optimal Trajectory Planning in UAV-Assisted IoT Networks." In: *IEEE Transactions on Wireless Communications* (2025), pp. 1–1. DOI: 10.1109/TWC.2025.3543042.

[62] Youssef Hussein, Mohamad Assaad, and Thierry Clessienne. "Opportunistic Scheduling With Beam Focusing in Distributed RIS-Aided MU-MIMO Systems." In: *IEEE Open Journal of the Communications Society* (2025).

[63] TEXAS INSTRUMENTS. *Low-Power PIR Motion Detector With Bluetooth® Smartand 10-Year Coin Cell Battery Life Reference Design*. 2014.

[64] Kusumlata Jain and Smaranika Mohapatra. "Taxonomy of edge computing: Challenges, opportunities, and data reduction methods." In: *Edge Computing: From Hype to Reality* (2019), pp. 51–69.

[65] Muhammad Ali Jamshed, Kamran Ali, Qammer H Abbasi, Muhammad Ali Imran, and Masood Ur-Rehman. "Challenges, applications, and future of wireless sensors in Internet of Things: A review." In: *IEEE Sensors Journal* 22.6 (2022), pp. 5482–5494.

[66] Baofeng Ji, Xueru Zhang, Shahid Mumtaz, Congzheng Han, Chunguo Li, Hong Wen, and Dan Wang. "Survey on the internet of vehicles: Network architectures and applications." In: *IEEE Communications Standards Magazine* 4.1 (2020), pp. 34–41.

[67] Gulraiz J Joyia, Rao M Liaqat, Aftab Farooq, and Saad Rehman. "Internet of medical things (IoMT): Applications, benefits and future challenges in healthcare domain." In: *J. Commun.* 12.4 (2017), pp. 240–247.

[68] Simon Kaboyo, Mohammed Abo-Zahhad, Osamu Muta, Ahmed H Abd El-Malek, and Maha M Elsabrouty. "Optimization of Age of Information in Adaptive FD/HD Cooperative SWIPT NOMA/OMA System." In: *IEEE Access* (2025).

[69] Igor Kadota and Eytan Modiano. "Age of Information in Random Access Networks with Stochastic Arrivals." In: *IEEE INFOCOM 2021 - IEEE Conference on Computer Communications*. 2021, pp. 1–10. DOI: 10.1109/INFOCOM42981.2021.9488897.

[70] Rashmi Kamran, Shwetha Kiran, Pranav Jha, Abhay Karandikar'T, and Prasanna Chaporkar. "Green 6G: Energy Awareness in Design." In: *2024 16th International Conference on COMmunication Systems & NETworkS (COMSNETS)*. 2024, pp. 1122–1125. DOI: 10.1109/COMSNETS59351.2024.10427334.

[71] J.-M. Kang and C.-J. Chun. "Joint Trajectory Design, Tx Power Allocation, and Rx Power Splitting for UAV-Enabled Multicasting SWIPT Systems." In: *IEEE Systems Journal* 14.3 (2020), pp. 3740–3743. DOI: 10.1109/JSYST.2020.2966534.

[72] Norman Kerle. "Disasters: Risk assessment, management, and post-disaster studies using remote sensing." In: *Remote Sensing Handbook, Volume VI*. CRC Press, 2024, pp. 153–198.

[73] Nizar Khalfet and Ioannis Krikidis. "Information Energy Capacity Region for SWIPT Systems Over Rayleigh-Fading Channels." In: *IEEE Transactions on Communications* 71.3 (2023), pp. 1416–1429. DOI: 10.1109/TCOMM.2022.3174068.

[74] Nasir Ullah Khan, Farid Ullah Khan, Marco Farina, and Arcangelo Merla. "RF energy harvesters for wireless sensors, state of the art, future prospects and challenges: a review." In: *Physical and Engineering Sciences in Medicine* 47.2 (2024), pp. 385–401.

[75] Pasi Koivumäki, Andreas F. Molisch, and Katsuyuki Haneda. "Line-of-Sight Probability in Cluttered Urban Microcells: Analyses Using Poisson Point Process and Point Cloud."

In: *IEEE Transactions on Antennas and Propagation* 70.3 (2022), pp. 2161–2173. DOI: 10.1109/TAP.2021.3119116.

[76] Ioannis Krikidis, Stelios Timotheou, Symeon Nikolaou, Gan Zheng, Derrick Wing Kwan Ng, and Robert Schober. "Simultaneous wireless information and power transfer in modern communication systems." In: *IEEE Communications Magazine* 52.11 (2014), pp. 104–110.

[77] Laboni Kundu et al. "Towards Energy Efficient RAN: From Industry Standards to Implementation Practice." In: *arXiv preprint arXiv:2402.11993* (2024).

[78] Sachitha Kusaladharma, Wei-Ping Zhu, Wessam Ajib, and Gayan Amarasuriya Aruma Baduge. "Stochastic Geometry Based Performance Characterization of SWIPT in Cell-Free Massive MIMO." en. In: *IEEE Trans. Veh. Technol.* 69.11 (Nov. 2020), pp. 13357–13370. ISSN: 0018-9545, 1939-9359. DOI: 10.1109/TVT.2020.3025746. URL: https://ieeexplore.ieee.org/document/9201540/ (visited on 05/10/2022).

[79] Thanh Tu Lam, Marco Di Renzo, and Justin P Coon. "System-level analysis of SWIPT MIMO cellular networks." In: *IEEE Communications Letters* 20.10 (2016), pp. 2011–2014.

[80] Junse Lee and François Baccelli. "On the Effect of Shadowing Correlation on Wireless Network Performance." In: *IEEE INFOCOM 2018 - IEEE Conference on Computer Communications*. 2018, pp. 1601–1609. DOI: 10.1109/INFOCOM.2018.8485965.

[81] Quanzhong Li and Liang Yang. "Robust Optimization for Energy Efficiency in MIMO Two-Way Relay Networks With SWIPT." en. In: *IEEE Systems Journal* 14.1 (Mar. 2020), pp. 196–207. ISSN: 1932-8184, 1937-9234, 2373-7816. DOI: 10.1109/JSYST.2019.2904721. URL: https://ieeexplore.ieee.org/document/8680752/ (visited on 05/10/2022).

[82] Yingzhe Li, François Baccelli, Harpreet S. Dhillon, and Jeffrey G. Andrews. "Statistical Modeling and Probabilistic Analysis of Cellular Networks With Determinantal Point Processes." In: *IEEE Transactions on Communications* 63.9 (2015), pp. 3405–3422. DOI: 10.1109/TCOMM.2015.2456016.

[83] Sergi Liesegang, Olga Munoz-Medina, and Antonio Pascual-Iserte. "Stochastic geometry analysis and design of wireless powered MTC networks." In: *2020 IEEE 21st International Workshop on Signal Processing Advances in Wireless Communications (SPAWC)*. IEEE. 2020, pp. 1–5.

[84] Jiansheng Lin, Youjia Chen, Haifeng Zheng, Ming Ding, Peng Cheng, and Lajos Hanzo. "A data-driven base station sleeping strategy based on traffic prediction." In: *IEEE Transactions on Network Science and Engineering* (2021).

[85] Joakim Lindh, Christin Lee, and Marie Hernes. "Measuring bluetooth low energy power consumption." In: *Application Note AN092* (2017).

[86] Anna Litvinenko, Arturs Aboltins, Sergejs Tjukovs, and Dmitrijs Pikulins. "The impact of waveform on the efficiency of RF to DC conversion using prefabricated energy harvesting device." In: *2017 Advances in Wireless and Optical Communications (RTUWO)*. 2017, pp. 61–66. DOI: 10.1109/RTUWO.2017.8228506.

[87] Wanchun Liu, Xiangyun Zhou, Salman Durrani, Hani Mehrpouyan, and Steven D. Blostein. "Energy Harvesting Wireless Sensor Networks: Delay Analysis Considering Energy Costs of Sensing and Transmission." In: *IEEE Transactions on Wireless Communications* 15.7 (July 2016), pp. 4635–4650. ISSN: 1558-2248. DOI: 10.1109/TWC.2016.2543216.

[88] O. L. López et al. "Energy-Sustainable IoT Connectivity: Vision, Technological Advances, and Challenges." In: *IEEE Open Journal of the Communications Society* 4 (2023), pp. 2609–2651. DOI: 10.1109/OJCOMS.2023.3343360.

[89] Weidang Lu, Xiaohan Xu, Guoxing Huang, Bo Li, Yuan Wu, Nan Zhao, and F. Richard Yu. "Energy Efficiency Optimization in SWIPT Enabled WSNs for Smart Agriculture." en. In: *IEEE Trans. Ind. Inf.* 17.6 (June 2021), pp. 4335–4344. ISSN: 1551-3203, 1941-0050. DOI: 10.1109/TII.2020.2996672. (Visited on 04/07/2022).

[90] Yang Luo, Chunbo Luo, Geyong Min, Gerard Parr, and Sally McClean. "On the Study of Sustainability and Outage of SWIPT-Enabled Wireless Communications." en. In:

*IEEE J. Sel. Top. Signal Process.* 15.5 (Aug. 2021), pp. 1159–1168. ISSN: 1932-4553, 1941-0484. DOI: 10.1109/JSTSP.2021.3092136. URL: https://ieeexplore.ieee.org/document/9464720/ (visited on 04/07/2022).

[91] Wanting Lyu, Yue Xiu, Jun Zhao, and Zhongpei Zhang. "Optimizing the Age of Information in RIS-Aided SWIPT Networks." In: *IEEE Transactions on Vehicular Technology* 72.2 (2023), pp. 2615–2619. DOI: 10.1109/TVT.2022.3208612.

[92] Zaki Masood, Hosung Park, Han Seung Jang, Sunyong Yoo, Sokhee P. Jung, and Yonghoon Choi. "Optimal Power Allocation for Maximizing Energy Efficiency in DAS-Based IoT Network." In: *IEEE Systems Journal* 15.2 (2021), pp. 2342–2348. DOI: 10.1109/JSYST.2020.3013693.

[93] Louis Meile, Anja Ulrich, and Michele Magno. "Wireless Power Transmission Powering Miniaturized Low Power IoT devices: A Revie." In: *2019 IEEE 8th International Workshop on Advances in Sensors and Interfaces (IWASI)*. 2019, pp. 312–317. DOI: 10.1109/IWASI.2019.8791433.

[94] Michela Meo, Daniela Renga, and Zunera Umar. "Advanced Sleep Modes to comply with delay constraints in energy efficient 5G networks." In: *VTC Spring*. 2021, pp. 1–7. DOI: 10.1109/VTC2021-Spring51267.2021.9448695.

[95] Pranay Kamal Miriyala, P Nitin Srinivas, et al. "On-Chip 5&6-GHz RF Energy Harvesting System for Implantable Medical Devices." In: *2024 IEEE International Symposium on Circuits and Systems (ISCAS)*. IEEE. 2024, pp. 1–5.

[96] Thomas Moscibroda. "The worst-case capacity of wireless sensor networks." In: *Proceedings of the 6th international conference on Information processing in sensor networks*. 2007, pp. 1–10.

[97] F. Mukhlif, K.A.B. Noordin, and O.B. Abdulghafoor. "Energy Harvesting Technique for Efficient Wireless Cognitive Sensor Networks Based on SWIPT Game Theory." In: *KSII Transactions on Internet and Information Systems* 14.6 (2020), pp. 2709–2734. DOI: 10.3837/tiis.2020.06.021.

[98] M. Sajid Mushtaq, Scott Fowler, and Abdelhamid Mellouk. "Power saving model for mobile device and virtual base station in the 5G era." en. In: *IEEE ICC*. Paris, France, May 2017, pp. 1–6. ISBN: 978-1-4673-8999-0. DOI: 10.1109/ICC.2017.7997473. (Visited on 04/07/2022).

[99] Ali A. Nasir, Xiangyun Zhou, Salman Durrani, and Rodney A. Kennedy. "Relaying Protocols for Wireless Energy Harvesting and Information Processing." In: *IEEE Transactions on Wireless Communications* 12.7 (2013), pp. 3622–3636. DOI: 10.1109/twc.2013.062413.122042. URL: https://doi.org/10.1109%2Ftwc.2013.062413.122042.

[100] Ali A Nasir, Xiangyun Zhou, Salman Durrani, and Rodney A Kennedy. "Relaying protocols for wireless energy harvesting and information processing." In: *IEEE Transactions on Wireless Communications* 12.7 (2013), pp. 3622–3636.

[101] Dinh C. Nguyen, Ming Ding, Pubudu N. Pathirana, Aruna Seneviratne, Jun Li, Dusit Niyato, Octavia Dobre, and H. Vincent Poor. "6G Internet of Things: A Comprehensive Survey." In: *IEEE Internet of Things Journal* 9.1 (2022), pp. 359–383. DOI: 10.1109/JIOT.2021.3103320.

[102] Solmaz Niknam, Balasubramaniam Natarajan, and Reza Barazideh. "Interference Analysis for Finite-Area 5G mmWave Networks Considering Blockage Effect." In: *IEEE Access* 6 (2018), pp. 23470–23479. DOI: 10.1109/ACCESS.2018.2829621.

[103] Dusit Niyato, Dong In Kim, Marco Maso, and Zhu Han. "Wireless powered communication networks: Research directions and technological approaches." In: *IEEE Wireless Communications* 24.6 (2017), pp. 88–97.

[104] SERDAR Özyurt, AF Coşkun, S Büyükçorak, G Karabulut Kurt, and O Kucur. "A survey on multiuser SWIPT communications for 5G+." In: *IEEE Access* 10 (2022), pp. 109814–109849.

[105] Gaofeng Pan, Hongjiang Lei, Yansha Deng, Lisheng Fan, Jing Yang, Yunfei Chen, and Zhiguo Ding. "On Secrecy Performance of MISO SWIPT Systems With TAS and Im-

perfect CSI." In: *IEEE Transactions on Communications* 64.9 (2016), pp. 3831–3843. DOI: 10.1109/TCOMM.2016.2573822.

[106] Abhinav Singh Parihar, Pragya Swami, and Vimal Bhatia. "On Performance of SWIPT Enabled PPP Distributed Cooperative NOMA Networks using Stochastic Geometry." en. In: *IEEE Trans. Veh. Technol.* (2022), pp. 1–1. ISSN: 0018-9545, 1939-9359. DOI: 10.1109/TVT.2022.3155358. URL: https://ieeexplore.ieee.org/document/9723559/ (visited on 05/10/2022).

[107] Tharindu D Ponnimbaduge Perera, Dushantha Nalin K Jayakody, Ioannis Pitas, and Sahil Garg. "Age of information in SWIPT-enabled wireless communication system for 5GB." In: *IEEE Wireless Communications* 27.5 (2020), pp. 162–167.

[108] Tharindu D Ponnimbaduge Perera, Dushantha Nalin K Jayakody, Shree Krishna Sharma, Symeon Chatzinotas, and Jun Li. "Simultaneous wireless information and power transfer (SWIPT): Recent advances and future challenges." In: *IEEE Communications Surveys & Tutorials* 20.1 (2017), pp. 264–302.

[109] Jens F Peters, Manuel Baumann, Benedikt Zimmermann, Jessica Braun, and Marcel Weil. "The environmental impact of Li-Ion batteries and the role of key parameters–A review." In: *Renewable and Sustainable Energy Reviews* 67 (2017), pp. 491–506.

[110] Yury Polyanskiy, H. Vincent Poor, and Sergio Verdu. "Channel Coding Rate in the Finite Blocklength Regime." In: *IEEE Transactions on Information Theory* 56.5 (2010), pp. 2307–2359. DOI: 10.1109/TIT.2010.2043769.

[111] *Prepare Yourself for the "Tsunami of Data" Expected to Hit by 2025*. https://futurism.com/prepare-yourself-tsunami-data-expected-hit-2025. (Accessed on 05/09/2022).

[112] Constantinos Psomas and Ioannis Krikidis. "Blockage effects on joint information and energy transfer in directional ad-hoc networks." In: *2016 24th European Signal Processing Conference (EUSIPCO)*. 2016, pp. 808–812. DOI: 10.1109/EUSIPCO.2016.7760360.

[113] Constantinos Psomas, Minglei You, Kai Liang, Gan Zheng, and Ioannis Krikidis. "Design and Analysis of SWIPT With Safety Constraints." In: *Proceedings of the IEEE* 110.1 (2022), pp. 107–126. DOI: 10.1109/JPROC.2021.3130084.

[114] Zakria Qadir, Khoa N. Le, Nasir Saeed, and Hafiz Suliman Munawar. "Towards 6G Internet of Things: Recent advances, use cases, and open challenges." In: *ICT Express* 9.3 (2023), pp. 296–312. ISSN: 2405-9595. DOI: https://doi.org/10.1016/j.icte.2022.06.006. URL: https://www.sciencedirect.com/science/article/pii/S2405959522000959.

[115] Zexin Qiao, Ling Lyu, Yanpeng Dai, Nan Cheng, and Xuemin Shen. "Energy-aware sensor scheduling and opportunistic transmission for state estimation in industrial IoT systems." In: *2023 IEEE/CIC International Conference on Communications in China (ICCC)*. IEEE. 2023, pp. 1–6.

[116] Husam Rajab and Tibor Cinkler. "Enhanced Energy Efficiency and Scalability in Cellular Networks for Massive IoT." In: *5G and Beyond*. Ed. by Bharat Bhushan, Sudhir Kumar Sharma, Raghvendra Kumar, and Ishaani Priyadarshini. Singapore: Springer Nature Singapore, 2023, pp. 283–305. ISBN: 978-981-99-3668-7. DOI: 10.1007/978-981-99-3668-7_13. URL: https://doi.org/10.1007/978-981-99-3668-7_13.

[117] A. Rauniyar, P. Engelstad, and O.N. Østerbø. "Capacity enhancement of NOMA-SWIPT IoT relay system with direct links over rayleigh fading channels." In: *Transactions on Emerging Telecommunications Technologies* 31.12 (2020). DOI: 10.1002/ett.3913. URL: https://www.scopus.com/inward/record.uri?eid=2-s2.0-85082033976&doi=10.1002%2fett.3913&partnerID=40&md5=8e88c7f7224de1b925e37f9b190ad

[118] Yuan Ren, Xuewei Zhang, and Meruyert Makhanbet. "Interference Alignment Inspired Opportunistic Communications in Multi-Cluster MIMO Networks with Wireless Power Transfer." en. In: *Information* 12.8 (Aug. 2021), p. 335. ISSN: 2078-2489. DOI: 10.3390/info12080335.

[119] Balaji Rengarajan, Gianluca Rizzo, and Marco Ajmone Marsan. "Energy-optimal base station density in cellular access networks with sleep modes." In: *Computer Networks* 78 (2015), pp. 152–163.

[120] Iegor Riepin, Tom Brown, and Victor M. Zavala. "Spatio-temporal load shifting for truly clean computing." In: *Advances in Applied Energy* 17 (2025), p. 100202. ISSN: 2666-7924. DOI: https://doi.org/10.1016/j.adapen.2024.100202.

[121] Gianluca A. Rizzo and Marco Ajmone Marsan. "The energy saving potential of static and adaptive resource provisioning in dense cellular networks." In: *IEEE COMSNETS*. 2018, pp. 297–304. DOI: 10.1109/COMSNETS.2018.8328211.

[122] Gianluca Rizzo, Marco Ajmone Marsan, and Christian Esposito. "Energy-Optimal RAN Configurations for SWIPT IoT." In: *2022 20th International Symposium on Modeling and Optimization in Mobile, Ad hoc, and Wireless Networks* (*WiOpt*). 2022, pp. 169–176. DOI: 10.23919/WiOpt56218.2022.9930622.

[123] Gianluca Rizzo, Marco Ajmone Marsan, Christian Esposito, and Biagio Boi. "Green Operations of SWIPT Networks: The Role of End-User Devices." In: *IEEE Transactions on Green Communications and Networking* (2025), pp. 1–1. DOI: 10.1109/TGCN.2025.3552557.

[124] Gianluca Rizzo et al. "Energy-Optimal RAN Configurations for SWIPT IoT." In: *2022 IEEE Global Communications Conference* (*GLOBECOM*). IEEE. 2022, pp. 1–6. URL: https://arodes.hes-so.ch/record/11333/files/Rizzo_2022_energy-optimal_RAN.pdf.

[125] Abdu Saif, Kaharudin Dimyati, Kamarul Ariffin Noordin, GC Deepak, Nor Shahida Mohd Shah, Qazwan Abdullah, and Mahathir Mohamad. "An efficient energy harvesting and optimal clustering technique for sustainable postdisaster emergency communication systems." In: *IEEE Access* 9 (2021), pp. 78188–78202.

[126] Abdu Saif, Kaharudin Dimyati, Kamarul Ariffin Noordin, Nor Shahida Mohd Shah, Qazwan Abdullah, and Fadhil Mukhlif. "Unmanned Aerial Vehicles for Post-Disaster Com-

munication Networks." In: *2020 IEEE 10th International Conference on System Engineering and Technology (ICSET)*. 2020, pp. 273–277. DOI: 10.1109/ICSET51301.2020.9265369.

[127] Teodora Sanislav, George Dan Mois, Sherali Zeadally, and Silviu Corneliu Folea. "Energy harvesting techniques for internet of things (IoT)." In: *IEEE Access* 9 (2021), pp. 39530–39549.

[128] Stefan Schmickl, Thomas Faseth, and Harald Pretl. "A 1.9-μW 7-GHz IR-UWB Transmitter with RF-Energy-Harvester in 180-nm CMOS for Battery-Less Bio-Sensors." In: *2019 17th IEEE International New Circuits and Systems Conference (NEWCAS)*. 2019, pp. 1–4. DOI: 10.1109/NEWCAS44328.2019.8961228.

[129] Stefan Schmickl, Thomas Faseth, and Harald Pretl. "An RF-energy harvester and IR-UWB transmitter for ultra-low-power battery-less biosensors." In: *IEEE Transactions on Circuits and Systems I: Regular Papers* 67.5 (2020), pp. 1459–1468.

[130] Misbah Shahid, Moeenuddin Tariq, Zeshan Iqbal, Hussain Mobarak Albarakati, Noor Fatima, Muhammad Attique Khan, and Mohammad Shabaz. "Link-quality-based energy-efficient routing protocol for WSN in IoT." In: *IEEE Transactions on Consumer Electronics* 70.1 (2024), pp. 4645–4653.

[131] Faisal Karim Shaikh and Sherali Zeadally. "Energy harvesting in wireless sensor networks: A comprehensive review." In: *Renewable and Sustainable Energy Reviews* 55 (2016), pp. 1041–1054.

[132] Emiliano Sisinni, Abusayeed Saifullah, Song Han, Ulf Jennehag, and Mikael Gidlund. "Industrial internet of things: Challenges, opportunities, and directions." In: *IEEE transactions on industrial informatics* 14.11 (2018), pp. 4724–4734.

[133] Pawel Sroka et al. "Policy-Based Traffic Steering and Load Balancing in O-RAN-Based Vehicle-to-Network Communications." In: *IEEE Access* (2024), pp. 9357–9376.

[134] D. Stoyan, W. S. Kendall, and J. Mecke. *Stochastic geometry and its applications*. Wiley, 1987.

[135] Jie Tang, Jingci Luo, Mingqian Liu, Daniel K. C. So, Emad Alsusa, Gaojie Chen, Kai-Kit Wong, and Jonathon A. Chambers. "Energy Efficiency Optimization for NOMA With SWIPT." en. In: *IEEE J. Sel. Top. Signal Process.* 13.3 (June 2019), pp. 452–466. ISSN: 1932-4553, 1941-0484. DOI: 10.1109/JSTSP.2019.2898114. URL: https://ieeexplore.ieee.org/document/8636993/ (visited on 05/11/2022).

[136] Jie Tang, Daniel K. C. So, Arman Shojaeifard, Kai-Kit Wong, and Jinming Wen. "Joint Antenna Selection and Spatial Switching for Energy Efficient MIMO SWIPT System." In: *IEEE Transactions on Wireless Communications* 16.7 (2017), pp. 4754—4769. ISSN: 1558-2248. DOI: 10.1109/TWC.2017.2702575.

[137] Jie Tang, Daniel K. C. So, Nan Zhao, Arman Shojaeifard, and Kai-Kit Wong. "Energy Efficiency Optimization With SWIPT in MIMO Broadcast Channels for Internet of Things." en. In: *IEEE Internet Things J.* 5.4 (Aug. 2018), pp. 2605–2619. ISSN: 2327-4662, 2372-2541. DOI: 10.1109/JIOT.2017.2785861. URL: https://ieeexplore.ieee.org/document/8233108/ (visited on 05/10/2022).

[138] Jie Tang, Daniel KC So, Arman Shojaeifard, Kai-Kit Wong, and Jinming Wen. "Joint antenna selection and spatial switching for energy efficient MIMO SWIPT system." In: *IEEE Transactions on Wireless Communications* 16.7 (2017), pp. 4754–4769.

[139] Sotiris A. Tegos, Panagiotis D. Diamantoulakis, Koralia Pappi, and George K. Karagiannidis. "Optimal Simultaneous Wireless Information and Power Transfer with Low-Complexity Receivers." In: *2018 IEEE 19th International Workshop on Signal Processing Advances in Wireless Communications (SPAWC)*. 2018, pp. 1–5. DOI: 10.1109/SPAWC.2018.8446009.

[140] Ha-Vu Tran, Georges Kaddoum, and Kien T. Truong. "Resource Allocation in SWIPT Networks Under a Nonlinear Energy Harvesting Model: Power Efficiency, User Fairness, and Channel Nonreciprocity." In: *IEEE Transactions on Vehicular Technology* 67.9 (2018), pp. 8466–8480. DOI: 10.1109/TVT.2018.2848963.

[141] Lam-Thanh Tu, Abbas Bradai, and Yannis Pousset. "Performance Evaluation of SWIPT-enabled Cellular Networks with Adaptive Modulation -A Stochastic Geometry Approach." In: *Réseaux du futur : 5G et au-delà*. Paris, France, Mar. 2020. URL: https://hal.science/hal-02486816.

[142] Lav R Varshney. "Transporting information and energy simultaneously." In: *2008 IEEE international symposium on information theory*. IEEE. 2008, pp. 1612–1616.

[143] S. Vishnu, S.R. Jino Ramson, and R. Jegan. "Internet of Medical Things (IoMT) - An overview." In: *2020 5th International Conference on Devices, Circuits and Systems (ICDCS)*. 2020, pp. 101–104. DOI: 10.1109/ICDCS48716.2020.243558.

[144] Kehao Wang. "Optimally myopic scheduling policy for downlink channels with imperfect state observation." In: *IEEE Transactions on Vehicular Technology* 67.7 (2018), pp. 5856–5867.

[145] Shuai Wang, Minghua Xia, Kaibin Huang, and Yik-Chung Wu. "Wirelessly Powered Two-Way Communication With Nonlinear Energy Harvesting Model: Rate Regions Under Fixed and Mobile Relay." In: *IEEE Transactions on Wireless Communications* 16.12 (2017), pp. 8190–8204. DOI: 10.1109/TWC.2017.2758767.

[146] Shuai Wang, Minghua Xia, and Yik-Chung Wu. "Space-time signal optimization for SWIPT: Linear versus nonlinear energy harvesting model." In: *IEEE Communications Letters* 22.2 (2017), pp. 408–411.

[147] Z. Wen, Y. Liu, X. Liu, S. Li, and X. Chen. "Power allocation for SWIPT in K-user interference channels using game theory." In: *Eurasip Journal on Advances in Signal Processing* 2018.1 (2018). DOI: 10.1186/s13634-018-0547-7. URL: https://www.scopus.com/inward/record.uri?eid=2-s2.0-85046400494&doi=10.1186%2fs13634-018-0547-7&partnerID=40&md5=05c71066b2aa49f98fe91bb144e06d56.

[148] Adam Wierman, Zhenhua Liu, Iris Liu, and Hamed Mohsenian-Rad. "Opportunities and challenges for data center demand response." In: *International Green Computing Conference*. 2014, pp. 1–10. DOI: 10.1109/IGCC.2014.7039172.

[149] Jeffrey Wildman, Pedro Henrique Juliano Nardelli, Matti Latva-aho, and Steven Weber. "On the joint impact of beamwidth and orientation error on throughput in directional wireless poisson networks." In: *IEEE Transactions on Wireless Communications* 13.12 (2014), pp. 7072–7085.

[150] Jingjin Wu, Eric W. M. Wong, Yin-Chi Chan, and Moshe Zukerman. "Power Consumption and GoS Tradeoff in Cellular Mobile Networks With Base Station Sleeping and Related Performance Studies." In: *IEEE Transactions on Green Communications and Networking* 4.4 (2020), pp. 1024–1036. DOI: 10.1109/TGCN.2020.3000277.

[151] Yuan Wu, Yanfei He, Liping Qian, Jianwei Huang, and Xuemin Shen. "Joint Scheduling and Power Allocations for Traffic Offloading via Dual-Connectivity." In: *arXiv preprint arXiv:1509.09241* (2015).

[152] Ke Xiong, Beibei Wang, and K. J. Ray Liu. "Rate-Energy Region of SWIPT for MIMO Broadcasting Under Nonlinear Energy Harvesting Model." In: *IEEE Transactions on Wireless Communications* 16.8 (2017), pp. 5147–5161. DOI: 10.1109/TWC.2017.2706277.

[153] Jie Xu, Liang Liu, and Rui Zhang. "Multiuser MISO Beamforming for Simultaneous Wireless Information and Power Transfer." In: *IEEE Transactions on Signal Processing* 62.18 (2014), pp. 4798—4810. ISSN: 1941-0476. DOI: 10.1109/TSP.2014.2340817.

[154] Pengcheng Xu, Denis Flandre, and David Bol. "Analysis, Modeling, and Design of a 2.45-GHz RF Energy Harvester for SWIPT IoT Smart Sensors." en. In: *IEEE Journal of Solid-State Circuits* 54.10 (Oct. 2019), pp. 2717–2729. ISSN: 0018-9200, 1558-173X. DOI: 10.1109/JSSC.2019.2914581.

[155] J. Yaswanth, S.K. Singh, K. Singh, and M.F. Flanagan. "Energy-Efficient Beamforming Design for RIS-Aided MIMO Downlink Communication with SWIPT." In: *IEEE Transactions on Green Communications and Networking* 7.3 (2023), pp. 1164–1180. DOI: 10.1109/TGCN.2023.3273031.

[156] Le Ye, Zhixuan Wang, Ying Liu, Peiyu Chen, Heyi Li, Hao Zhang, Meng Wu, Wei He, Linxiao Shen, Yihan Zhang, et al. "The challenges and emerging technologies for low-power artificial intelligence IoT systems." In: *IEEE Transactions on Circuits and Systems I: Regular Papers* 68.12 (2021), pp. 4821–4834.

[157] S. Yin, Y. Zhao, and L. Li. "UAV-assisted Cooperative Communications with Power-splitting SWIPT." In: 2018, pp. 162–167. DOI: 10.1109/ICCS.2018.8689232. URL: https://www.scopus.com/inward/record.uri?eid=2-s2.0-85065016793&doi=10.1109%2fICCS.2018.8689232&partnerID=40&md5=fa032f7526a11d0cf3e644fc4f74dfd1.

[158] Xiangbin Yu, Junya Chu, Kai Yu, Tao Teng, and Ning Li. "Energy-Efficiency Optimization for IoT-Distributed Antenna Systems With SWIPT Over Composite Fading Channels." en. In: *IEEE Internet of Things Journal* 7.1 (Jan. 2020), pp. 197–207. ISSN: 2327-4662, 2372-2541. DOI: 10.1109/JIOT.2019.2946581.

[159] Xiong Yu, Geng Li, and Wenbing Lu. "Power consumption based on 5G communication." In: *2021 IEEE 5th Information Technology,Networking,Electronic and Automation Control Conference (ITNEC)*. Vol. 5. 2021, pp. 910–914. DOI: 10.1109/ITNEC52019.2021.9587128.

[160] Yi Yuan, Yanqing Xu, Zheng Yang, Peng Xu, and Zhiguo Ding. "Energy Efficiency Optimization in Full-Duplex User-Aided Cooperative SWIPT NOMA Systems." en. In: *IEEE Trans. Commun.* 67.8 (Aug. 2019), pp. 5753–5767. ISSN: 0090-6778, 1558-0857. DOI: 10.1109/TCOMM.2019.2914386. URL: https://ieeexplore.ieee.org/document/8704259/ (visited on 05/10/2022).

[161] Zhiling Yue, Howard H Yang, Meng Zhang, and Nikolaos Pappas. "Age of information under frame slotted ALOHA-based status updating protocol." In: *IEEE Journal on Selected Areas in Communications* 41.7 (2023), pp. 2071–2089.

[162] Kasim Sinan Yıldırım, Ruggero Carli, and Luca Schenato. "Safe Distributed Control of Wireless Power Transfer Net-

works." In: *IEEE Internet of Things Journal* 6.1 (2019), pp. 1267–1275. DOI: 10.1109/JIOT.2018.2813420.

[163] Haiyang Zhang, Yongming Huang, Chunguo Li, and Luxi Yang. "Secure Beamforming Design for SWIPT in MISO Broadcast Channel With Confidential Messages and External Eavesdroppers." In: *IEEE Transactions on Wireless Communications* 15.11 (2016), pp. 7807–7819. DOI: 10.1109/TWC.2016.2607705.

[164] Rui Zhang and Chin Keong Ho. "MIMO Broadcasting for Simultaneous Wireless Information and Power Transfer." In: *IEEE Transactions on Wireless Communications* 12.5 (2013), pp. 1989–2001. DOI: 10.1109/TWC.2013.031813.120224.

[165] Xuhui Zhang, Huijun Xing, Yanyan Shen, Jie Xu, and Shuguang Cui. "Age of Information Minimization in UAV-Enabled IoT Networks via Federated Reinforcement Learning." In: *IEEE Transactions on Wireless Communications* (2025), pp. 1–1. DOI: 10.1109/TWC.2025.3563426.

[166] Yunpu Zhang and Changsheng You. "SWIPT in Mixed Near-and Far-Field Channels: Joint Beam Scheduling and Power Allocation." In: *IEEE Journal on Selected Areas in Communications* 42.6 (2024), pp. 1583—1597. ISSN: 1558-0008. DOI: 10.1109/JSAC.2024.3389115.

[167] Fangming Zhao, Nikolaos Pappas, Meng Zhang, and Howard H. Yang. "Age of Information in Random Access Networks with Energy Harvesting." In: *IEEE Journal on Selected Areas in Communications* (2025), pp. 1–1. DOI: 10.1109/JSAC.2025.3584549.

[168] Nan Zhao, F. Richard Yu, and Victor C. M. Leung. "Opportunistic communications in interference alignment networks with wireless power transfer." In: *IEEE Wireless Communications* 22.1 (Feb. 2015), pp. 88–95. ISSN: 1558-0687. DOI: 10.1109/MWC.2015.7054723.

[169] Xun Zhou, Rui Zhang, and Chin Keong Ho. "Wireless Information and Power Transfer: Architecture Design and Rate-Energy Tradeoff." en. In: *IEEE Trans. Commun.* 61.11 (Nov. 2013), pp. 4754–4767. ISSN: 0090-6778. DOI: 10.1109/TCOMM.2013.13.120855. (Visited on 04/07/2022).

[170] Jiang Zhu, Yonghui Song, Dingde Jiang, and Houbing Song. "A new deep-Q-learning-based transmission scheduling mechanism for the cognitive Internet of Things." In: *IEEE Internet of Things Journal* 5.4 (2017), pp. 2375–2385.

[171] Özen Özkaya and Berna Örs. "Model-based, fully simulated, system-level power consumption estimation of IoT devices." In: *Microprocessors and Microsystems* 105 (2024), p. 105009. ISSN: 0141-9331. DOI: https://doi.org/10.1016/j.micpro.2024.105009. URL: https://www.sciencedirect.com/science/article/pii/S0141933124000048.

*La borsa di dottorato è stata finanziata dal D.M. n. 351 del 9.4.2022, a valere sul PNRR - finanziato dall'Unione europea -NextGenerationEU - Missione 4 "Istruzione e ricerca", Componente 1 "Potenziamento dell'offerta dei servizi di istruzione: dagli asili nido all'Università" - Investimento 4.1 "Estensione del numero di dottorati di ricerca e dottorati innovativi per la pubblica amministrazione e il patrimonio culturale*

Finanziato dall'Unione europea NextGenerationEU | Ministero dell'Università e della Ricerca | Italiadomani PIANO NAZIONALE DI RIPRESA E RESILIENZA